Framework for neurosphere growth modelling under phase-contrast microscopy

Stephane Ulysse Rigaud

THÈSE DE DOCTORAT DE
l'UNIVERSITÉ PIERRE ET MARIE CURIE

Spécialité

Informatique

École doctorale Informatique, Télécommunications et Électronique de Paris

Présentée par

Stéphane Ulysse RIGAUD

Pour obtenir le grade de

DOCTEUR de l'UNIVERSITÉ PIERRE ET MARIE CURIE

Sujet de la thèse :

Méthodologie de Modélisation de la Croissance de Neurosphères sous Microscope à Contraste de Phase

soutenue le 10 Mars 2014

devant le jury composé de :

Dr. Patrick Bouthemy	INRIA Rennes	Rapporteur
Dr. Xavier Descombes	INRIA Sophia Antipolis	Rapporteur
Dr. Thomas Boudier	Université Pierre et Marie Curie, Sorbonne Universités	Examinateur
Dr. Vincent Mouly	Université Pierre et Marie Curie, Sorbonne Universités	Examinateur
Dr. George Stamon	Université Paris-Descartes	Examinateur
Dr. Nicolas Loménie	Université Paris-Descartes	Encadrant
Dr. Joo-Hwee Lim	A*STAR Institute for Infocomm Research	Co-Directeur
Prof Daniel Racoceanu	Université Pierre et Marie Curie, Sorbonne Universités	Directeur

DOCTOR OF PHILOSOPHY (PhD) THESIS OF
PIERRE ET MARIE CURIE UNIVERSITY

Specialisation

Computer Science

Paris doctoral school of Computing, Communications and Electronic

Presented by

Stéphane Ulysse RIGAUD

Submitted for the partial requirement of

Doctor of Philosophy from UNIVERSITY OF PIERRE AND MARIE CURIE

Thesis subject :

Framework for Neurosphere Growth Modeling Under Phase-Contrast Microscopy

defended the 10th Marsh 2014

comity composed of :

Dr. Patrick Bouthemy	INRIA Rennes	Rewiewer
Dr. Xavier Descombes	INRIA Sophia Antipolis	Rewiewer
Dr. Thomas Boudier	Université Pierre et Marie Curie, Sorbonne Universités	Examiner
Dr. Vincent Mouly	Université Pierre et Marie Curie, Sorbonne Universités	Examiner
Dr. George Stamon	Université Paris-Descartes	Examiner
Dr. Nicolas Loménie	Université Paris-Descartes	Supervisor
Dr. Joo-Hwee Lim	A*STAR Institute for Infocomm Research	Co-Director
Prof Daniel Racoceanu	Université Pierre et Marie Curie, Sorbonne Universités	Director

University Pierre and Marie Curie,
Sorbonne Universities, Paris, France
I^2R / A*STAR, Singapore
Image & Pervasive Access Lab
IPAL UMI CNRS 2955

1 Fusionopolis Way
#21-01 Connexis (South Tower)
Singapore 138632

À mon grand-père.

Heureux qui, comme Ulysse, a fait un
beau voyage,

Joachim Du Bellay

Acknowledgments

First of all, I would like to thank all the people who supported and collaborated with me to achieve this work. Without your help I could not be at this stage today.

I wish to extend my sincerest gratitude to my thesis directors, Prof. Daniel Racoceanu and Dr. Lim Joo Hwee, for giving me the opportunity to realize this work, for their precious advices, ideas and support that brought this work to completion, and for the confidence they had in me and for the freedom and responsibility I received in my work. It was really a wonderful experience to work with them and to learn from them.

I express my sincere thanks to the president of the thesis jury, Prof. George Stamon, and the official referees, Dr. Patrick Bouthemy and Dr. Xavier Descombes for reviewing my thesis.

A special thank to Alexandre Gouaillard, for his support and teaching, and the volley at Sentosa. I would like also to thank all my colleagues from the lab for their help and support, especially my colleagues Hamdi Aloulou, Thibaut Tiberghien, Antoine Fagette, Coralie and Ludovic.

A part of this research work was realized in close collaboration with the Institute for Infocomm Research (I^2R), the Bio-Imaging Institute (BII) and the Institute of Medical Biology (IMB). I would like to thank Sohail Ahmed, Lee Hwee Kuan, Shvetha Sankaran, Hariharan Srivats, Chao-Hui Huang and their teams for the collaboration we had, and the long meetings and discussions.

I would like to thank also all the great people I have met in Singapore those past three years, my dear Sir Harish and his best pal Mahmood; Loic, Pierre and Elianor who were working so far away; Pei Hua, Massi, Farhan, Debra, Mika, Teppo for all the good time we had and the travel.

Finally, I would like to thank my family and my friends for their understanding and support during the past three years.

Thanks to all of you.

Framework for Neurosphere Growth Modeling Under Phase-Contrast Microscopy Time-Lapse Images

Abstract

The study of the stem cells is one of the most important current biomedical research field. The recently discovered neural stem cells, that can be found in the brain, represent, most certainly, the key factor of our brain high plasticity and recovery capacities. This is even much more relevant since the neural stem cells may also be responsible for the formation of brain cancer.
Despite significant advances in this area, a lot of questions still remain open about the neural stem cells. Studying their behaviour and their possible reaction to specific drugs, could lead to multiple applications in regenerative medicine. Computer vision and image processing recently gain a considerable interest in the biomedical field, for the development of automated solutions for live cell monitoring, allowing observation and analysis of high quantity of information generated through multiple experiments.
High fragility and complex evolution of neural stem cells pose many challenges in image processing and image analysis. Dealing with some of these challenges, this thesis proposes a new methodology for the observation and modelling of neurosphere formation under phase contrast time lapse microscopy, by considering these difficulties, and by proposing an augmented 3-D visualisation capability. From the single neural stem cell to the proliferation and formation of middle size spherical aggregates called neurosphere, we analyse the two dimensional microscopic images series (analysis phase) and extract a three dimensional model of the neurosphere (synthesis phase). Using image processing and analysis methods, we extract information from the neurosphere growth monitoring sequences given by the microscope. Using this information and combing it with *prior* biomedical knowledge about the experiment, we define a three dimensional model of the observed cells. The model is then validated through a 3-D to 2-D registration approach.
Overall, our framework proposes an automated visualisation and monitoring solution for neural stem cell proliferation sequence into neurosphere under phase contrast microscopy. The scientific challenge of 2-D analysis 3-D synthesis has been treated using an original multi-parametric, genetic algorithm approach. The perspectives of this study are very important, related to augmented capabilities for neural stem cell selection, drug testing, stem cells selection and even - in the near future - fate early prediction capabilities.

Keywords

Neural Stem Cell, Phase-Contrast Microscopy, Neurosphere, Rigid Model, 2-D to 3-D Registration, Cell Detection, 3-D Microscopy, Biomedical Imaging, Genetic Algorithm, Mesh, Delaunay Triangulation

Méthodologie de Modélisation de la Croissance de Neurosphères sous Microscope à Contrast de Phase

Résumé

L'étude des cellules souches est l'un des champs de recherches les plus importants dans le domaine biomédical. Découvertes récemment au niveau du cerveau, les cellules souches neuronales sont très probablement à l'origine de la forte plasticité et de la capacité de régénération de notre cerveau, jouant un rôle prépondérant dans la rééducation de ce dernier, par exemple, suite à un traumatisme. De plus, ces mêmes cellules partagent de nombreux points communs avec les cellules cancéreuses que l'on peut observer dans certains cancers du cerveau, principalement, leur capacité à se diviser et à proliférer. De nombreuses questions existent autour de ce type de cellules et l'étude de leur développement, comportement, ainsi que l'influence de certains produits actifs sur ces dernières pourraient ouvrir la voie vers de nouvelles applications en médecine régénérative, ainsi que pour le traitement de tumeur cérébrale. La vision par ordinateur et le traitement d'images ont été fortement mis en avant dans le domaine biomédical pour le développement de solutions automatiques d'observation et de culture de cellules. En effet, l'outil informatique permet, d'une part, l'automatisation et la parallélisation de protocole d'expérience minimisant ainsi l'intervention humaine et augmentant la quantité de données générées, et d'autre part, le traitement et l'analyse de larges quantités de données générées par ces mêmes expériences. La combinaison entre la modalité de contraste de phase utilisée pour l'observation des cellules, leur grande fragilité, ainsi que leur complexe processus de prolifération, soulèvent d'importants challenges en traitement et analyse d'image. Ce travail de thèse propose une nouvelle méthodologie pour l'observation et la modélisation des neurosphères sous microscope à contraste de phase. À chaque observation réalisée par le microscope, à partir d'une seule souche jusqu'à sa prolifération et la formation d'un agrégat de cellules de taille moyenne (appelée neurosphère), notre système permet l'extraction d'un modèle en trois dimensions de la structure de cellules observées. Une analyse de la séquence d'images de contraste de phase permet la segmentation de la neurosphère ainsi que des cellules la constituant. À partir de ces informations, combinées avec des connaissances a priori sur la prolifération des cellules souches neuronales, plusieurs modèles 3-D possibles sont alors générés. Ces modèles sont ensuite évalués par rapport à l'image d'observation, grâce à un recalage 3-D vers 2-D.

À travers cette approche, nous présentons un outil automatique de visualisation et d'observation augmentées de la prolifération de cellules souches neuronales sous microscope à contraste de phase.

Mots-clefs

Cellule Souche Neuronale, Image à Contrast de Phase, Neurosphère, Model Rigide, Recalage 2-D–3-D, Détection de Cellules, Microscopies 3-D, Imagerie Biomédicale, Algorithme Génétique, Maillage, Triangulation de Delaunay

Author's Publications

Conference Papers

S. U. Rigaud, C.-H. Huang, S. Ahmed, Joo-Hwee Lim, and D. Racoceanu. An analysis-synthesis approach for neurosphere modeling. In *Engineering in Medicine and Biology Society,EMBC, 2013 Annual International Conference of the IEEE*, pages 1–6, 2013.

S. U. Rigaud, N. Loménie, S. Sankaran, S. Ahmed, Joo-Hwee Lim, and D. Racoceanu. Neurosphere fate prediction: An analysis-synthesis approach for feature extraction. In *Neural Networks (IJCNN), The 2012 International Joint Conference on*, pages 1–7, 2012.

S. U. Rigaud and Nicolas Loménie. Neural stem cell tracking with phase contrast video microscopy. In *SPIE Medical Imaging*, pages 796230–796236, 2011.

White Papers

H. Irshad, **S. U. Rigaud**, and A. Gouaillard. Primal/dual mesh with application to triangular/simplex mesh and delaunay/voronoi. *Insight Journal*, pages 1–14, 2012.

S. U. Rigaud and A. Gouaillard. Incremental delaunay triangulation. *Insight Journal*, pages 1–5, 2012.

S. U. Rigaud and A. Gouaillard. Walk in a triangulation : Straight walk. *Insight Journal*, pages 1–3, 2012.

Reports

H. K. Lee, A. Sohail, J. H. Lim, D. Racoceanu, W. Xiong, W. Yu, L. Cheng, C. H. Huang, **S. U. Rigaud**, M. Kulikova, and S. C. Chia. A*STAR JCO Project Report : Intelligent vision system for neural stem cell, 2013.

H. K. Lee, A. Sohail, J. H. Lim, D. Racoceanu, W. Xiong, W. Yu, L. Cheng, Y. N. Law, W. Huang, C. H. Huang, **S. U. Rigaud**, M. Kulikova, and S. C. Chia. A*STAR JCO Grant Proposal : Integrated autonomous microscopy systems, 2014.

S. U. Rigaud. Neural stem cell tracking under phase-contrast time-lapse microscopy. Master's thesis, University of Pierre and Marie Curie (Paris 6), IPAL Lab (Singapore), 2010.

Contents

List of Figures

List of Tables

Acronyms

CPU Central Processing Unit. xxi, 71, 75, 78

CT Computed Tomography. 14, 31, 94

DAPI 4',6-diamidino-2-phenylindole. xix, 17

DIC Differential Interference Contrast. 31, 40, 41

DoG Difference of Gaussian. 33, 97

FACS Fluorescence-Activated Cell Sorting. 20, 21

FN False Negative. 50, 51

FP False Positive. 50

GFP Green Fluorescence Protein. xix, 13, 17, 36

GPU Graphics Processing Unit. xxi, 70–72, 75, 78

ICP Iterative Closest Point. 119

iPS Cells induce pluripotent stem cells. 10

ITK Insight ToolKit. 79, 80, 83, 85

LMA Levenberg-Marquardt Algorithm. 99

MI Mutual Information. 95, 96

MRI Magnetic Resonance Imaging. 14, 31, 93, 94

MSE Mean Square Error. 95, 99

NCC Normalised Cross-Correlation. 95, 96, 99, 105

NFA Neurosphere Formation Assay. xix, xxi, 14, 19, 22, 24, 27, 65, 123–126

PET Positron Emission Tomography. 93

PSF Point Spread Function. 41, 42

RGD Regular Gradient Descent. 99, 107

ROC Receiver Operating Characteristic. 51

ROI Region Of Interest. xx, 43–45

SVG Subgranular Zone. xix, 16

SVZ Subventricular Zone. xix, 16

TN True Negative. 50, 51

TP True Positive. 50, 51

VTK Visual ToolKit. 108

Introduction

Recently, the improvement of microscopy imaging technology and the automation of the different experiment protocols, led to a new methodology for cell analysis and drug testing in biology and biomedical science fields. Indeed, the capacity to accumulate high volumes of microscopy image data from automated experiments, created the need for bioimage analysis systems, to be able to process and extract knowledge and information from the massive data produced.

The monitoring of living cells *in vitro*, especially their growth, has become essential for the understanding of the mechanisms of development, as for drug testing. In the particular case of stem cells, for which our knowledge remains limited, the monitoring of their growth and behaviour is critical for a better understanding of their role in the body, the effect of specific drug on their behaviour, and the possible control for modern medical application.

Intelligent Visual System for Neural Stem Cell Observation

Mammalian cell culture techniques have proved to be invaluable to the pharmaceutical industry. Two dimensional monolayers of adherent cell cultures have been widely used for drug discovery and for toxicity testing. However, such in vitro systems very badly approximate the physiology of their in vivo counterparts, in particular humans, in which the anatomy is inherently three dimensional.

Complex 3-D culture systems, consisting of a matrix of different cell types, would more accurately reflect mammalian physiology. Furthermore, the use of tissue-specific stem cells, makes 3-D culture system even more attractive for the study of as disease processes such as cancer. For the aforementioned reasons, it becomes very important to study stem cell based 3-D culture systems, as: neurospheres, reconstructed skin and intestinal crypts.

Advanced microscopy has enabled large and complex culture systems to be analysed at high resolution. The ability to effectively develop 3-D cell cultures, microscopy and data analysis is tightly coupled, forming a tripartite dependency that re-enforces each other. The effectiveness of analysing the image data and deriving new knowledge, depends on the

quality of the data, while the experimental design depends on what type of data is more suitable for image analysis.

Currently, there is no system with an effective integrated pipeline of 3-D cell culture, microscopy and image analysis. Building a complete set of image analysis tools to analyse complex cell culture to give prompt feedback as well as to automatically control the microscope is important for physiological studies of tissues and drug discovery. Advanced microscopy is at present, semi-automated, in the sense that manual monitoring and intervention are still essential. We propose a much more automated imaging suite, including automated control of stages, refocusing, light illumination and detection of aberrant events *etc.* Such system will allow us to follow the growth of live cells, in 3-D and in real-time automatically contiguously for several days or weeks. Such a system will be very attractive to the biotechnology industry.

This work take is a component of the Intelligent Visual System for Neural Stem Cell Observation Project[1] involving the Institute for Medical Biology (IMB), the Bio-Informatics Institute (BII) and the Institute for Infocomm Research (I^2R) of which the Image and Pervasive Access Laboratory (IPAL) is part of. Its specific aim is to build a microscopy suite endowed with sufficient intelligence to effectively understand and analyse biomedical images. Results of analysis will be directly used to control microscopy equipment in real time, for a contiguous period of several days or weeks. The microscopy suite is specifically built to analyse the anatomies of complex 3-D cell cultures, which have been the focus of much research recently and will experience an expanding market in the near future.

As part of this project, our study focusses on the 3-D cells organisation appearing during the cell culture growth. Thus, we propose a framework solution to estimate the 3-D cells configuration of a growing 3-D structure (neurospheres in the case of this work), starting from time lapse phase contrast 2-D microscopic observations.

[1]IVSNSC - `www.ipal.cnrs.fr/project/ivs4nsc-intelligent-biomedical-vision-system`

Organisation of the Thesis

This thesis concentrates its research efforts on the modelling of the neurosphere structure during its formation. The framework is composed of three main processes: (i) the analysis - extracting information from the microscope observation, (ii) the synthesis - generating possible structural configuration of cells using information from the analysis process and the *prior* knowledge of neurosphere, and (iii) the selection - using a three-dimensions to two-dimensions registration process to evaluate the generated model based on the microscope observation. The work is presented in four chapters, following the different part of the framework. In the first chapter, we introduce the biological background and motivations related to this doctoral work. The second chapter consists in the analysis process, in which the neurosphere is tracked, segmented and the visible cells detected using tracking and segmentation methods. We cover the state of the art of the methods used in this module, the choice, the methods and the results obtained by application on our data. The third chapter presents the three-dimensional modelling process. Two approaches are introduced: an iterative modelling using Delaunay mesh and an evolution construction model using evolution algorithm. The fourth chapter provides the selection process to score and rank the different models generated using a three-dimensions to two-dimensions registration process between the models and the observation, as an analysis of the results of the two methods.

Chapter 1

Biological Context Related to Neural Stem Cells

1.1 Stem Cells

An adult mammalian body is composed of different type of cells (*e.g.* an adult human has around 300 differentiated types of cells). Each of these cells has its specification and function, before it ends its cycle, by entering into mitosis (division) and producing two new identical cells, or by entering into apoptosis (death). In 1960, new type of cells was defined which, in opposition to the rest of the cells of the body, are undifferentiated and called stem cells. However, due to their rarity and the absence of definitive biological marker, their identification is done through the observation of specific and measurable characteristics during *in vitro* experiment, which will define them as stem cells [51]. The observed characteristics are the following:

Self-renewal - the cells are capable of going through multiple division cycle and maintaining their existence over an extended period of time.

Proliferation - the cells, through division cycle, are capable to increase their population and proliferate.

Potency - the cells, through division cycle, are able to generate differentiated cells.

These characteristics may be defined more precisely depending on the type of stem cell observed. Two different types of stem cells are identified: embryonic stem cells and somatic stem cells.

The embryonic stem cells were identify for the first time in a human body in 1998 [98] but were already identify for the mouse since 1981 [35]. They are present during the embryonic stage of mammalian individual, when the proliferation and potency properties play a major role in the embryo development and the creation of different major tissues that will form an individual. Indeed, the embryonic stem cells present a high degree of potency at the beginning of the formation, in order to generate all possible types of differentiated cells.

The somatic stem cells (also called adult stem cells) are stem cells recently discovered in adult mammalian tissue. Relatively rare in comparison with the embryonic stem cells, they are located in the different major tissues of the adult body. In opposition with the

omni-potency of the embryonic stem cells, the somatic stem cells are defined as *plury*-potency. They will only generate cells that will differentiate into primary cells type of the tissue from which they are coming. Their role in the adult body is not properly defined, and may change with the tissue hosting them. It is assumed that they maintain a similar role than the embryonic stem cells but at low and controlled speed, providing the tissue with a regeneration capacity, by renewing the pool of differentiated cells. The first somatic stem cells discovered were in the hematopoietic system (bones marrow) of mice in 1963 [14], and they could generate all the different type of blood cells.

A methodology to artificially produce *plury*-potent stem cell *in vitro* was discovered in 2006 [95]. They are defined as induce pluripotent stem cells (iPS Cells). Their creation consist in reactivating genes corresponding to the *plury*-potency using an retrovirus. This approach give the possibility of production of stem cells in laboratory, bypassing most of the ethical problems that surround the study of stem cells. However, it was observed that such generated stem cells are prone to express tumorous behaviour.

1.1.1 Progenitor Cells

The generation process of differentiated cells from stem cells is done through an intermediate type of cells called progenitor cells [51, 82]. The stem cells are capable of two types of division. The first is a symmetrical division that generates two identical stem cells (Fig. 1-1a). The second is an asymmetrical division, producing a new stem cell and a progenitor cell (Fig. 1-1b). The progenitor cells have a short division cycle, and are bound to become differentiated cells. It is important to notice that progenitor cells do not physiologically differ from stem cells and one cannot be visually identified from the others. Though, they are not stem cells as they already have in their genetic code, a specialisation, related to the lineage cell type in which they will differentiate. The progenitor cells will only be able to do symmetrical division and produce two new identical progenitor cells with the same genetic code (Fig. 1-1c). In case the concerned tissue is composed of multiple different lineage cell types, the generated progenitor cell will only be related to one lineage cell type. If other lineage cell type is necessary, the stem cells will have to produce a new progenitor cell related to this particular lineage cell type. The purpose of the progenitor cells is to

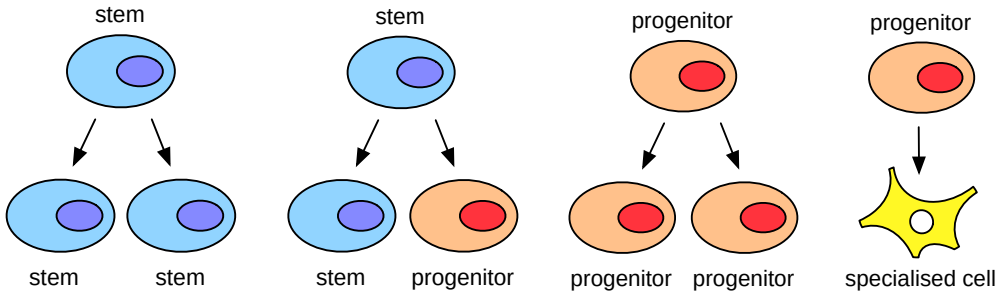

Figure 1-1: Division pattern of neural stem cells and neural progenitor cells. (a) Symmetrical division of stem cells. (b) Asymmetrical division of stem cells. (c) Division of progenitor cells. (d) Progenitor cell differentiation.

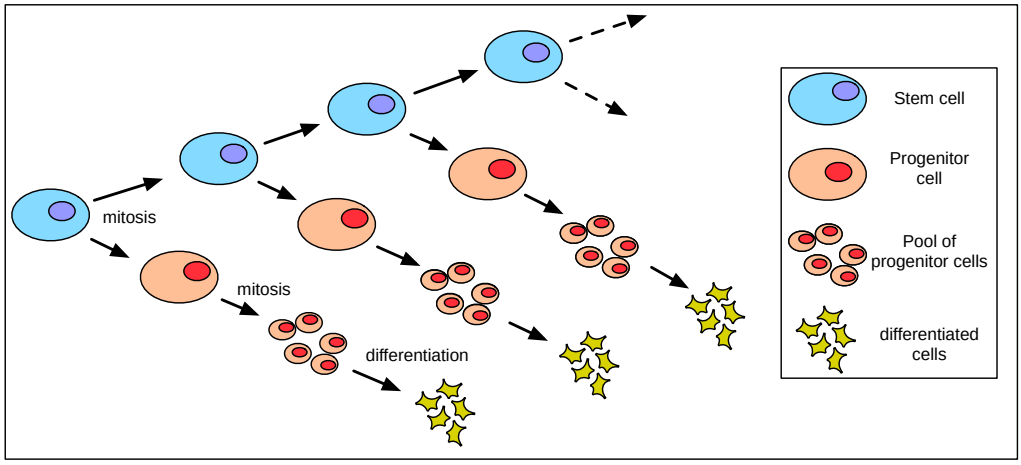

Figure 1-2: Differentiation transient amplification process induced by progenitor cells.

allow a transient amplification process. The stem cells produce one progenitor which will rapidly divide itself a limited number of times, before ongoing into a differentiation process, to transform themselves into lineage cells (Fig. 1-2) With this process, the stem cells only go into one division but will result in producing a several differentiated cells through the division process of the progenitor cells.

1.1.2 Neural Stem Cells

For a very long time, it was stated that cells in the central nervous system (*e.g.* neurons) could not be replaced, and that, in general, the body could not produce new nerve cells to replace damaged or old nerve cells. The recent discovery of somatic stem cells in

the central nervous system of adult mammalian, have brought this general believe down [83, 84]. The embryonic and somatic stem cells of the central nervous system, are also called neural stem cells. The embryonic types are responsible for the development of the central nervous system during the embryonic stage, while the somatic type play a role in the elasticity of the nervous system tissue. In the same way as the other type of somatic stem cells, the neural stem cells can produce all the lineage cell types present in the central nervous system: neurons (Fig. 1-3b), astrocytes (Fig. 1-3a) and olygodentrocytes (Fig. 1-3c); through the generation of neural progenitor cells.

The discovery of the neural stem cells has opened new possibility of research, having naturally raised new questions:

- Where do they come from? Are they embryonic stem cells that stayed undifferentiated, or are they other cells appearing at a particular moment?

- What are their roles in the neural tissue? Do they have a direct relation with disease and injury recovery of the brain? Do they have a relation with tumour cells?

- Can we identify neural stem cells without expressing their stem cell properties?

- Can we manipulate neural stem cell to increase their ability to proliferate *in vitro* for the development of tissue for possible transplantation? And *in vivo* to enhance the production of new neural cells as a cure for degenerative disease and help injury recovery?

There are still no biological marker to identify neural stem cells and their definition must be done through the measurement of the three main properties of stem cells *in vitro*. This increases the difficulty to study them as they present a very high fragility and sensibility to any external factors.

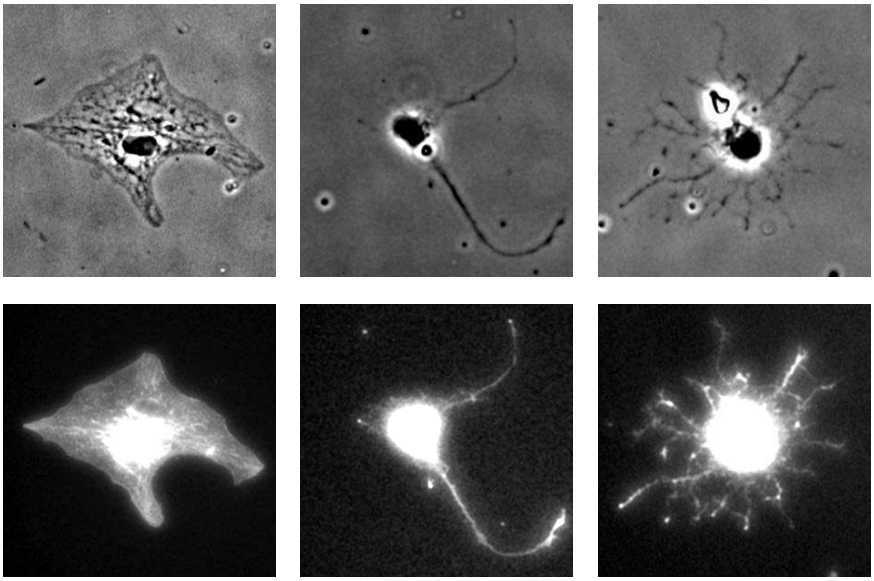

(a) (b) (c)

Figure 1-3: Cell lineage type of the central nervous system image in phase contrast (first row) and with GFP marker fixed to the cytoskeleton (second row). (a) Astrocyte, characterised by dense body. (b) Neuron, characterised by its 1 3 long neurites. (c) Olygodendrocyte, characterised by a star shape with multiple branches.

1.2 Cell Culture and Experimentation

1.2.1 Adhesive and Floating Culture

It exists different way to culture cells, depending (among others) on the type of cells to be cultured, the observation intended by the biologist and the modality used to observe them. However, it is possible to define two principal ways to culture cells: two-dimensional culture and three-dimensional culture.

Two-dimensional culture is the first and most used culture process. It consists of placing the cells at the bottom of a culture dish, on a flat substrate, on which they will fix themselves. The dish is filled with a media liquid, providing cells nutriments, for their development. The cells will divide, move, be in contact with other cells and die freely over time, on the substrate plan. Using the media, it is possible to introduce drugs in the culture to observe their effects on the living cells. With such approach, the observation of the cells is straight forward, as the culture can only be composed of isolated cells to monolayer tissue. Some cell overlapping is possible, but in overall, the cells are visible and

do not need any manipulation, except the addition of biological marker for fluorescence microscopy.

Three-dimensional culture is a more recent approach and less widespread. It consists in providing the cells with an environment similar to what they would have *in vivo*. It will make the cells develop in a 3-D space in opposition of the 2-D space of flat culture, and the cells will proliferate into 3-D structure of cells. Several approaches of three-dimensional culture exist [56]: Cell spheroids, microcarrier culture and tissue-engineered model [40]; And some cells may require a scaffold to support their development and keep a spatial control on their development. The observation of this type of culture can be more complex, as the visual depth of confocal microscope is less than $500\mu m$, and other visualisation process such as Magnetic Resonance Imaging (MRI) or Computed Tomography (CT) are used [97].

It is common to observe and culture cells on a flat surface, usually the bottom of a glass or a polystyrene culture dish, but is it still the best way to do? The question concerning the impact of the substrate supporting the cells on their development and behaviour was raised since 1972 and continues to still oppose sides [79, 85]. The interest of three-dimensional culture is the enhancement of high-content microscopy and a more adapted approach for stem cells culture that seams to have better development in three dimensions [49]. However, the complexity of such culture makes the automation and the visualisation difficult and costly, leaving three-dimensional culture still under-used. In our case, three-dimensional cell spheroids assay will be used for the culture and the proliferation of neural stem cells.

1.2.2 Neurosphere Formation Assay

The NFA (Fig. 1-4) is an experiment, proposed in 1992 by Reynolds and Weiss [83, 84, 87], which shown the existence of neural stem cells in the central nervous system of adult mammalian, and that these neural stem cells were able to produce neurons. In a more generic *in vitro* application, the NFA allows exhibiting and measuring the neural stem cells characteristics and therefore, the identification of such cells.

The neural cells are extracted from central nervous system tissue of adult mammalian

or embryo, and placed into a serum-free solution containing growth factors. The neural stem cells contained in the pool of cells, placed into the dish, will react to the growth factors and will divide over time, expressing their self-renewal property. They will form spherical agglomerate of cells, called neurosphere, composed of neural stem cells and neural progenitor cells, while non-stem cells will only be able to divide a limited number of time before dying. Once neurospheres are formed, it is possible to dissociate them into single cells again, which will form, under the same conditions, new neurospheres. The repetition process can be virtually done indefinably but in application had shown some limitations, as the observation of a increase of apoptosis among the cells.

If the growth factors are removed, the neurosphere will dissociate itself and the neural progenitor cells will differentiate into the different lineage cell types. After the differentiation, the presence of all the lineage cell type is an expression of the *multi*-potency property of the neural stem cells. More details explanations on the experiment [30] and experimental protocol can be found in the literature [8, 9, 7].

1.2.3 Neurosphere

A neurosphere is the results of the expression of the self-renewal and proliferation properties of neural stem cells *in vitro*. A neurosphere is a three-dimension spherical agglomerate of neural stem cells and neural progenitor cells. The neurosphere structure is not fully characterised and understood, and remain an important unknown of the neural stem cell research. Recent study has described neurosphere as environmental adaptability from the neural stem cells, being structures that allow neural stem cells to express the plasticity needed for *in vivo* engraftment and differentiation [105]. The specific form of the neurosphere, a sphere, is possibly due to the optimisation of the interaction cell-environment through the most optimise shape from a thermodynamic aspect. Indeed, the environment is the direct link to the cells for nutriment and oxygen needed for it survival, and the distribution of biological phenomenon (mitosis, apoptosis, *etc.*) is directly linked to the position of the cells in the structure.

The importance of the neurosphere in biomedical research is its use for neural stem cells

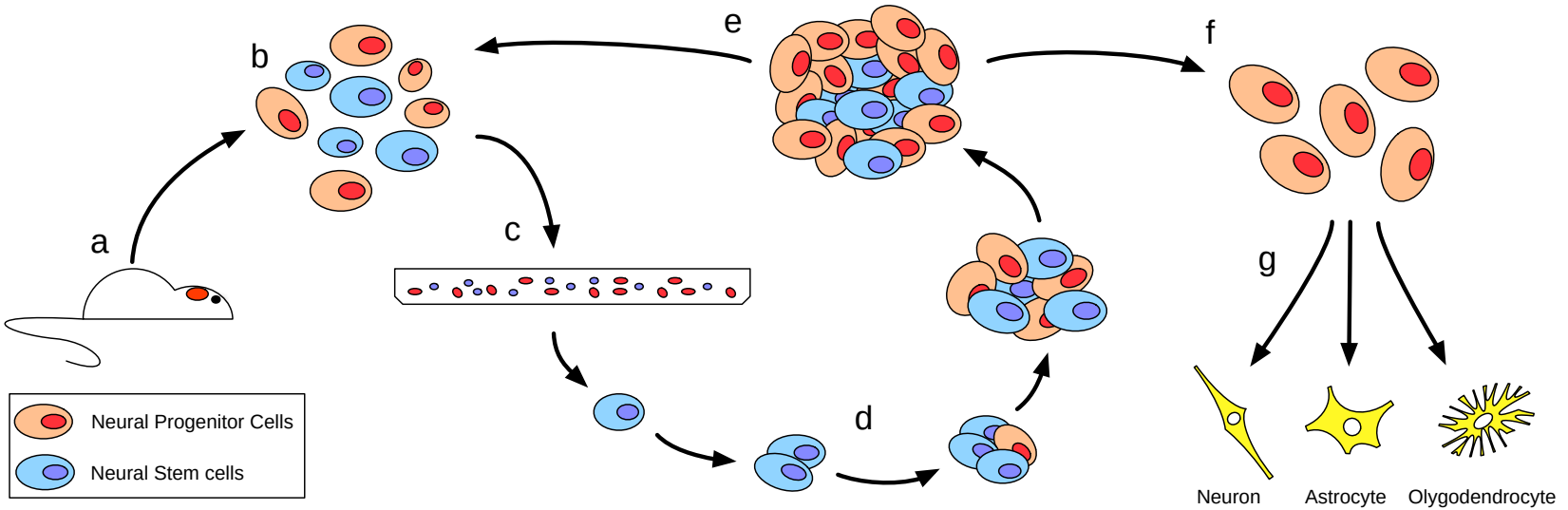

Figure 1-4: Neurosphere Formation Assay. (a) Extraction of neural cells from embryonic mammalian central nervous system or from the SVZ or SVG of adult mammalian central nervous system. (b) Creation of a pool of multiple types of cells, which contain some neural stem cells and neural progenitor cells. (c) The cells are cultured into free-suspension serum-free condition with a growth factor for several days. (d) During the culture period, neural stem cells will go through multiple cell cycles and proliferate. (e) After a certain time, neural stem cells will have created agglomerate of neural stem cells and neural progenitor cells that we call neurosphere. At this point, the neurosphere is dissociated into single cells again and either re-cultured into a dish to form again neurosphere, or the growth factors are removed and the cells enter a differentiation process. (f) The neural progenitor, without the growth factors will differentiate themselves into their lineage cell type. (g) After the differentiation process done, the three main lineage cell type of neural tissue should be visible.

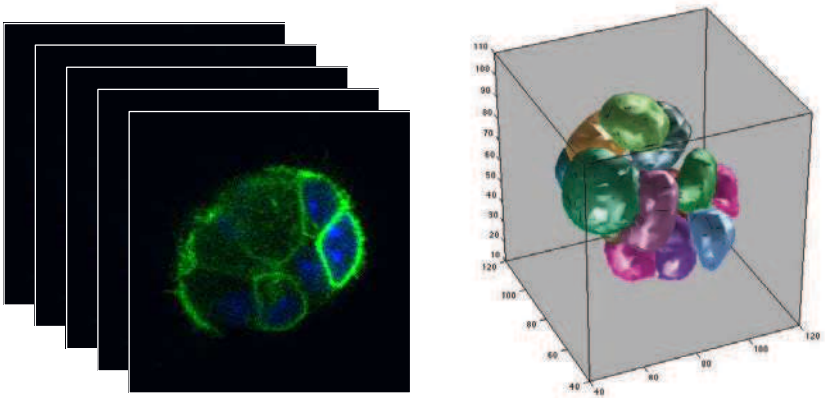

(a) (b)

Figure 1-5: Confocal microscope observation of neurosphere. (a) Image z-stack of a neurosphere marked with DAPI and GFP. (b) Reconstructed model from the three-dimensional segmentation of the cells in the z-stack [111].

culture and its possibility to culture pool of specialised neural cells that allows drug test screening to determine possible factor to influence the production of specific specialised neural cells. It also has an importance as a possible way for neural stem cells transplantation.

1.2.4 Imaging of Neurosphere

Observation Through Confocal Microscope

The neurosphere is a three-dimensional object. Using two fluorescent biomarkers, DAPI for marking the nuclei and GFP for marking the cells membrane, three-dimensional observations were done using a confocal microscope (Fig. 1-5a). The cells and neurospheres imaged in this way, where segmented and reconstructed in three-dimensions (Fig. 1-5b). However, the bio-toxicity of the markers and the photo-toxicity of the confocal laser needed to excite the markers are to high, and are not supported by the neural cells. All the neurospheres imaged in this way died quickly after performing one stack of images. The confocal modality was put aside, as it did not allow us to observe the neural stem cells and neurosphere over time.

Observation Through Phase-Contrast Microscope

Due to the high fragility of the observed cells, the observation of the neurosphere formation was done using a light microscope [15]. In contrast with the laser microscope [92], their photo-toxicity is lower and more adapted for live cells observation [113]. A phase-contrast microscope was used as it offered a better contrast observation of the cells. We use a multi-position time lapse experiment (Fig. 1-6). Particular site in the dish are registered into the microscope and, over time, the microscope will loop over the entire registered site and take an image. A predefined number of sites can be observed at the same time. Often used in living cells observation, as it is a non-invasive modality, it does not allow to observe three-dimensional structure. The focus of the microscope can be done on a specific depth but all the structure on a different depth will create out of focus artefacts making the observation difficult. However, the phase-contrast modality can be coupled with fluorescence markers to create multi-modalities images (Fig. 1-7). This approach was possible even with the high fragility of the cells but need to augment the time-scale of the time lapse and to use external membrane fluorescence markers.

1.2.5 Experimental Limitations

The neurosphere formation assay is very popular as it opened new possibilities in stem cell and brain research, by leading to several open questions on the central nervous system formation process and its regenerative capacity. However, the experiment has several drawbacks and restrictions that make it difficult to control and to extract information from it. One of the first and main problems is the low percentage of neurosphere formation. If the cells are extracted from adult tissue or embryo tissue, the percentage of first generation neurosphere to be formed, varies from 2.5% to 10%, and require a minimum of 5 to 7 days of experiment to form neurospheres. A high number of cells have to be process in order to have a minimum amount of neurospheres at the end of the experiment. The second main problem is the duration of the experiment. In live microscopy, a long experiment time-scale brings a problem of stability and viability, as it increases the possible effect of different variable from the experiment, such as the variation of temperature, photo-toxicity, random interaction or event between specimens, *etc.* The third major problem is the image time

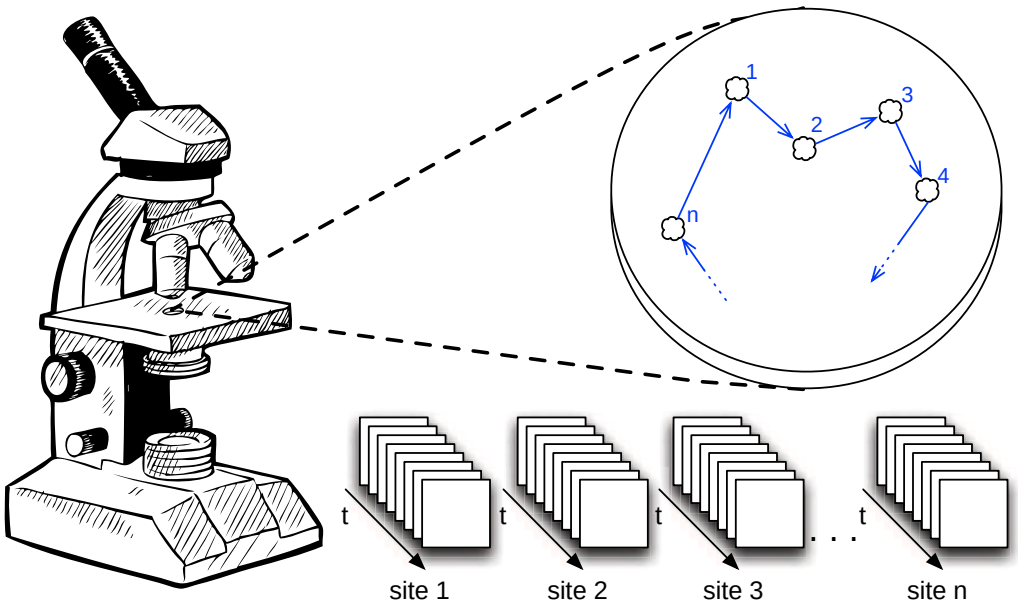

Figure 1-6: Parallel site imaging of NFA experiment using a phase contrast microscope. The dish contains multiple neural cells. Position of singular cells is registered as observation site in the microscope. Over time, the microscope goes through all the observation sites to imaged the current state of the cells and create a time-lapse of all the sites. The whole experiment is done under a controlled environment.

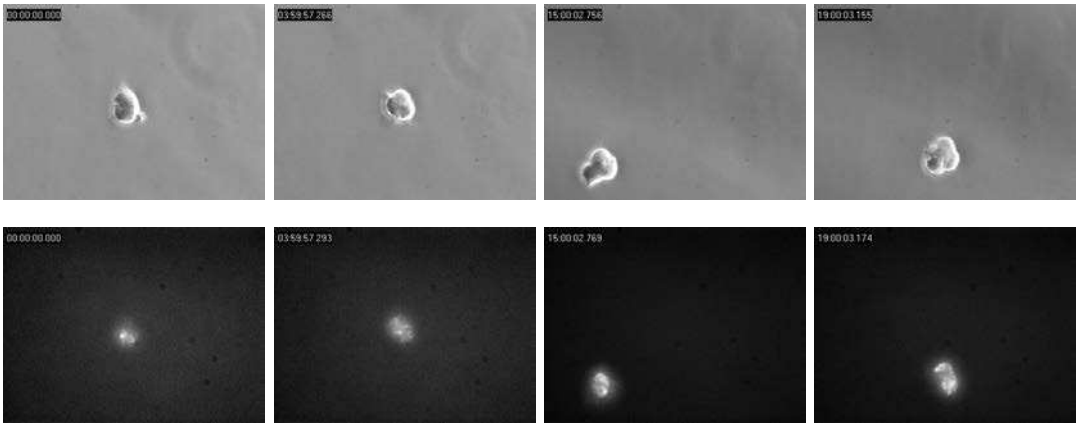

Figure 1-7: Extract of a time-lapse sequences using both (top row) phase-contrast and (bottom row) fluorescence brightfield microscopy using the *CD93* protein.

Figure 1-8: A*STAR IMB Phase-contrast microscope installation with incubator for living cells observation.

acquisition. As a high number of specimens are observed at the same time, the experiment is done through multi-position time-lapse sequences. Such process brings a mechanical limitation of how many observation can be done over a certain time, and is defined by the efficiency of the stage motor and the overall distances between site observation in the observed dish.

1.2.6 Data

We observed the neural stem cells development into neurosphere through a time lapse acquisition in phase contrast (Fig. 1-8). We have build two data sets of time-lapse sequences that contain cells developing in neurosphere and cells failing to develop in neurosphere.

Training Data Set

It is an early stage observation of the neurosphere development. The acquisition was done over two days, and 20 cells were observed in a glass dish at x40 magnification with a 2x2 binning modality using an Zeiss phase-contrast microscope (Fig. 1-9a). The cells were preliminary sorted using a Fluorescence-Activated Cell Sorting (FACS) and a *CD98* marker. The cells acquisition was performed with the automatic microscope tracking algorithm

[42]. On the 20 cells, nine managed to divide to reach a 2-cells configuration, four reached 3-cells and 4-cells configuration, and five did not survive the experiment. Five sequences are however not usable due to the presence of dust biasing the process. The data generated appear with a high contrast between the cells and the background however does not contain much visible details inside the cells. Due to the high contrast present in the images and the low complexity of the cells configuration reached in the different sequences, this data set is use to test the framework.

Test Data Set

It is a longer observation of the neurosphere development. The acquisition was done over 5 days, and 20 cells were observed in a glass dish at x40 magnification with a 1x1 binning modality using a Olympus phase-contrast microscope (Fig. 1-9b). The cells acquisition was performed with the automatic microscope tracking algorithm [42]. On the 20 cells, only four manage to divide and survive to an early neurosphere structure and fourteen did not form a neurosphere, as they died after one or two division. Similar to the first data set, two sequences are not usable due to the presence of dust biasing the process. The difference of surviving cell is due to the absence of FACS sorting. The data generated appear with lesser contrast than the first data set however the inside of the cells and neurosphere are much more details. Also, much higher cells configuration are reached, making the different sequences more difficult to process. Therefore, this data set is mostly used as a test data set due to its higher complexity compared to the *Training* data set.

1.3 Challenges and Perspectives

The recent years have seen the merge of biology with informatics solution, opening new possibilities in terms of observation of biological event. In stem cells research, computational solution are mostly used for automatically gather data on living cultured cells (size, movement, division, *etc.*) and process those data to extract knowledge on the cells (*e.g.* behaviour to particular chemical factors).

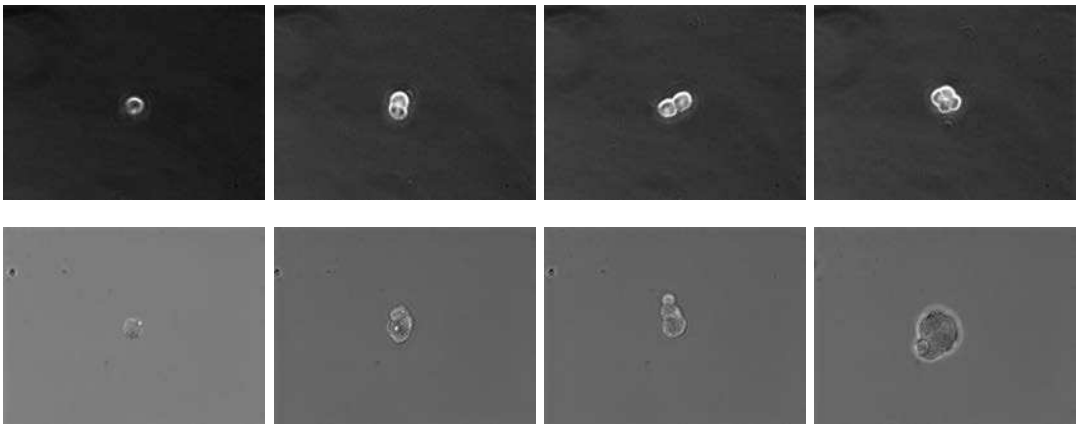

Figure 1-9: Extract of a time-lapse sequences from (top row) *Training* data set and (bottom row) *Test* data set.

1.3.1 Biological

Related to our case of application, neural stem cells discovery is still considered new to the field, and not much is know about those particular cells. The NFA is the most used experiment for neural stem cells culture and identification, thus it represents our best method to gather information on neural stem cells and better understand how they work [1].

The monitoring and the observation of the development of neurosphere over time can help us to extract and analyse various information related to the cells and to their possible use as clinical solution for regenerative medicine [99]. Currently, NFA are not observed. The dish is stored into an incubator and analysis of the cells is done after several days once neurosphere already started to form. The observation and analysis are done on the already formed neurosphere (size, number of cells, *etc.*), but the formation of the neurosphere itself is left apart. It is during the formation of the neurosphere that the self-renewal and the proliferation properties of the neural stem cells are fully observable, and that we could extract behaviour information linked to the formation process. However, the observation of such part of the experiment is not simple, as fluorescence microscope, such as confocal are not usable, being too toxic for the cells. More classic observation modality is used, but the observation results are not always simple to read, because of the complexity of the neurosphere. The development of new computer science solutions to enhance the neurosphere formation observation, and extract and analyse information

related to this formation (such as neurosphere movement, cell division rate, cell division tracing, proliferation speed, *etc.*), represents a strong need and challenge for the biological research.

Drug testing via high-throughput screening or high-content screening, is an important approach in the search of new drugs in biomedical research. In the case of neural stem cell, possible new drugs are investigate in order to see if it is possible to favour the production of a specific type of cells by the neural stem cells, to enhance or diminish the proliferation capacity of the neural stem cells, and even specifically kill neural stem cells. It has been proven that neural stem cells participate in the replacement of damaged tissue after an injury [4], and several work are done to investigate the specific properties and mechanisms in ageing and brain cancer [29]. Multiple hypotheses relate the neural stem cells to the brain plasticity and to specific brain tumour [36, 28]. Identifying chemical compound to control neural stem cells, for possible clinical application in regenerative medicine, is an important objective of the neural stem cell research, in general. Being able to favour the production of a specific type of cells by the neural stem cells, to enhance or diminish the proliferation capacity of the neural stem cells, and even specifically kill neural stem cells would be an important step in the biomedical field.

1.3.2 Computational

In a more computational and mathematical aspect, general biological experiment raises challenges in image processing and analysis. Problematic, in term of image processing and analysis, usually remain the same between classic application and biological application as in both cases we try to understand the content of the image through segmentation, identification and tracking of objects. Still, new challenges are raised mostly by the particularity of the studied object (cells, molecules, *etc.*) and to the modality of observation.

Object detection, segmentation and tracking to be applied to living cells *in vitro*. Contrary to persons, cars or other daily life object, they are all nearly exact replica of each other for the human eye. Their life spam is much shorter and they can divide and die in a very short window of time. Such challenge applied to living cells is not new but continue to

be an important challenge, especially with the high diversity of cells and various modality of observation. It is an important point in order to follow the cells in the image and gather information related to these cells.

Three-dimension object structural modelling from time-lapse two-dimension image. From two-dimension to three-dimension by reconstructing objects or places from pictures or video is an important topic in image processing. We observe three-dimensions object that will divide and form a three-dimension structure over time using a two-dimensions modality. This difference of dimension creates a loss of information that may be restored and extrapolated. Though such reconstruction is done using multiple view of the object at the same or different time, in our case only a time-lapse observation of a deformable object and a set of *prior* knowledge on the experiment is available.

1.3.3 Scope and Objectives

Focusing on the fact that neurosphere structure and the visualisation of its formation would enhance the observation of the NFA, we oriented our work in the elaboration of an observation framework for the biologist. The objectives of this framework is to provide the biologist with: First, an alternative or enhance observation tool. Allowing them to better understand the phase-contrast image of neurosphere, how many cells they were looking at and their configuration. Second, a visualisation platform. Through the generated model, new information can be encoded visually for the biologist, such as the tracking of a particular cell, the age, *etc.* Methods and work from other would be directly integrated in the model for the biologist to visualise.

1.4 Overview

Our framework proposes a corresponding three-dimensional neurosphere model, by extracting relevant information from on-line neurosphere formation sequences taken by the microscope, estimating a possible configuration of cells in the observed neurosphere and selecting the most relevant accordingly to the observation.

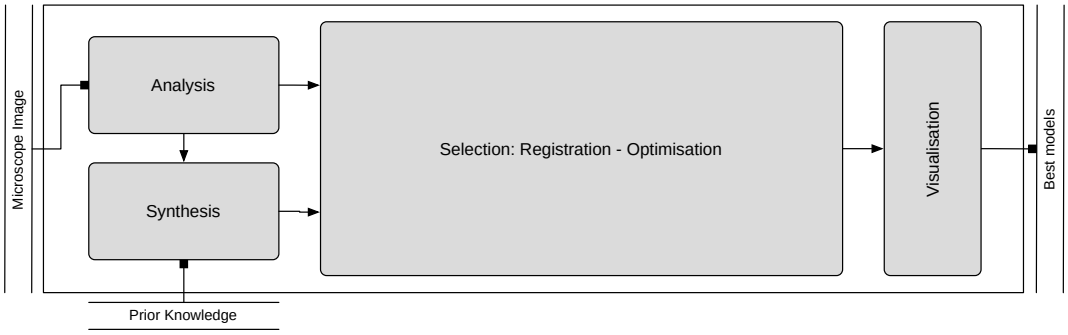

Figure 1-10: High level diagram of the neurosphere modelling framework.

The system is composed by three modules (Fig. 1-10):

1. An *analysis module* that takes the microscope output image and processes it to detects the neurosphere and segment the visible cells present in the image.

2. A *synthesis module* which takes the different information extracted from the image by the analysis module and, in combination with generation rules defined from *prior* knowledge of neural stem cells and neurosphere, generates a defined number of possible model.

3. A *selection module* finalises the process, by ranking each generated three-dimensions model, according to how close it is to the current observation. The result of the process is a ranked list of possible three-dimensions model that can be visualised by the user off-line or on-line.

1.4.1 Analysis

The analysis module is the first step of the framework and directly takes the output of the microscope if the framework is used on-line, or the time-lapse sequence of microscope images if used off-line. The role of the module is to extract relevant information from the image using image processing algorithms. Those information can be various and extended depending on the type of modality used, the type of cells observed and the goal of the global process. In our application, we look at the neurosphere itself through its shape, position and orientation, and to the cells that compose this same neurosphere, how many

cells, their position in the neurosphere, their respective size. Those information are then used in both synthesis and selection module.

1.4.2 Synthesis

The synthesis module is taking two inputs information: the results of the analysis module and the *prior* knowledge given by the user on the problematic. From those two inputs, the synthesis module generates a set of three-dimensional model that are possible according to the *prior* knowledge and close to the observation through the information extracted from the previous module. Depending on the method applied for the model generation, the generated set size can vary from one to multiple models, each of them representing a possible configuration of cells. For our application, two methods for generating the model are proposed.

1.4.3 Selection

The selection module is the last part of the process and takes the two previous module output as input. Using a three-dimensions to two-dimensions registration process, each model is evaluated regarding on how well it fits to the microscope observation. A list of the best models is defined according to the score given to each of them. A visualisation of the results is proposed to the user through the merge of the selected model and the microscope observation.

1.4.4 Contribution

Leveraging our experience with traditional approach to biomedical imaging which rely on high content image analysis, this work proposes a method to determine the 3D cell configuration of a structure such as neurosphere from a phase-contrast microscope observation.

1. In the analysis module, we proposed a new approach for detecting and segment highly clustered cell using partial circle shape present in the image.

2. In the synthesis module, focussing on the structural aspect of the neurosphere, we proposed two approaches, respectively using Delaunay mesh structure and evolution

algorithm, merged with *prior* knowledge on the neurosphere, to extract the cells configuration of the neurosphere.

3. Finally, the global framework, gathering methods from different field such as image processing, biomedical imaging, bioinformatics and artificial intelligence, proposes a new approach for the enhancement of neurosphere proliferation monitoring, and for the extraction of structural information from the NFA experiment.

Overall, this work opens new perspectives for neural stem cells research, in term of observation and high-content analysis.

Chapter 2

Analysis:

Cell Detection under Phase Contrast

2.1 Introduction

The analysis represents the first process of the neurosphere modelling framework. The corresponding analysis module is directly linked to the microscope, taking the image of the observed neurosphere as an input. Its purpose is, using image processing algorithms, to extract relevant parameters from the microscope image. These parameters are to be used for two purposes: the first role is to feed the synthesis module, in order to limit the model generation only to possible solution; the second role is related to the synthesis module, in order to support the evaluation of each generated model.
Three processes are used in this module. First, a tracking method determines the position of the neurosphere and remove possible dust, or dead cells, in the image. Second, using the physics of the phase contrast microscopy, a restoration process removes the phase contrast artefacts from the image, increasing the contrast of the image. Finally, based on circle fitting, a cell detection in dense aggregate, determines how many cells are present in the neurosphere.

2.2 State of the Art Related to Image Analysis of Living Cells

2.2.1 Fluorescence and Non-Fluorescence Cells

In biological image analysis, one of the major challenges is related to the type of modalities and cells to be observed [115, 70]. This is similar to medical image analysis with all the different imaging modalities like MRI, CT, *etc.* and the different tissue and organs to be observed. The two main families of observation in cell biology are fluorescence, that include the confocal microscope and non-fluorescence, that include phase contrast and Differential Interference Contrast (DIC) microscope.

In phase contrast and DIC images, the cell does not always appear as being very contrasted, compared to the background, but more like a region with different texture and non-uniform intensity. Beside, the images contain several artefacts, depending on their position with regards to the microscope objectives and the light orientation, such as the phase halo and out-of-focus blur. Such effects are difficult to reproduce as they are very

dependent of the cell type and the parameters of the microscope.

In fluorescence, it is actually possible to dye specific cellular structure like the nuclei or the membrane of the cells. The marker is made to target and dye only a specific structure of the cell, giving the assurance of what is observed. This is time consuming as the dye must get in the cells and attach itself to the specific structure, but it fully highlights the target structure and the cells, even if they are deep in a multilayer tissue. As the microscope will detect the fluorescence at a precise wavelength and discard any other sources of light, the fluorescence images do not contain any artefacts or background. The intensity at a point only corresponds to the concentration of fluorescence markers at that point. It is also possible to have multiple fluorescence markers on one image, to highlight different structures.

Depending on which type of modality the image was taken, even if the objectives are similar, the methods, parametrisations and results can be very different. Most research use fluorescence modalities as they present more reliable and cleaner data to work on, but the time needed for marking the cells, the cost of the markers to be used, and the high intensity of the laser used in fluorescence imaging are high requirement that are not always easy to meet for certain type of cells and certain type of experiments.

2.2.2 Cell Segmentation

The first step of every cell analysis is to detect and/or segment the cell present in the image, and to do so with an automatic approach. It is a wide field of research and a lot has been done on the subject, and an important number of methods exist [104].

Intensity Threshold is one of the most common approaches widely used in generic image segmentation [90]. In cell segmentation, it makes the assumption that the cells are highly contrasted with the background. In this case, a global or a local threshold determined from the histogram of the image can provide good results in an efficient and simple way. On non-fluorescence image, this will allow to detected contrasted object present in the image (Fig. 2-1d), and for fluorescence image, this will detect the cellular structure

that has been marked (Fig. 2-1f). However the results are too dependent from the image contrast and its illumination and, if used alone, can produce poor segmentation results. The cells may not be completely segmented due to non-uniform intensity of the pixels of the cells but only part of the cells are segmented (Fig. 2-1e), and touching cells may be detected as one large cell, degrading the segmentation precision (Fig. 2-1f). Therefore, pre-processing such as illumination correction, histogram equalisation and noise reduction are often used before any intensity threshold, and post-processing using morphological filter such as opening, closing and hole filling, usually follow the threshold to remove noise, smooth the detection, separate lightly connected cells and overall improve the final detection 2-1g. Such method was used by Al-Kofahi *et.al.* [2] as a cell detection step in phase contrast images. This is a good method for simple case, were the cells are not touching each other and the contrast in the images is high, but may be insufficient for more complex images. A variance of thresholding approach is local thresholding. Usually much easier to adapt, the intensity values, means and variance are observed on a smaller patch of the image, usually containing a cell to be segmented, and the threshold is determined on the patch only [103, 3, 6].

Features Detection using linear filters is another classical approach for cell segmentation. Depending at which scale the cells are observed, they can be considered as blob, and in this case, blob detection method such as Difference of Gaussian (DoG) can be used, or as object, and in this case, a classic edge detection filter can be used. Such approach has similar problem as intensity threshold. The quality of the results is in relation with the visibility of the features to be detected in the image. Such approach behaves better when integrated as a process step of a pipeline. Several studies using this kind of approach can be found, like Sakuma *et.al.* [91], or in fluorescence, for example Bao *et.al.* [12].

Morphological Mathematics is an important approach in image segmentation and is used in cell segmentation as non linear approach. The *watershed algorithm* is an algorithm that use the image as a landscape map with high and low peaks that form different basins. Starting from the local minima, the relief is flooded, a metaphorical way for a region growth. Each basin fully flooded will form a region delimited by watershed (contours).

As it easily managing multiple objects segmentation in the same image, the watershed algorithm is an important tools for cells segmentation [76]. The main drawback of the algorithm is its sensitivity to noise and over-segmentation, being, however, well adapted to separate touching cells (Fig. 2-1h). Some other methods of morphological mathematics exist but are normally used as pre-processing steps, especially *open* and *close* operations, in order to improve a more complex step for the detection.

Deformable Model approaches are the more recently used for cell detection. It consists of detecting cells using a parametric contour or surface, having an energy function associated to it. The most well-known deformable models are active contours, also called *snakes*, and are defined as a minimisation energy problem. The energy function is associated with a parametric contour, usually a curve or a parametric shape, and is the sum of energy of the contour where

internal energy is the energy related to the shape, length and regularity of the contour.

external energy is the energy defined by the position of the contour on the image, and leads the contour toward the zone of interest in the image.

constrain energy is a constraint value given by the user in order to control and interact with the snakes.

written as

$$E_{snake}(\Theta) \;=\; E_{int}(\Theta) \;+\; E_{ext}(\Theta) \;+\; E_{con}(\Theta) \tag{2.1}$$

where Θ encodes the active contour representation (points, curve, *etc.*). The result of the active contour is then determined as

$$\Theta^* \;=\; \arg\min_{\Theta} \; E_{snake}(\Theta) \tag{2.2}$$

and the solution is found through an iterative optimisation procedure, where each step updates the contour. A variation of the active contour is the Level Set [17], very effective, for a higher cost, for managing topological changes in the segmented object, as for tracking these changes. Several studies propose to use active contours for segmenting cells, as they can easily adapt to different shapes of cells, being able to overcome non-uniform intensity

of cells (Fig. 2-1i). The segmentation is done by parametrising the active contours on the intensity of the image, to detect gradient [34, 108, 110, 32]. More adapted approach allow to define a specific shape of the object to be segmented [96, 64], improving the segmentation that particular type of object. Such approach has already been used for low magnification neurosphere segmentation in high throughput drug screening [106] in order to determine the effect of drugs on the size of neurospheres after an incubation time.

2.2.3 Cell Tracking

Automated cell tracking is an important process in *in vitro* cell analysis, especially in high throughput analysis of cells. Cell migration, cell contacts and interaction, mitosis, apoptosis, and overall, any information on cell behaviour or change of behaviour, provide important information on those particular cells and on the effects of their environment. Several methods exist for tracking living cells *in vitro*, in order to register this information, as for following the cells and even tracking their lineage division. They can be regrouped in two main methods:

Tracking by detection the cells present in the image at each time step of the sequence. It links each detected cell to cells detected at the previous and next time step, using association rules. Pairing the cells, in order to minimise the likelihood distance between the associated cells, can be used to do the association. Such distance can be the difference between two specific points (*e.g.* cell centroids, cell center of mass, *etc.*) but it can also be the distance between two sets of features that describe two cells. The features such as shape, size, *etc.* are extracted during the segmentation of the cells. Once build, a probability of likelihood is defined between each pair of features vectors [2]. The scores given to each possible pair then determine the best association configuration. Three types of association can be done, one cell to one cell, one cell to two cells and one cell to none, which correspond to cell movement, cell division and cell death. The detection based tracking is straightforward to use and provide good results. However, it usually fails in the case of high number of cells, especially in case of close or clustered ones.

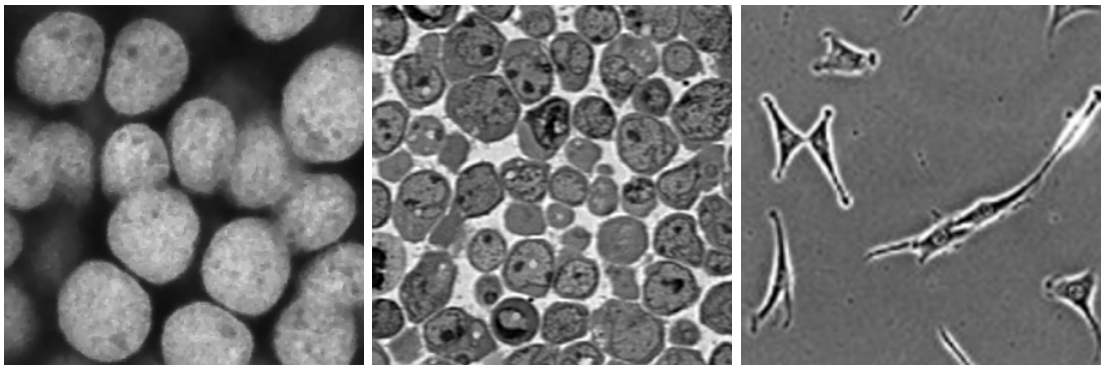

(a) Mammalian Cells marked by GFP under confocal microscope

(b) Histopathological slide under brightlight microscopy

(c) Mammalian living cells under phase contrast microscope

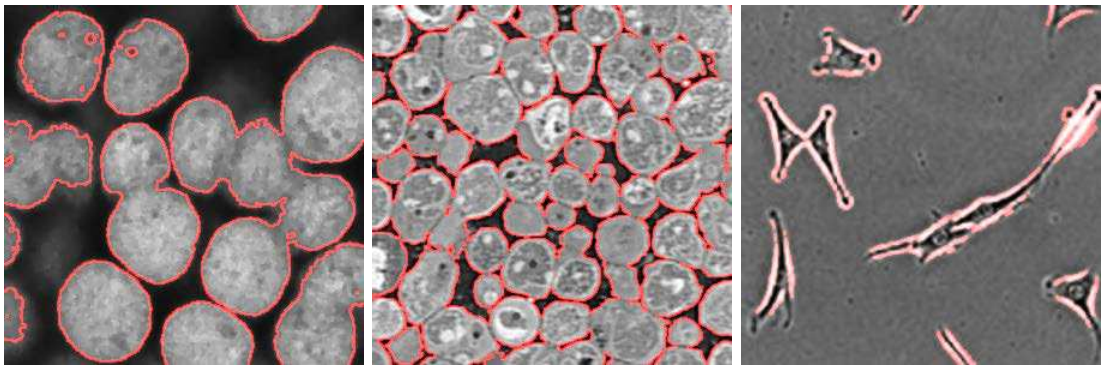

(d) Intensity based segmentation

(e) Intensity based segmentation

(f) Intensity based segmentation

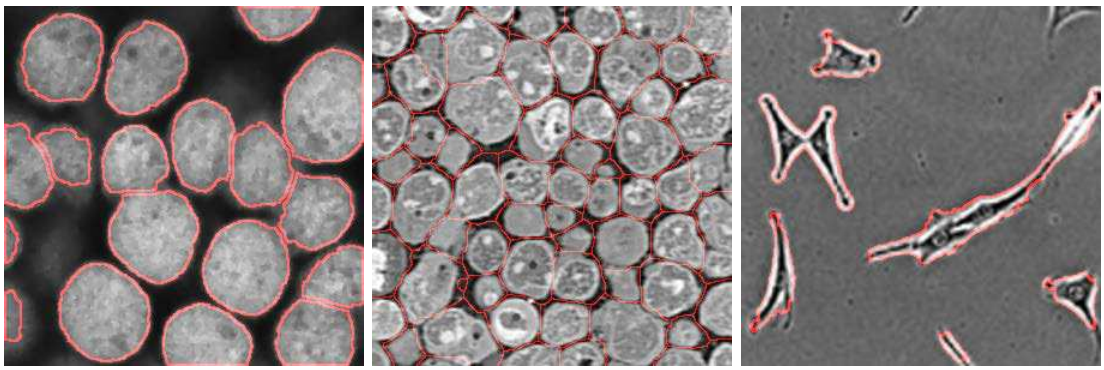

(g) Intensity threshold and morphomathematical reconstruction

(h) Watershed segmentation

(i) Active contour segmentation

Figure 2-1: Different type of cells under phase contrast and fluorescence microscopy and example of segmentation result using naive intensity based methods and more recent method.

Tracking by model evolution is a tracking method using deformable model such as active contours. With this approach, the cell is segmented with a deformable model, as described previously. The model carried on into the next frame with the same configuration, will be used as an initial step for the next frame to converge [12, 58, 114, 33]. Other approach exist that use more rigid model such as mean-shift algorithm [26, 18]. The advantage of such approach is the possibility to handle topology modification such as two cells that touch and separate, or overlapping cells. Among the drawbacks to these methods, we can point out the high number of empirical parameters dependent on the application case, and the high computational cost.

2.2.4 Cell Fate Prediction

Existing cell fate prediction methods treat simple cases - by determining if the cells are going to live, die, or divide [2, 44, 43] - , for advanced cases - by finding out if their evolution is affected by drugs or not [5] - , and finally, for complicated cases (*e.g.* with stem cells) - by anticipating if the cells are going to differentiate themselves and if so, into which cell type [21]. The approaches are based on feature extraction, usually done during the segmentation and tracking process. The features on which the prediction is based, depend of the type of modality, as they allow observing different processes characterising the cells behaviour. For example, on time lapse sequences, the cells movement is a key parameter to most of the existing process. Both the global movement, defined by the distance travelled by the cell from the beginning of the sequence, and the local movement, defined by the distance travelled by the cell between two time step, are monitored. The shape takes also an important role, usually observed through the eccentricity and the size of the cell. Fate prediction does not only apply to single cells, but also to tissue or structure formation, in which case, the time between division and the time taken for a division play an important role [102]. An important phase of learning is needed to train the process to recognise the different patterns in the features. Doing so, requires a consistent ground truth. Coupled with a tracking and tracing process, fate prediction becomes a powerful tool for studying cells [101].

2.3 Neurosphere tracking

Neurospheres are living objects in a moving environment. From the first neural stem cell to a large structure, the neurosphere will continually move in the dish. The movement is mostly the effect of cells movement in the suspension liquid, and also possible liquid current inside the dish, and the neurosphere would often go out of the field of view of the microscope. Therefore, the first important step in our study was to track the neurosphere in the time-lapse sequence. In order to do it, we use the $\Sigma - \Delta$ motion filter [65], a background estimator for motion detection. This estimator only uses time efficient operations that can be easily embedded for real-time applications. The use of a background estimator was decided over the observation that cells and neurospheres are living body in movement, in opposition with dead cells and dead neurospheres, which lose all motion.

The main idea of the algorithm, is to compare the image difference Δ_t, obtained by the subtraction between the current image I_t and a mean image I_m. The variance V of the sequence gives the temporal activity of every pixel in the image over time. The more a pixel changes its value, the more active it is considered. If a pixel has a higher Δ_t value than is current temporal activity, then it is likely to be part of the foreground as a moving object. This threshold discards small and regular movement in the background such as possible small dust. The strength of this method is its robustness to ghost and trace effects that can appear in the motion detection process. In order to eliminate these effects, a hybrid reconstruction (*HRec*), based on the so-called forgetting morphological operator erosion and dilatation [86], is applied on the gradient norm image of Δ_t and exponentially eliminates ghosts while it goes through the sequence. The overall process iterates over each new time step, updating the different value according to the new acquisitions as follow

M_t, V_t and I_t are respectively the mean image of the sequence, the variance image of the sequence and the current frame of the sequence at time t. M_0 is initialised at I_0 and V_0 at 1. α and N are the two only parameters to be defined. Morphological operations are used to fill possible holes in order to create binary masks of the detected objects. We increase the robustness of the process to consider possible miss-detections of neurospheres

Algorithm 1 $\Sigma - \Delta$ motion filter algorithm

loop
  $\Delta_t = M_t - I_t$
  if $|\Delta_t| \neq 0$ **then**
    $V_t = V_{t-1} + sgn(\ N \times |\Delta_t| - V_{t-1}\ )$
  end if
  $\Delta_t^{'} = HRec^{\alpha}_{\Delta_t}(\ Min(\ ||\nabla(\ I_t\ )||,\ ||\nabla(\ |\Delta_t|\ )||\ )\ )$
  if $\Delta_t^{'} < V_t$ **then**
    $D_t = 0$
  else
    $D_t = 1$
  end if
  $L_t = Rec^{D_t}(\ \varepsilon_{B_\lambda}(\ D_t\ )\ )$
  $M_t = M_{t-1} + sgn(\ \Delta_t - M_{t-1}\ )$
end loop

as possible detection of dust entering the field of view, by determining the compactness of the detected object in the images such as

$$C = \frac{4\ \pi\ A}{P^2} \tag{2.3}$$

where A is the surface and P the perimeter of the object. If the circularity is under the threshold, we can assume either a bad segmentation or that the observed cell is dividing. In our case, we assume a bad segmentation. The neurosphere will tend to compact spherical object and should have compactness close to 1, while dust and miss detection should have a value closer to 0.

2.4 Cell Detection in Neurosphere Cluster

The microscope observation contains two types of objects to detect and segment, each at different level: the neurosphere and the cells in the neurosphere. With the exception of dead cells or external cells, all the cells in which we are interested are part of the neurosphere, and it is the accumulation of those cells that form the neurosphere structure. Therefore, we aim to first detect and segment the neurosphere in the image, and then detect and segment the cells that are contained in the neurosphere. To do so, we first apply a restoration process on the image to remove unwanted artefacts contained into phase contrast images. Then, we use a Level Set method to segment and detect the neurosphere using the image

gradient, followed by a circle fitting detection method using the partial circles from the boundary of the neurosphere. Finally, we apply a post process to keep, reject or merge the detections.

2.4.1 Phase Contrast Restoration

Living cells can be imaged by several different image modality, DIC, phase contrast, confocal, *etc.* that impact on which methods that are used and how they are used. Even in the same modality, like phase contrast. In our case, the images vary in term of contrast, depending on positive or negative phase contrast, illumination, phase contrast artefacts, *etc.*. This brings several problems in term of robustness of the segmentation and the detection methods. Yin *et.al.* propose to overcome this aspect by presenting the phase contrast image as an image degraded by the phase contrast modality and by restoring the image using the phase contrast microscope physics. This restoration aim to create an artefact-free image, more appropriate for image processing.

A phase contrast image, that will be noted as g, is defined by the squared difference between the surround light wave l_s and the diffracted light wave l_s

$$g(x) \;=\; \| \; l_s(x) \;-\; l_d(x) \; \|^2 \tag{2.4}$$

where the surround light wave and the diffracted light wave are defined as

$$l_s(x) \;=\; i\theta_p A e^{i\beta} \tag{2.5a}$$

$$l_d(x) \;=\; i\theta_c A e^{i(\beta - f(x))} \;+\; (i\theta_p - 1)\theta_c A e^{i(\beta - f(x))} \;*\; \text{airy}(r) \tag{2.5b}$$

with θ_p and θ_c the amplitude attenuation factor of the phase ring and the specimen, A and β the illumination wave's amplitude and phase of the light, and airy(r) an obscure *Airy* pattern. From the equation 2.4, the phase contrast image g can be approximated by

$$g(x) \propto (\delta(r) - \text{airy}(r)) * f(x) + C \tag{2.6}$$

with C constant, δ Dirac function and f artefact-free image. We can see that the phase

contrast image is the result of the convolution of an unknown image with a convolution kernel which correspond to the Point Spread Function (PSF) of the microscope. The constant C corresponds to the objective lens imperfection that results in an non-uniform illumination.

The restoration of microscopy images was first proposed by Li *et.al.* [59] for DIC and phase contrast and more recently improved by Yin *et.al.* [109]. They proposed a linear model as

$$g \approx Hf + C \tag{2.7}$$

where H represents a symmetric sparse matrix, defined by the convolution between the PSF, discretised into a $(2M+1) \times (2M+1)$ kernel, and the artefact-free image, such as

$$(Hf)_j = \sum_{u}^{2M+1} \sum_{v}^{2M+1} PSF(u,v)\ f(x_j + u - M,\ y_j + v - M) \tag{2.8}$$

From this linear model, f can be approximated through an optimisation iterative process defined as a quadratic function

$$E(f) = \| Hf - g \|_2^2 + \lambda_s f^T L f + \lambda_r \| \Lambda f \|_1 \tag{2.9}$$

with L Laplacian matrix corresponding to similarity between spatial neighbours, Λ positive diagonal matrix associated to the sparseness regularisation, $\| \cdot \|_2$ and $\| \cdot \|_1$ respectively the l_2 and l_1-norm, and λ_r and λ_s weight factors.

The PSF used must be defined from the microscope such as

$$PSF(u,v) = \text{airy}(\sqrt{u^2+v^2}) - \delta(u,v) \tag{2.10}$$

The PSF is directly dependent of the *Airy* pattern function

$$\text{airy}(r) = R\frac{J_1(2\pi Rr}{r} - (R-W)\frac{J_1(2\pi(R-W)r)}{r} \tag{2.11}$$

with R and W the distance from the aperture and the aperture size of the objective, and

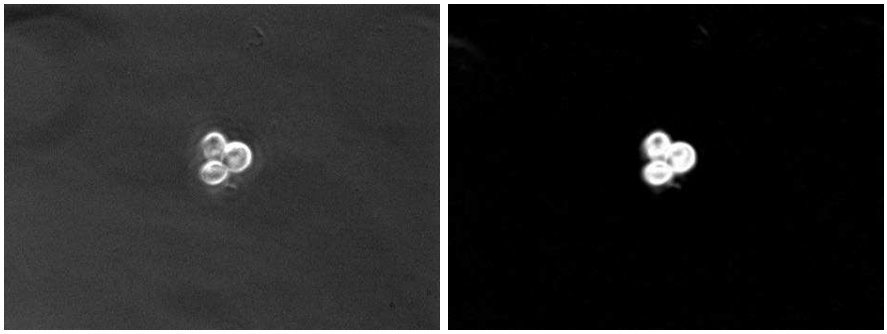

(a) (b)

Figure 2-2: Restoration results, before and after, on a ×40 two-cells neurosphere.

J_1 the Bessel function of the first order. In our case, as we have a particular type of images, where the cells are imaged in suspension in the cultured dish, this modifies the phase contrast artefacts. We are using the following $R = 8500\mu$m and $W = 1000\mu$m, directly extracted from our deployment. The cells observed are floating into the culture dish. Due to the suspension, the light effect (refraction, diffraction, *etc.*) is different for cells in fix culture. A perfect restoration of the cells would require the use of a three-dimensional PSF on a z-stack images, however such process would necessitate a higher number of acquisition which would lead to the death of our specimens.

The iterative process approximates the artefact-free image, converging to a dark background and light object image representation (Fig. 2-2). Thus, this approach alone is not enough in our case to extract the neurosphere, and only detects the cells present in it. This approach only proposes a new modality of observation of phase contrast image, and segmentation and detection process are still needed.

2.4.2 Partial Circle Detection

Once the neurosphere detected, we aim to detect the cells contained in it. This a challenging problem for two major reasons:

1. The cells are highly clustered and agglomerated.

2. The lack of contrast in the neurosphere allowing to detect the cells membrane in the neurosphere.

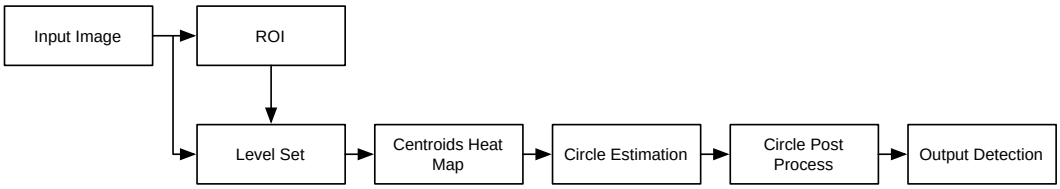

Figure 2-3: Clustered cells detection workflow process

Several methods exist for segmenting touching and clustered cells. Most of the approaches concentrate on segmenting the clusters, by then proceeding to a more precise segmentation of the cluster, using either active contours [75, 19, 110] or graph-cuts [23]. We decided to base or approach on curvature point of the cluster (*i.e.* how the border of the cluster is curved to determined the position of cells). However, the curvature point association method, which works well for simple agglomerates of two or three cells, is failing due to the high number of curvature points and their configuration in sphere. The active contour approach does not have better results as it is based on the intensity information contained into the clustered cells and the distance between the seeds. The cells do not have a clear separation between themselves, nor a clear visible nuclei, to define correct seed points.

Based on ellipse fitting approach for segmenting simple cluster cells [48], we propose to segment the cells contained into the neurosphere, using a circle fitting process. Circles, which will model the cells, are positioned using the external edge of the neurosphere (fig. 2-4b), and will, as they are positioned, create false edge that can be used to place new circles (Fig. 2-4c). The iteration process continues until no circle can be added (Fig. 2-4d), as the area of the neurosphere will be covered. First, we define a ROI around the the neurosphere and, using the ROI as initialisation state, we extract the boundaries of the neurosphere using a geodesic Level Set algorithm. Second, we define the center of the cells using a partial circle detection process based on the *Hough* transform [107]. Finally, each candidate cell position are kept, mixed or discard following a set of rules on their distance and size (Fig. 2-3)

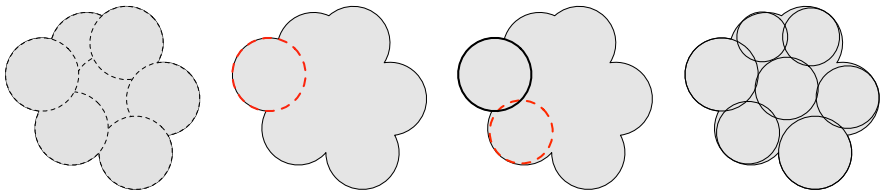

(a) (b) (c) (d)

Figure 2-4: Circle fitting iterative process. a) Initial cluster of cell with the dashed line as ground truth. b) Positioning circle using the boundary of the neurosphere. c) Positioned circle boundary are used for position other circle. d) Final results expected.

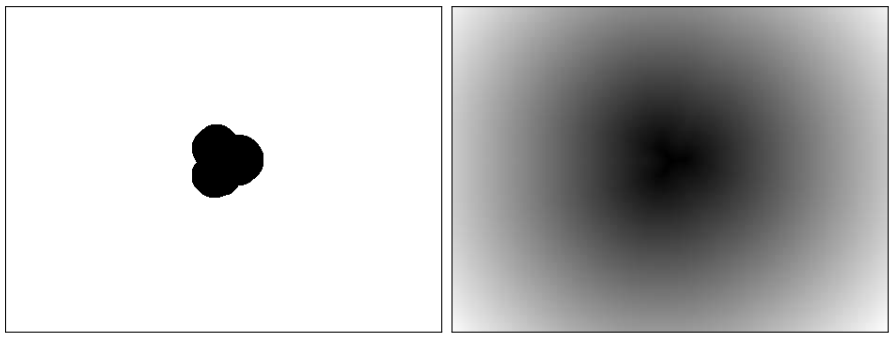

(a) (b)

Figure 2-5: Initialisation of the level set. (a) Extraction of a ROI which will be the initialisation curve of the level set. (b) Calculation of a distance map that will guide the convergence of the level set.

Region of Interest

The ROI is determined by an intensity based approach. *Otsu*'s threshold [77] is applied to create a binary mask which is then morphologically dilated using an important structural element (Fig. 2-5a). The size of this structuring element does not have a direct importance on the process, however, if too big, it may slow it down, by creating a too important ROI. If this element is too small, it can deteriorate the results, by not properly enclosing the neurosphere. In our case, the structural element is a circle element of radius $r = 10$ pixels, a size satisfying these constraints.

Neurosphere Boundary Extraction

The boundary of the neurosphere is extracted using a Level Set method [17] that will follow the gradient of the image, defined along a parametric planar curve $\Theta(p) \ : \ [0,1]$ in $\Re^2$,

such as the energy associate to Θ is

$$E(\Theta) \;=\; \alpha \int_0^1 \|\Theta'(p)\|^2 dp \;+\; \beta \int_0^1 g(\Theta(p))dp \tag{2.12}$$

with α and β non negative weight, ∇ the gradient norm operator, and g the external energy function given by the position of the Θ over the image, in this case, $g = \frac{1}{\|\nabla I\|}$ in order for the level set to converge to the edges present in the image. The first integral corresponds to the internal energy associated to the curve shape and stiffness and the second to the external energy associated to the image. Minimising equation 2.12 is equivalent to solving the following

$$E(\Theta) \;=\; \int_0^L \frac{1}{\|\nabla I(\Theta(s))\|} ds \tag{2.13}$$

where L the length of the parametric curve Θ parametrised by a set of points s. This approach will give, at each point of the curve, an energy value corresponding to the inverse of the edge norm of the image, and will try to minimise the sum of these values. Minimising the equation 2.13 will correspond to determining the smallest curve that follow the norm of the gradient of the image I.

The Level Set algorithm takes two inputs, a curve initialisation that will define the Level Set at its initial state E_0, and a gradient based feature image $g(\|\nabla I\|)$. The first input is defined by the ROI, from which an euclidean distance map from the edge of the ROI to its center of mass is calculated (Fig. 2-5b). It will provide to the Level Set the initial parametric curve associated with the energy E_0 and the direction of evolution of the curve, mainly if the curve is going to evolve outward or inward in our case. The edge-based feature image is directly calculated from the original image. An Anisotropic Smoothing filter [78] is applied to remove any noise contained in the image and to enhance the gradient of the image (Fig. 2-6a). This will be followed by an inverse gradient norm detection filter (Fig. 2-6b). However, the gradient norm may not be very contrasted in some cases. It is then advised to enhance the contrast through a sigmoid filter

$$f(x) \;=\; \min \;+\; \frac{\max - \min}{1 + \exp^{\frac{\beta - x}{\alpha}}} \tag{2.14}$$

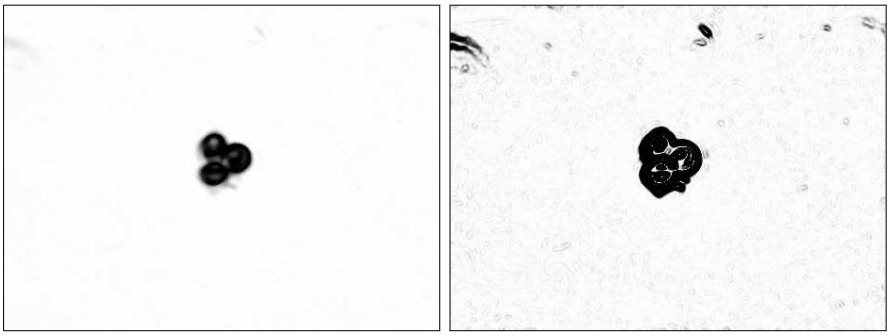

(a) (b)

Figure 2-6: Gradient information extracted from the image for the level set. (a) Anysotropic denoising filter. (b) Sigmoid gradient filter.

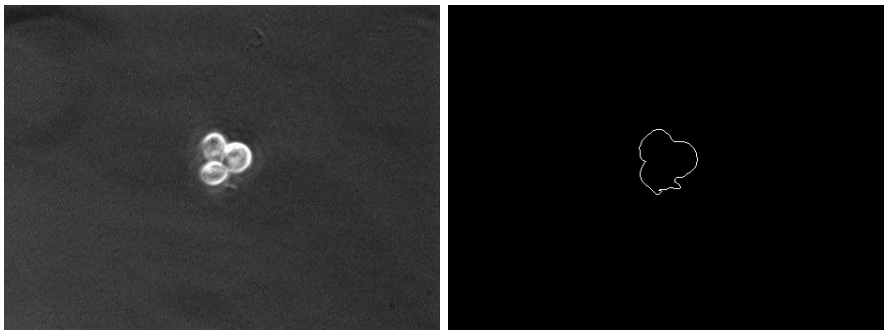

(a) (b)

Figure 2-7: Level set detection of the neurosphere.

that will map all the pixel values $x \in [\beta - \alpha \ : \ \beta + \alpha]$ respectively to the min and themax values of the image, isolating the pixels with intensity included in $[\beta - \alpha \ : \ \beta + \alpha]$ from the rest of the image. The edge-based feature image should have high value at low gradient area and low value at high gradient area of the image, and the pixel value will provide the evolution speed of the curve at each point. At each update step, the initial curve will follow the direction given by the distance map at a speed defined by the value of the edge-based feature image. When the curve arrives to a boundary, the edge-based feature value should be close or equal to zero, stopping the curve evolution. (Fig. 2-7b)

Candidate Circle Fitting

From the converged Level Set, we obtain a closed boundary, used to detect the cells present in the cluster. From the closed boundary, we want to find the circular included segments,

and to determine their corresponding centres which should provide us a map of possible positions of the cells. The circles defined by the cells are not complete and only partially visible, thus we perform a detection of the visible segments.

We based our approach on the *Hough* transform [11, 46] method for shape detection, in our case, circular, with search in the (a,b,R) space (Fig. 2-8). From each edge point $p = (x, y)$ - boundary point - we define in the (a, b) space a voting line orthogonal to the edge as

$$a = r\cos\theta \tag{2.15a}$$

$$b = r\sin\theta \tag{2.15b}$$

with $r \in \{r_{min}, r_{max}\}$, and θ the gradient orientation

$$\theta = \arctan\left(\frac{\partial I_y}{\partial I_x}\right) \tag{2.16}$$

Each line acts as a vote for its corresponding edge point and the accumulation of votes gives us potential position for cells. In other words, each point of the boundary is going to vote for a possible position of a cell, creating a heat map of possible position of cells in the image. Once applied to our data, we could observe that the boundaries of the cells are not be perfectly circular and the voting lines do not perfectly converge on a specific point. They are more likely to produce blobs with different size and intensity, depending on how regular and circular the boundaries are. To overcome this, the heat map is convolved with the negative normalised second derivative of a Gaussian function, also called a *Mexican Hat* function (Fig. 2-9c), defined

$$\phi(t) = \frac{2}{\sqrt{3\sigma}\pi^{\frac{1}{4}}}\left(1 - \frac{t^2}{\sigma^2}\right)\exp^{\frac{-t^2}{2\sigma^2}} \tag{2.17}$$

with σ, the variance of the Gaussian. The convolution will enhance the peaks, by detecting the different local maxima, in order to determine a set of position for cells (Fig. 2-9b).

The final step corresponds to determine, for each local maxima detected in the *(a,b)*

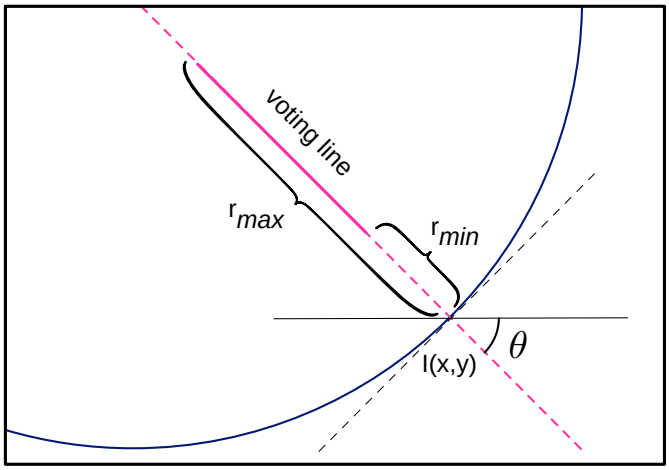

Figure 2-8: Centroid detection voting graph in the (a, b, R) space. From the point $I(x, y)$, a voting line is trace with an orientation of θ and a length $r = \{r_{min}, r_{max}\}$.

space, the best radius. This is done by accumulating the number of boundary pixel associated to a radius. For every radius $r \in \{r_{min}, r_{mqx}\}$, we sum the edge pixel on the circle defined by r. The best r^* is therefore given by

$$r^* = \arg\max_r \sum_{p \in circle(r)} edge(p) \quad \text{with} \quad edge(p) = \begin{cases} 1 & \text{if p is an edge} \\ 0 & \text{elsewise} \end{cases} \tag{2.18}$$

Circle Selection

The partial circle fitting process identifies the circular structures present in the image, but they do not all correspond to a cell. Some may correspond to the concave shape of the neurosphere leading to a detection outside of the neurosphere, other can multiple detected circle corresponding to the same cells. We have an over-detection of circular shape in the image and we need to eliminate these not corresponding to cells. We first do a primary selection through the radius range of the circles, between r_{min} and r_{max}, and the intensity of the detected centroid. The two parameters are defined by the biologist or, in the case of the radius range, determined by the size of the cells detected at the beginning of the experiment, during the single cell state of the neurosphere and, in the case of the centroids intensity, a threshold defined by the user and the previous cell detection, if available. Then, we test the position of the centroid, if they are located inside or outside of the neurosphere

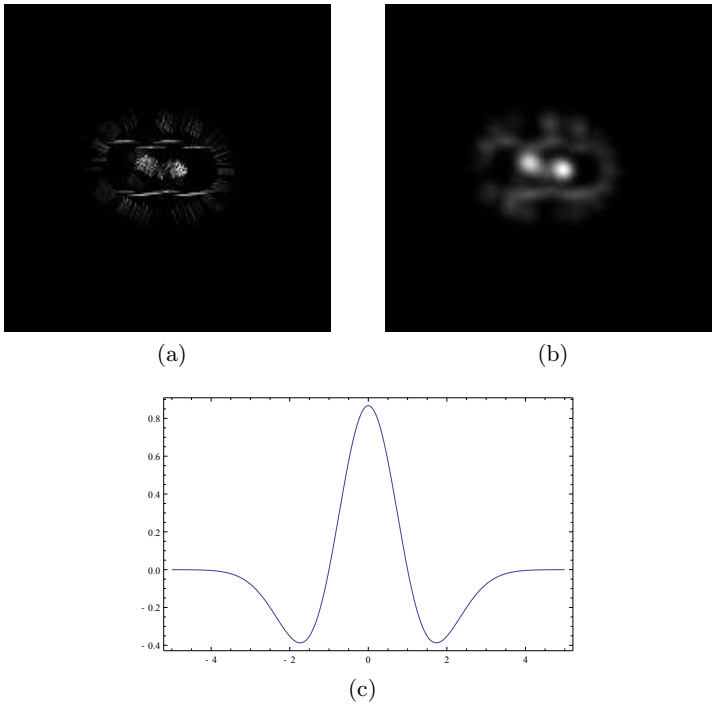

Figure 2-9: Convolution of the voting map with a 2-dimensional Mexican Hat function to concentrate the vote in peaks and remove low local maxima.

detected previously, using a binary mask of the neurosphere area. Finally we test the overlapping and the content of the different circles. If a circle is included inside another circle or if two circles overlap, we merge the two. We allow a minimum overlapping, as the boundaries of the cells are not always clear.

2.5 Results and Analysis

2.5.1 Neurosphere Tracking

In the first data set, the neurosphere formation is observed over five days and the microscope does not track them. In the different sequences, we can observe that during their proliferation, the cells start to move in the culture dish, requiring the biologist to move the microscope stage in order to keep the cells in the field of observation of the microscope.

We have tested the process on this data set to determine in real time the position of the neurosphere and discard non-neurosphere objects from the data. The overall process

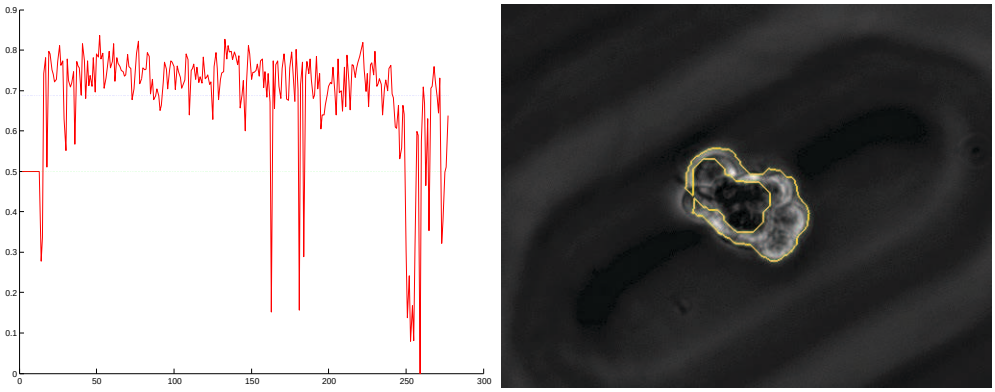

(a) (b)

Figure 2-10: (a) The overall circularity over a time lapse sequence. The value fluctuate between 0.65 and 0.85 with a mean at 0.7. Misdetections due to moving dust or low movement can be observed where the circularity value drops drastically. (b) A visualisation of the misdetection, corresponding to the most important pikes between frame 150 and 200 in the circularity graph (a)

provides good results, except during particular behaviour of the neursophere. Indeed, once the neurosphere reaches a certain size, it happens that it slows down or even stops moving considerably for a certain time. This possibly leads to a misdetection as our process will start to include the neurosphere into the background as a dust or dead cells (Fig. 2-10).

2.5.2 Cell Detection

We tested our method on a large data set which merge the *Training* data set and *Test* data set, that contain early neurosphere with various configuration of cells observed under different microscope.

The evaluation of the method was done by comparing four value: True Positive (TP), False Positive (FP), True Negative (TN) and False Negative (FN). The following are define as

TP a correct identification, in our case a cell correctly detected.

FN an incorrect rejection, in our case a cell that was not detected.

FP a incorrect identification, in our case, a detection that does not correspond to a cell.

TN a correctly rejected, which there is no equivalent in our case.

In order to evaluate our method, we used the *precision-recall* approach [24] as

$$\text{precision} \;=\; \frac{TP}{TP+FP} \quad \text{recall} \;=\; \frac{TP}{TP+FN} \tag{2.19}$$

from which it is common to determine the F-measure

$$F \;=\; 2 \cdot \frac{\text{precison} \cdot \text{recall}}{\text{precison} + \text{recall}} \tag{2.20}$$

The Receiver Operating Characteristic (ROC) [24] approach, which would usually be used to evaluate methods for binary detection process such as ours, was not used as it consists in comparing the ratio of TP over FN. However, in our case, we do not know how to define what is a TN.

The data set for the evaluation was composed of 20 time lapse sequences each of 135 images containing from 1 to 5 cells that survived until the end of the experiment. We removed from the test the five sequences (sequence 6, 7, 10, 12 and 17) as they contain an abnormal density of dust and particle that disturb behaviour of the experiment and would bias the evaluation of our detection and segmentation methods (Fig 2-11a). The other sequences may still contain a few particle or dust but they remain limited or temporary in the sequence.

We have calculated, the *precision-recall* and the F-measure (Tab. 2.1) for each sequence of the data set and for the totality of the sets (Tab. 2.2). Overall, our method gives good results, both in term of precision and recall, with respectively ~ 0.88 and ~ 0.91, and a F-measure close to ~ 0.9. If we look at each sequence however, we can observe that three sequences distinct themselves from the rest: sequence 5, 14 and 15. The sequence 5 has a very bad results, with a F-measure under 0.6, much lower than the rest of the sequences. The sequence 15 and 14, on the contrary, have perfect results, with a F-measure of 1. These results can be explained by the particularity of the corresponding sequences. The sequence 14 and 15 only contain each one late division, which makes the sequences containing only one cell in most of the images, without cell cluster. The sequence 5 contain a dust in

some part of the sequence, which is misdetected as a cell, lowering the result of the whole sequence. We recalculated the F-score without the sequence 14 and 15, but keeping the sequence 5, in order to have a more honest results on the accuracy of the method. Without those two results, we can observe a lower F-score of 0.88, which still remains a good results.

We can observe different results of the detection process on different size neurospheres from the *Training* data set (Fig. 2-12) and *Test* data set. In both data set the detection works on single cells and small cluster of 2 cells (Fig. 2-12a) or 3 cells (Fig. 2-12b, 2-13a), but also worked quite well on a bit more complicated cluster of 4 (Fig. 2-12c, 2-12d, 2-13b) and 5 cells (Fig. 2-13c, 2-13d).

As we have seen, the method proposed provides us with good detection on our different data. However, the process has some drawbacks in is current state.

It is sensible to the presence of external object as we assume that the sequence only contains cells and all the different external objects have been removed or detected as external. A learning and classification process applied on the detection results could lower false positives found due to over-detection.

The shape of the cells during the detection is also an important variable in the method. We assumed that the cells are spherical due to the particularity of the experiment, *i.e.* floating cell culture. This hypothesis is not always correct as the cells may actually change form when they move in the solution, losing their spherical towards an ellipsoid shape (Fig. 2-11b) Finally, the approach is limited by the observation modality itself, in our case, phase-contrast microscopy, as it only acquire two-dimensional images of the neurospheres, that are three-dimensional structures. Some cells may not be visible as they are behind other cells or out of focus of the microscope. The proposed method detects the visible cells of the neurosphere but do not allow a full three-dimensional detection of the cells present in the neurosphere. Such detection would need to have multiple views of the structure either by rotating it, using proximal two-beam optical tweezers [52, 53] or by multiplying the number of observation angles. Those two solutions were not explored, as they would

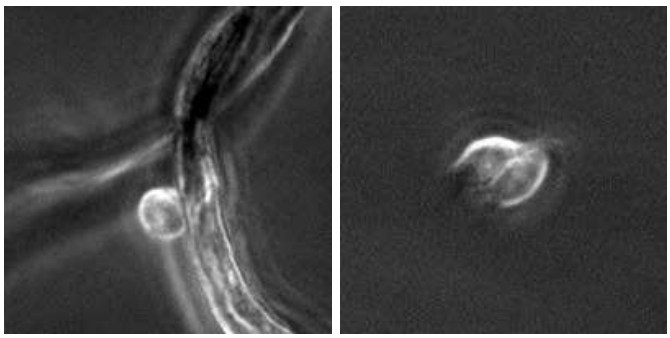

(a) (b)

Figure 2-11: (a) External object (dust) disturbing the proliferation of the cells. (b) Cell deformation due to movement during the observation.

Sequence	1	2	3	4	5	8	9	11
Precision	0.925	0.929	0.875	0.978	0.574	0.744	0.897	0.950
Recall	1.000	0.956	0.931	0.983	0.576	0.947	0.913	0.936
F-measure	0.961	0.943	0.902	0.980	0.575	0.833	0.906	0.943

Sequence	13	14	15	16	18	19	20	
Precision	0.991	1.000	1.000	0.876	0.835	0.871	0.968	
Recall	0.809	1.000	1.000	0.972	0.929	1.000	0.876	
F-measure	0.891	1.000	1.000	0.922	0.879	0.931	0.919	

Table 2.1: *Precision-Recall* and F-measure.

highly increase the complexity of an already complex structure and experiment.

2.6 Conclusion

We propose a method to extract the number, size and position of cells in dense clusters. Through a validation on our data, we shown that the method was quite efficient, both in terms of results and cost. An extension to ellipsoid shape could allow the process to be more easily applied to different type of data or problematic. The information extracted from the detection, with the shape and texture information are then sent to both the synthesis and the selection module. However, the module can be improved with new methods, able to enhance the information extraction from the image.

	Precision	Recall	F-measure
with 14 and 15	0.884	0.906	0.895
without 14 and 15	0.874	0.898	0.886

Table 2.2: Global *Precision-Recall* and F-measure.

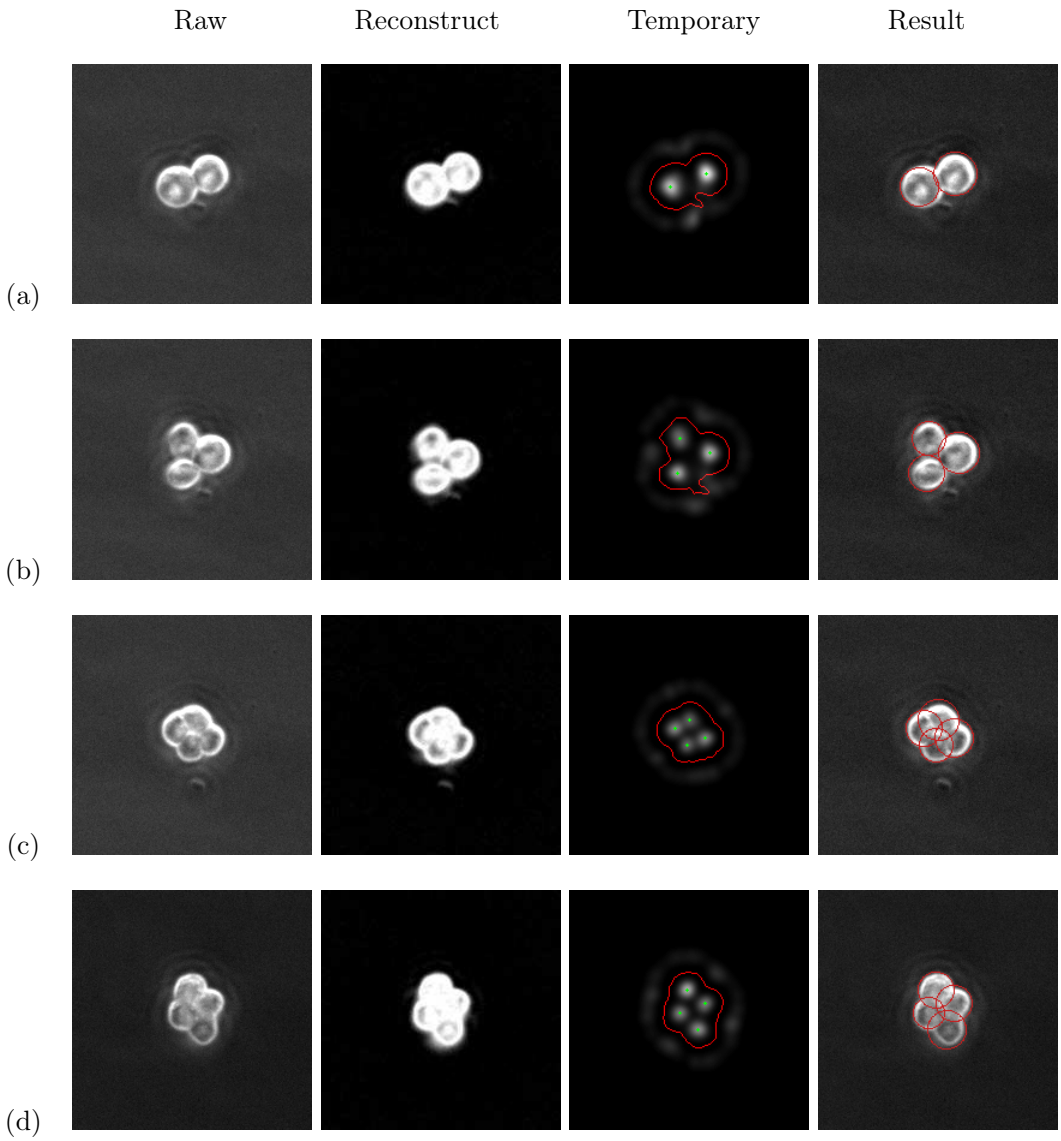

Figure 2-12: Results and temporary steps of the cell detection method on different neurosphere stages, from the *Training* data set. Left column, the raw observation from the microscope. Middle column, the temporary results of the neurosphere detection and centroids position. Right column, the final results of the cell detection.

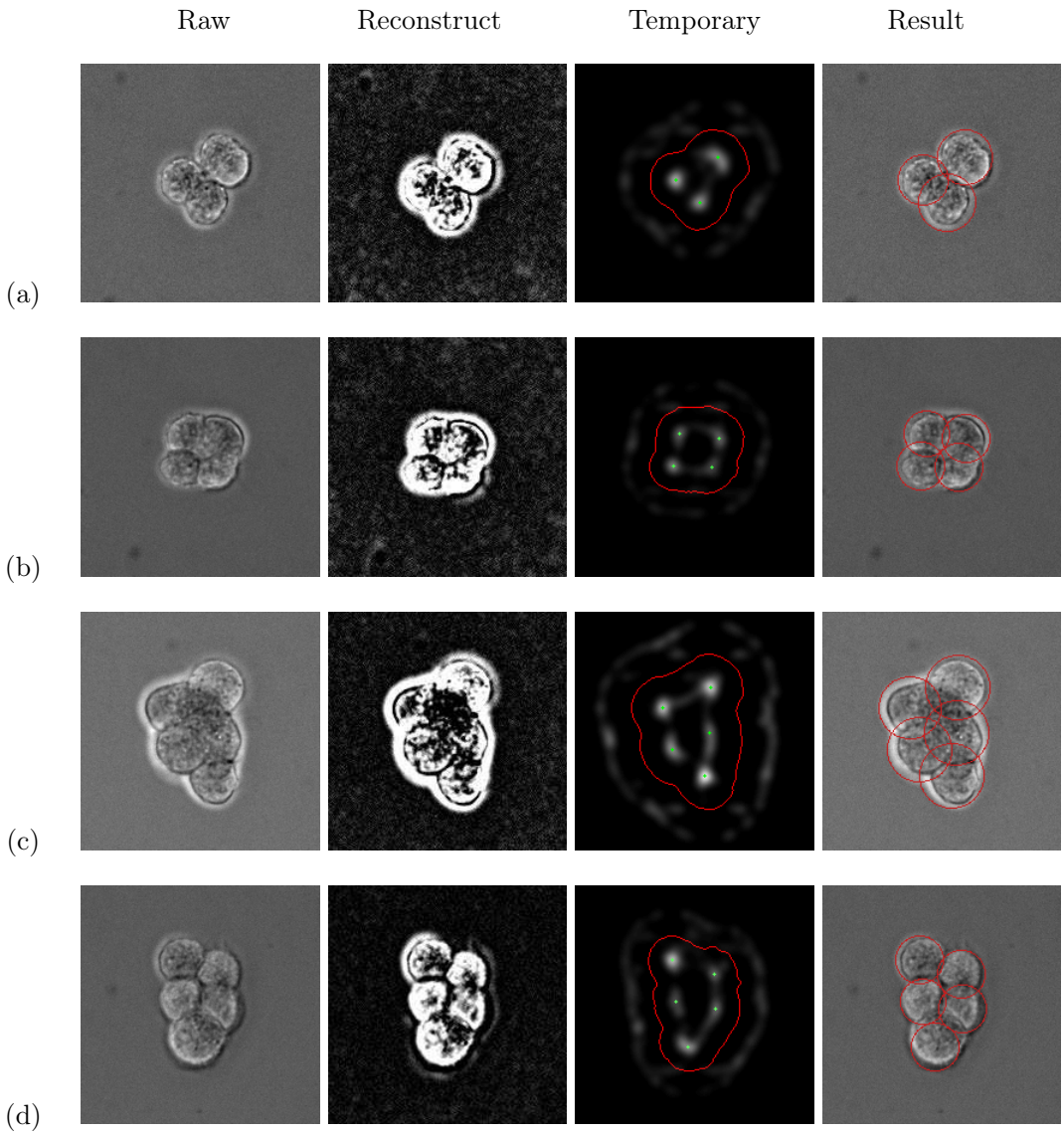

Figure 2-13: Results and temporary step of the cell detection method on different neurosphere stage from the *Test* data set. Left column, the raw observation from the microscope. Middle column, the temporary results of the neurosphere detection and centroids position. Right column, the final results of the cell detection.

Chapter 3

Synthesis:

Neurosphere Model Generation

3.1 Introduction

In the overall framework proposed in our study, the synthesis naturally follows the analysis. The synthesis module will generate a set of models, using information provided by the analysis module, with respect to the *prior* knowledge predefined by the biologist on neurosphere and neural stem cells. It is too difficult to define the exact model, as many solutions are possible starting form the 2D analysis results. Therefore, multiple models are generated, in order to cover the solution space, limited by the *prior* knowledge and the analysis module information.
First, we will list and explain the different *prior* knowledge information used in the module. Then, we will describe the model generation methods. As multiple methods are possible for the model generation, two methods respectively based on evolution algorithm and on Delaunay triangulation, are proposed and implemented.

3.2 Using Biological *Prior* Knowledge

Different types of model exist. The mostly used are mathematical models describing or simulating a process or event. This was, for example, used for cancer cell cycle analysis [13], or applied to plant growth and development [81]. We inspired our process from models used in medical imaging, that were proven effective in matching and tracking anatomic structures by exploiting constrains from the image mixed with *prior* knowledge about the shape, size and localisation of the structure [69]. Such models, usually deformable, are widely used in assisted surgery approach.

We extract data from the microscope information and from *prior* knowledge, in order to define a deformable model, giving use the size, shape and configuration of the object to be observed. A particularity of our method is the definition of the model using a *structural composition* approach. Therefore, we define cells as building blocks that will give shape and structure to the model [80]. *Prior* knowledge about the biology and the physics of the neurosphere, induces the definition of rules that will guide the synthesis of our model.

We classified this knowledge in three relevant clusters: appearance, configuration and proliferation;

Appearance The phase contrast modality renders cells with a visible grey level variation, from high intensity on cells membrane to low intensity in the centre of the cells. We can use that intensity effect as a texture configuration, specific to each cell, in order to improve their localisation. Also, the mitotic process interferes with the cell's organelles density and disposition, in particular DNA, and should impact on the phase contrast observation, making the global cell intensity change, usually increase and saturate, until the cell division.

Configuration We know that a cell division forms two new cells from a unique parent cell. Those two new cells will be neighbours and stay in contact. Also, as all division occur in the neurosphere, all new cells will necessary appear in contact with already existing cell, and all neighbour of a cell shall be a close parent to this one. Furthermore, cell membrane is composed of extrinsic protein in charge of the cell interaction with neighbour cells and creates links between cells membranes. Combined with tension applied on the boundaries of deformable object such as neurosphere, the overall structure will keep all the cells connected to each other and tend to a sphere shape. The only exception is when a cell dies, as the remains of the cell will detached itself from the structure.

Proliferation A cell can either deform and move, divide into two new cells, or die. In our case, deformation and movement are defined by the neurosphere itself and not any more by the cell. If no division nor death are determined, new detection are due to cells entering or leaving the field of view. In the context of our study, this may apply if the neursophere rotate on itself, occluding some of the cells. A cell reaches its mitosis phase after a $24 \sim 30$ hours cycle. If a cell does not divide, then it will most likely die.

Most of the current proposed rules concern: cells rendering under phase-contrast microscopy, which provide information on the type of material encountered by the phase light and can possibly provide information about overlapping objects; cell life cycle, providing information on division frequency and mechanism; and neurospheres global shape. These observations are used in both the generation of the model, limiting the space of possibilities for the model generator, and in the elaboration of an evaluation function for providing a score to the model during the selection process.

3.2.1 Structural and Topological Constrains

By definition, a neurosphere is a spherical agglomeration of neural stem and progenitor cells. As there is no visible difference between neural stem cells and neural progenitor cells, we simplify the structure as an agglomerate of similar cells of the same size and properties.

A cell floating in a liquid, like nutritious water, will have a spherical shape as the membrane will take the most compact structure, due to the tension forces at its surface (Fig. 3-2a). A similar behaviour can be observed in daily life with soap bubble, that is a volume of air surrounded by a wall of water with the relation

$$P_i - P_o = \frac{4T}{r} \tag{3.1}$$

with P_i and P_o respectively the pressure inside and outside the cell, T the tension at the surface and r the radius of the cell. The same observation apply to neurospheres which constitutes an agglomeration of cells [50] (Fig. 3-2b). Each cell in the neurosphere will have its internal pressure, that will be opposed with the external pressure of the dish solution and create a tension surface. The force tension at the surface of the neurosphere, as the necessity of the structure to optimise its contact with the environment that contains nutriment, will make the neurosphere converge to a sphere. At equilibrium, the agglomerate has a uniformly curved shape that is directly dependent to the surface tension and the inside pressure. The relation between the pressure applied to the agglomerate and its deformation is given by the Laplace relation as

$$\Pi = 2\sigma r\| = \sigma \left(\frac{1}{R_1} + \frac{1}{R_2} \right) \tag{3.2}$$

where Π is the pressure, σ the surface tension, $\|$ the curvature, R_1 and R_2 are the radii of curvature of the agglomerate. If no specific pressure is applied to the agglomerate, it tends to a perfect sphere.

Cells are deformable objects by nature and, even if they tend to keep a spherical shape while in suspension, they are deformed at the contact of other cells, creating a visual

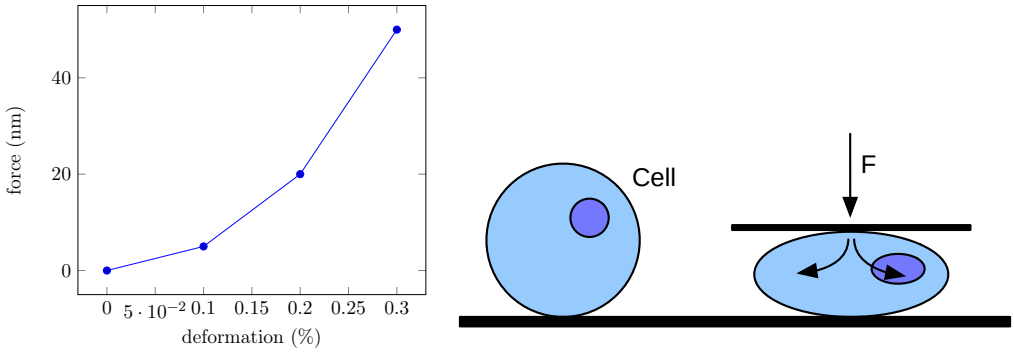

(a) (b)

Figure 3-1: Cell maximum deformation. (a) A cell can support a maximum of 30% of deformation. (b) The deformation is similar to a balloon filled of incompressible fluid.

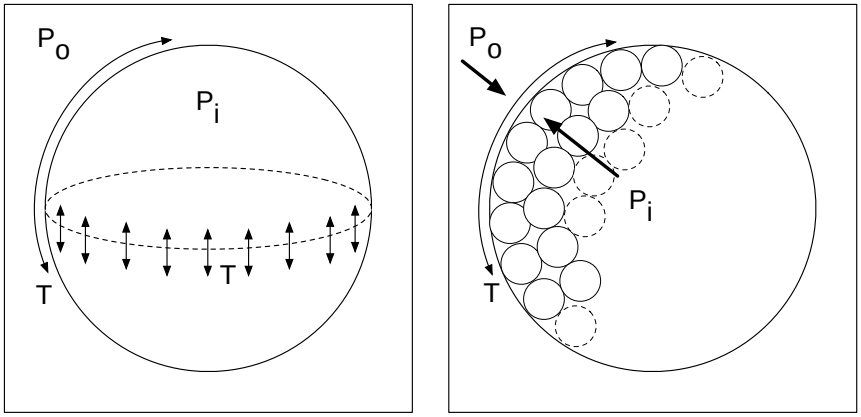

(a) (b)

Figure 3-2: Relation between surface tension T and the pressures P. (a) Tension T at the surface of a bubble directly in relation with the internal pressure P_i and the external pressure P_o. (b) Same observation applied on a collection of bubbles.

impression of overlapping. Studies have shown that cells are actually not compressible, but are deformable. They behave like balloons filled with incompressible fluid, and will be able to support a certain deformation to a limit of 30% and come back to their original shape [62, 60] (Fig. 3-1). Pass this limit, the membrane will not be impermeable any more and the cell content will start to leak, damaging the cell and preventing it to return to its original form.

3.2.2 Neurosphere Proliferation Speed

How many cells compose the neurosphere at each time of the proliferation process, is an important question, both for a better understanding of the neurosphere formation process and also to generate the model. We can deduce the number of cells present in a neurosphere from several information: the age of the neurosphere, the size of the neurosphere and the visible cells of the neurosphere.

From observation, we know that neural stem cells and neural progenitor cells finish their cycle and divide in a time fork between 24 to 30 hours (Fig. 3-4). Before this time, cells are unlikely to divide, and past this time, if the cell did not divide, it is likely to die. Based on a normal distribution, we can determine probabilistic law for the cell to divide, providing at each time how many cells are in the neurosphere (Fig. 3-3).

As we know, cells are deformable but cannot be compressible. Therefore, is should be a direct relation between the size of the neurosphere and the number of cells that it contains. An empirical experimentation was done where the number of cells contained in neurosphere was determined at different of time of development (Fig. 3-5). We can observe an exponential relation, between x the size of the neurosphere and y the number of cells contained in the neurosphere, given by

$$y = \alpha \exp^{(\beta x)} \tag{3.3}$$

with the constants $\alpha = 0.473$ and $\beta = 0.0972$. However, the size of a neurosphere varies depending on the measure, as even if the structure tend to a sphere, it may be ellipsoidal depending on it stage of maturity. In this case, the longest axe was used to determine the size.

Our last information on how many cells are present in a neurosphere is extracted from the cell detection and segmentation process, and detection results from the previous acquisition time. This method only provides the number of visible cells, as a reference number, from which we can estimate, through the size and age of the neurosphere, how

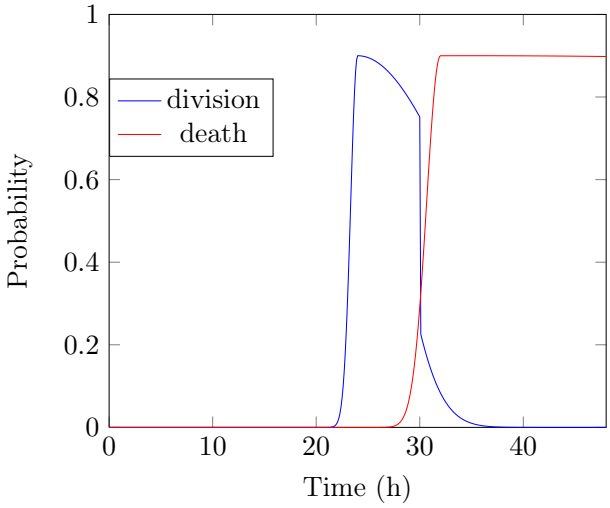

Figure 3-3: Plot of the probability of division and death over time of a cell.

many cells are present.

3.2.3 Phase Contrast Halo Artefact

As discussed previously, the phase contrast modality displays the cells with some particular texture artefacts. The most well known is the halo effect. It gives the observed cells a specific representation, which we are using to improve the positioning of cells located in the middle of the cluster or on a different layer. Under the microscope, the cells will be represented by two concentric circle of intensity that can be model by a mixture of inverted Gaussian functions. The difference of the intensity is due to the density of the material that the phase encounters. The membrane of the cell and nuclei is normally denser than the rest of the cell. The orientation of the phase touching the limit between the cell and the outside, also affects the output signal of the observation. Such information will not be used during the model generation, it will however be incorporated in the model during the projection process (see section 4.3.2) and will play a role in the ranking of the different models.

3.3 Random Sphere Approach

We first tried to determine the cell configuration with a random generation of structure. In the model space $\mathbb{M} \mapsto \mathcal{R}^3$, we define a neurosphere configuration N composed of a set

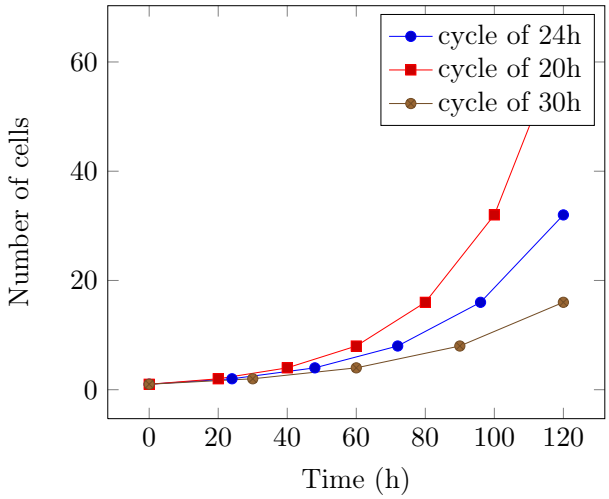

Figure 3-4: Plot of evolution of the number of cells in neurosphere over time, in the case that all the cell cycle where identical and synchronised.

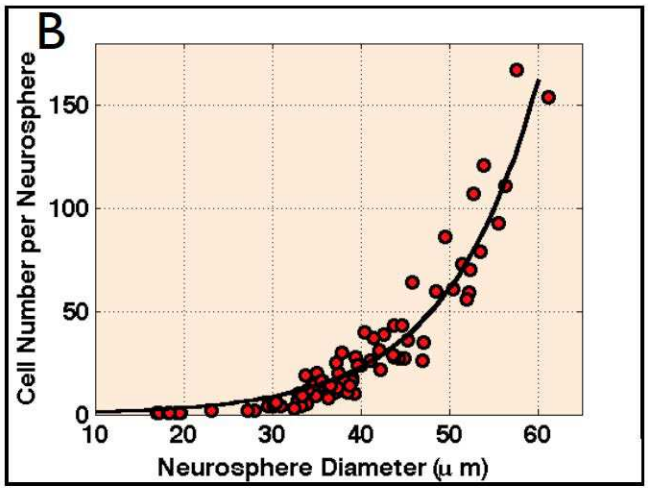

Figure 3-5: Plot of number of cells in a neurosphere at different time of the NFA experiment over their diameters (μm). Courtesy of Institute of Molecular and Cell Biology.

of cells $S = \{s_0, s_1, ..., s_n\}$. Each cells s_i is characterised by a radius r_{s_i} and a position $c_{s_i} \in \mathbb{M}$. An important number of random neurosphere configurations are generated in order to cover the entire possible configuration. In the totality of the configuration generated this way, one or more will fit to our observation. However, the space of possible configuration is too important and has to be narrowed. A set of restrictions were defined into the random process to limit the number of output to only possible solutions.

First, to prevent the sphere to be scattered, the space M, containing the sphere, is defined as a sphere itself of a radius

$$R = Nr - \frac{\mu}{2} \tag{3.4}$$

with μ the maximum deformation coefficient. This will prevent the sphere to disperse into in-compact structure while leaving enough space for various configurations. Second, to prevent full overlapping, two cells cannot overlap up to a threshold. We use the deformation coefficient μ to determine the threshold, for two sphere A and B, as

$$A \cap B \leqslant 2\pi\mu r^2 \tag{3.5}$$

Finally, a cell must always be touching another cell, as isolated cell is not compatible with a neurosphere configuration.

3.4 Evolution Algorithm Approach

The last approach was done by using evolution algorithm, which can be defined as search and optimisation algorithm based on the Darwin principle of evolution. Such algorithm is built following a generic construction (Fig. 3-6) that consists in generating an initial population of individuals, assignment of a score according to a defined fitness function, and finally generating a population of offspring using the current population, by applying mating operations and mutation operations. The mating operations are the creation of an offspring using two individuals and the mutation is creating an offspring from the deformation of one individual. The offspring population created then replaces the current

population in the iteration and is evaluated using the fitness function. The process loops and proceeds until a termination criterion is reached, such as for the most common cases, an individual reaching a score below a threshold, the mean score of the population below a threshold or simply a maximum iteration of the whole process.

The first step consists in defining a population P of individual. We use the same approach as for the random model, and define a neurosphere $p \in P$ as a set of N spheres such as $p = \{s_1, s_2, ..., s_n\}$ and each sphere is defined as $s = \{c, r\}$ where c and r are respectively the coordinate of the centre and the radius of the sphere. The fitness function f used to score and rank each individual is based on three values: The projected shape formed by the model once projected into the microscope observation space; the texture associated to the model and how well it fits to the microscope observation; and how well the model fits *prior* knowledge defined as generation rules, such as distance between cells for example. The function f can be defined such as

$$f(x) \; = \; \omega_1 E_{shape}(x) \; + \; \omega_2 E_{texture(x)} \; + \; \omega_3 E_{violation}(x) \tag{3.6}$$

with x an individual to be rated. The violation value is a penalty that increases when the individual does not fit the *prior* knowledge rules identified in section 3.2. More information on the shape and texture evaluation can be found in section 4.3. The evaluation function will provide an individual with a score, determining how good is the individual. The algorithm will then use those scores to define good and bad individual for the next iteration, making the population converge to a better solution.

From the initial population, the evolution algorithm will proceed to a search in the solution space. The mutation and mating operations are here to modify and evolve the current population, which represent the solution, toward a better solution.

3.4.1 Selection Operation

The selection operation is the first step in generating the offspring population by selecting one or two individual, depending of the purpose of the selection, to be given to the mating

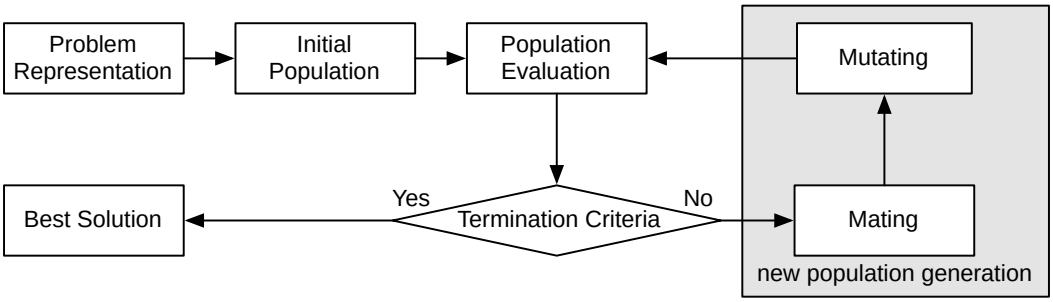

Figure 3-6: Generic process of evolution algorithm. An initial population is created and evaluated. Using this population, a new population is created using mutating and mating process to mimic an evolution process. The process loop until a population meet the termination criteria.

and the mutation operation that will follow. The selection process is independent from the individual representation, on the contrary of the mating and the mutation parts, but only depends on its score. We tried two approaches, the *stochastic sampling* and the *tournament selection*, both already existing and proven for selecting individual. The stochastic sampling is a probabilistic selection approach. Each individual has a certain probability to be selected according to its current score. The better the score is, the more chances the individual has to be selected. For the tournament selection approach, we randomly take n individuals and oppose them. The individual with the best fitness score at the end, is selected. For our application, we tested both approaches and have selected the tournament method.

3.4.2 Mutation Operation

The mutation operation is also to be defined according of the representation of an individual, and consists in modifying the selected individual to create a different one. It is associated to a mutation rate, a probability that an individual mutates, to be defined by the user or parametrised by some tests. In genetic algorithm, a simple and common mutation process would be the modification of coding bit of the gene. This modification could be a random change of value or also a swap between two bits. In our case, a good mutation would be the application of a transformation to the individual to form a different individual. The first option is a global mutation that modifies the entire individual using a minor mutation. For an individual of n cells, a random small translation t is applied to

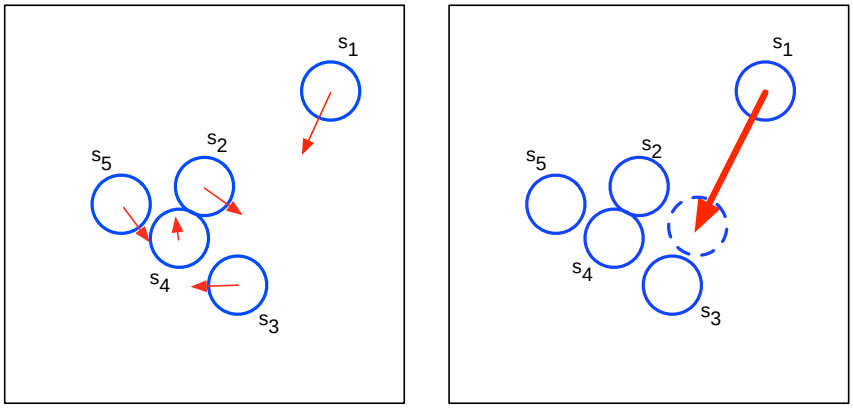

(a) (b)

Figure 3-7: Global or local mutation applied to an individual (a) A global mutation, small translation applied to each cells. (b) A local mutation is a random translation of the sphere.

the centre coordinates c of each sphere s_i of the individual (Fig. 3-7a) such as

$$c_{s_i} = c_{s_i} + t \quad \forall i \in \{0, 1, ..., n\} \qquad \text{with } ||t|| = 1 \tag{3.7}$$

The second option is a local mutation that modifies only one part chosen randomly in the individual using a important mutation. For an individual of n cells, a random cell s is translate of a random vector t such as

$$c_s = c_s + t \qquad \text{with } 0 \leq ||t|| \leq \frac{\sqrt{(w^2 + h^2)}}{2} \tag{3.8}$$

where w and h the dimension of the microscope image (Fig. 3-7b). As the goal of the mutation is to produce a different individual close to the original one but enough different to be consider as a new individual, the global mutation which affect the overall individual should remain small in order to not go too far from the original individual. On the contrary, the local mutation that only affects one cell, should be more important, in order to create a different individual.

3.4.3 Mating Operation

The mating operation is directly dependent on the representation of an individual. It is associated to a mating rate, a probability that an individual mate, to be defined by the user or parametrised by some tests. In the process of genetic algorithm dealing with gene representation, the most common mating process is the crossover. Mimicking the biological crossover, it consists in cutting two individual in two, and generate two new individuals by merging the parts from different individual. We kept this approach but applied to our model representation. Called CrossCut, this approach is realised by dividing the individuals in two parts and by merging them, to create an offspring. We applied also an alternate approach called CrossMix, which consist in creating an offspring which will be the weighted mean of N individuals as

$$\text{offspring} \;=\; \sum_{i}^{N} \omega_i x_i \tag{3.9}$$

We tried two possible CrossMix: CrossMix-Fit, where the weight is determined by the fitness of the individual. The fitter, the better weight he will have, such as a weight of $0.5 \leqslant \omega \leqslant 1$ and $\sum \omega_i = 1$. The other variant, called CrossMix-Rand, is applying the weight randomly, without taking in account the fitness of the two individuals. These operations are used to merge the coordinate of the different spheres of the individuals and create a new offspring (Fig. 3-8).

3.4.4 Algorithm GPU Design

As we saw, evolution algorithms is an iterative process in which each member of a population mate, mutate and are then evaluated according to a fitness function. In our case, and in the majority of the applications, the most costly part of an evolutionary algorithm is the evaluation process of each individual of the population. In order to make the process usable in term of time processing, we decided to use the processing capacity of a GPU. The GPU is designed to do multiple repetitive independent process in parallel which is our case for the evaluation of the individual. The use of such technology requires an adaptation of the design of the code and algorithm that is originally made for a central process unit. We tried two different designs: computation in blocks and computation in series.

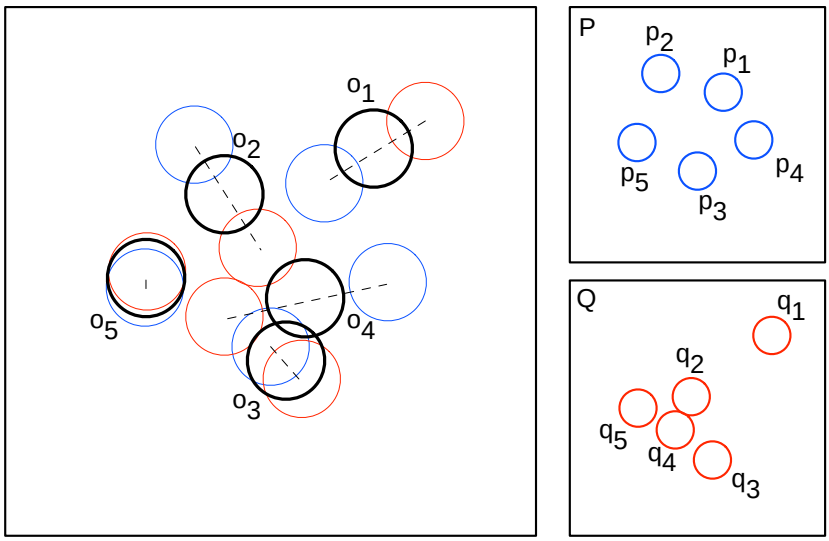

Figure 3-8: A mating process using CrossMix between two individual P and Q using equal weights. The spheres of P is paired with he spheres in Q to give a new offspring.

Computation in blocks associates one thread of the GPU to one individual of the system (Fig. 3-9). All the individuals would be processed and evaluated in parallel, at the same time, by the GPU. Each thread is in charge of processing the fitness function to the individual and gives the results in output. For example, from a population of 1000 individuals, the same amount of threads is used from the GPU, and the 1000 individuals are processed in the same time. The advantage of such model is that it is a straightforward translation of the evolution algorithm to a GPU design, in which the main loop over the population is parallelised in order to process all the population at the same time. However, a major inconvenient is that it requires to load the totality of the individuals into the GPU memory, which is separated from the memory of the computer. This memory is limited and in direct relation with the type of GPU used. As the latest generation of GPU have more memory than the previous generation, the transfer from the computer memory to the GPU memory is a very costly operation. For complex individuals such as in our case, there is a critical need for recent GPU, in order to be able to manage the memory cost.

Computation in series associates one pixel to one thread of the GPU (Fig. 3-10). The individuals of the population are still processed in series like they would be on a CPU, but each pixels of the model projection is processed in parallel. Each thread will calculate the

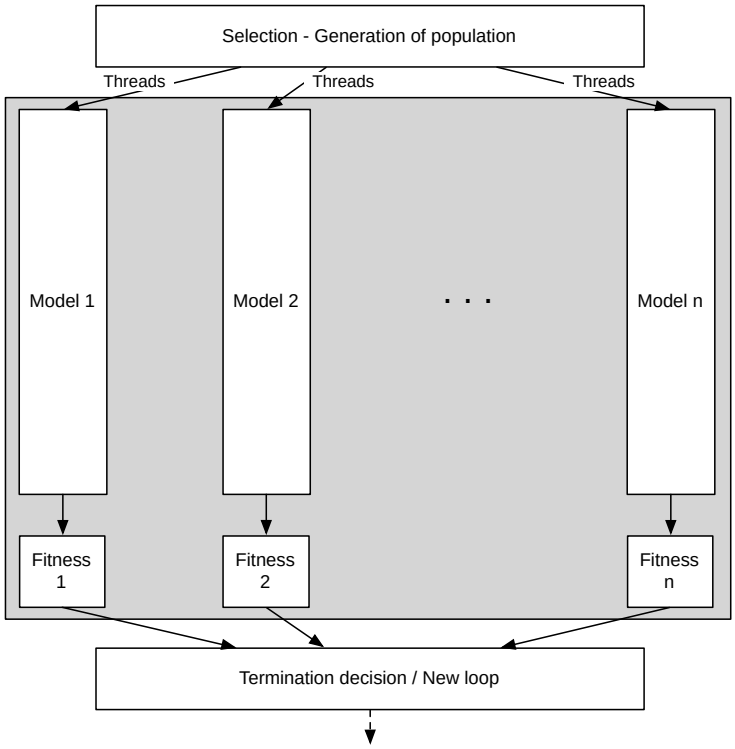

Figure 3-9: Parallel GPU implementation of the evolution algorithm. All the model are given to the GPU, and one thread is allocated for each model to process its score.

fitness score on a pixel scale and then, the final fitness score is determined for the individual. The advantage of this approach is the association of one thread to one pixel, in order to fully use the totality of the threads available in the GPU. Also, only one projection is loaded at a time, making the memory cost irrelevant. The main difficulty of this approach is that we only get the fitness score for each pixel. A sum is then to be done on the results of the threads output.

3.4.5 Evolution Algorithm Test

The evolution process is possible through different approaches, each associated with specific parameters. In order to determine the best configuration that allowing us to minimise as much as possible the error in the most efficient way, we have performed a series of comparisons tests between the different possible evolution strategies. We have first defined an evolution process with the most common choices in the literature. The individual selection

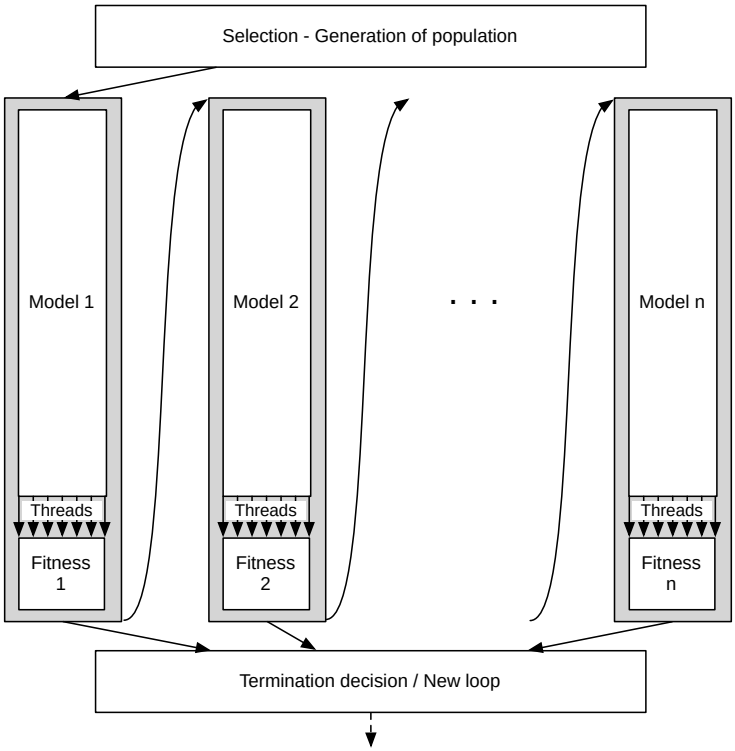

Figure 3-10: Serie GPU implementation of the evolution algorithm. The models are given in series by the GPU, and each model has his score process by n threads of the GPU.

is done using a stochastic sampling selection, and the mating process by a CrossCut 50% method. We run the overall with 35 individual through 1000 iteration. This configuration was defined as the default configuration from which we would define a more optimised configuration. We have run the different tests on an artificially generated dummy basic configuration. Most of the tests were done on a 3-cell planar configuration.

As there is no default mutation process in our first configuration, we first compare the mutations approach that was considered. We use a mating rate of 70% and a mutation rate of 40%. We have proposed and compared two possible approaches, local or global (Fig. 3-11). With no doubt, the local approach is much more efficient in our case. It allows the process to converge to a close solution before the end of the maximum iteration. The global approach is also converging but in a much slower pace, failing to reach a 0.5 error rate at the maximum iteration.

Next to the mutation process, we have tested the mating process. Similar as for the mutation, we defined the mutating rate at 10% and the mating at 90%. The CrossCut, the default choice, is compare to two possible variations, the Cross Mix Fit and the Random Cross Mix. Same as with the mutation process, one of the approaches clearly detached itself from the two other. The CrossCut and the Cross Mix Fit have both similar results, and seam to converge to a solution but fail to reach an acceptable solution as they stagnate to a 0.4 error at the end of the maximum number of iterations. The Random Cross Mix successfully reached a good error rate in less than 500 iterations, half of the maximum number of iterations.

The last part to be defined in the algorithm is the selection process. We compared the stochastic sampling approach with a tournament approach. For the tournament approach, a new parameter is defined as the importance given to the fitness score of an individual. We tried with several tournament rates and found that the tournament approach with a 80% rate gave us the best results (Fig. 3-13). However, the other possibilities succeeded in reaching close results.

As we defined the algorithm qualitative parameters (*e.g.* selection, mutation, *etc.*), we

have now to define the quantitative parameters, in our case, the number of individual per populations, the maximum iterations, the mutation rate and the mating rate.

With our default approach we have defined a population of 35 models and a maximum iteration of 1000. Those two parameters are directly linked to the memory and speed cost of the algorithm. We tried to limit the algorithm to a maximum of 25000 tests that would allow to keep an acceptable cost for the process while giving enough search tests to reach a solution. We define different couples of number of individual, noted ind, and maximum iteration, noted ite, and test their effects on the process (Fig. 3-14). The two couples that concentrate on large population, $ind = 60,\ ite = 416$ and $ind = 80,\ ite = 312$, do not have enough iterations to actually reach a solution. Both their process are ended, reaching the maximum iteration criteria, in the middle of their convergence. The two other couples, $ind = 40,\ ite = 625$ and $ind = 20,\ ite = 1250$, which are focussing a smaller population but higher iteration managed to reached a viable solution. We did more tests on those in order to defined the best couple of parameters to be used in our application (Tab. 3.1), and we decide to use $ind = 20,\ ite = 1250$ as it seams to perform better on larger tests.

The two last parameters to be defined are the mutation and the mating rate. As they are quantitative parameters, we selected the best rate for each through multiple runs of the algorithm (Tab. 3.2). The couple $ind = 20,\ ite = 1250$ globally show better results over the different tests we did.

Concerning the GPU design of the algorithm, the main choice of design was made in term of speed processing. Both GPU design are faster than the classical CPU design (Fig. 3-15). However we can observe that the GPU series is much fast. This is due to the low GPU memory and the much important amount of thread used. The memory transfer cost use at the beginning of the process is visible on the GPU blocks design curve as we need to process at least 200 individual to see an improvement of speed and the increase of the size of the population highly impact the speed process of the design.

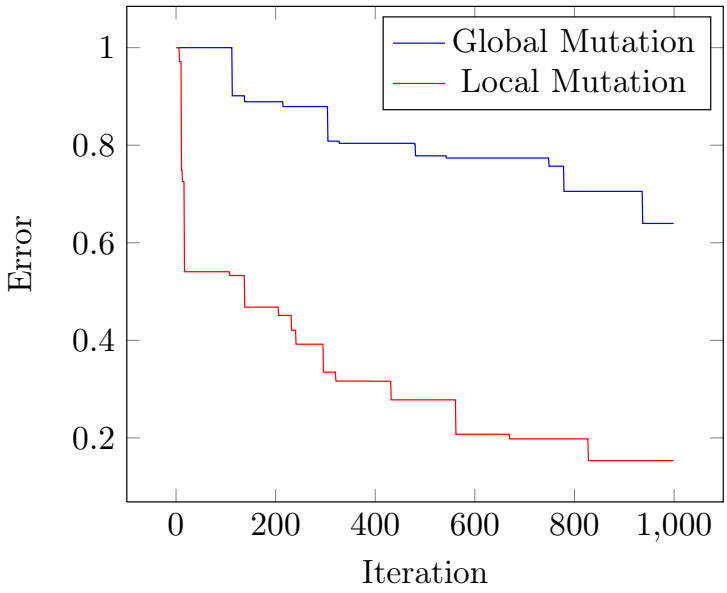

Figure 3-11: Comparison run between two mutation processes, global small translation of all the spheres or translation of a single sphere.

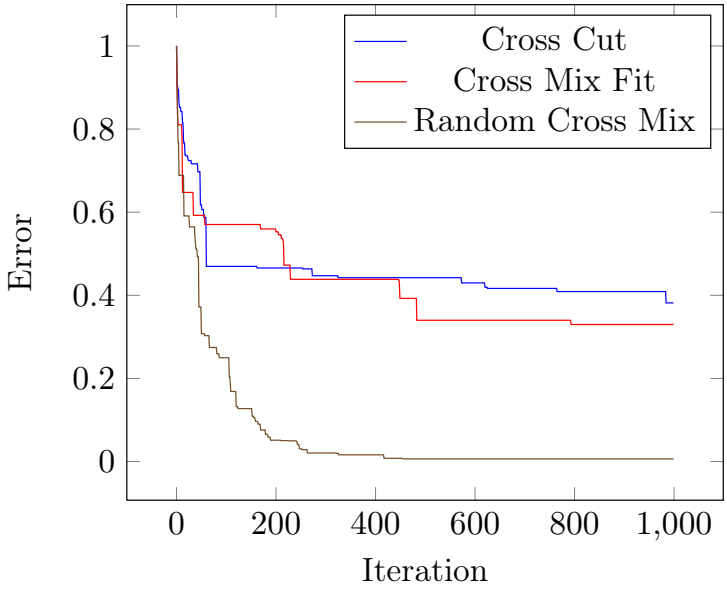

Figure 3-12: Comparison run between mating processes Cross Cut, Cross Mix and Random Cross Mix.

Number of Cells	$ind = 20,\ ite = 1250$	$ind = 40,\ ite = 625$
3	0.05	0.14
4	0.09	0.25
5	0.23	0.21

Table 3.1: Mean error values over ten runs of the evolutionary algorithm on different dummy data using two different population size and maximum iteration.

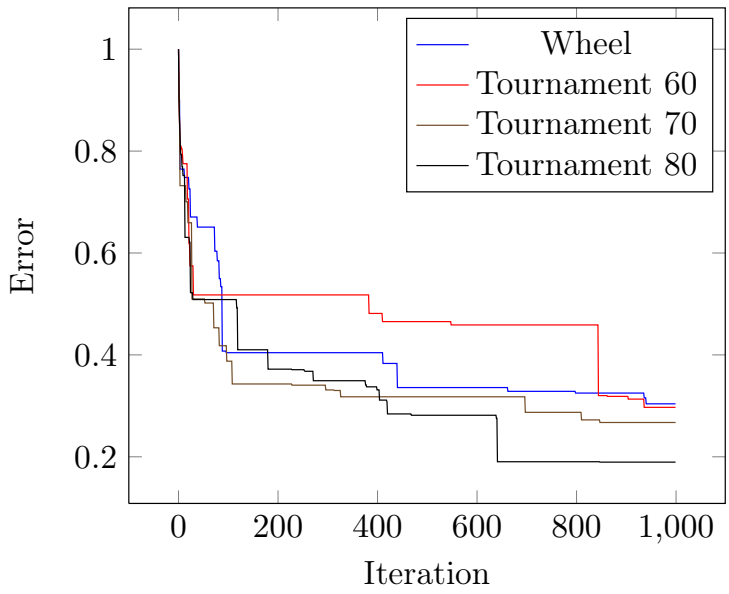

Figure 3-13: Comparison run between the selection process stochastic selection and tournament selection. The percentage link to the selection is rate associated to the tournament process.

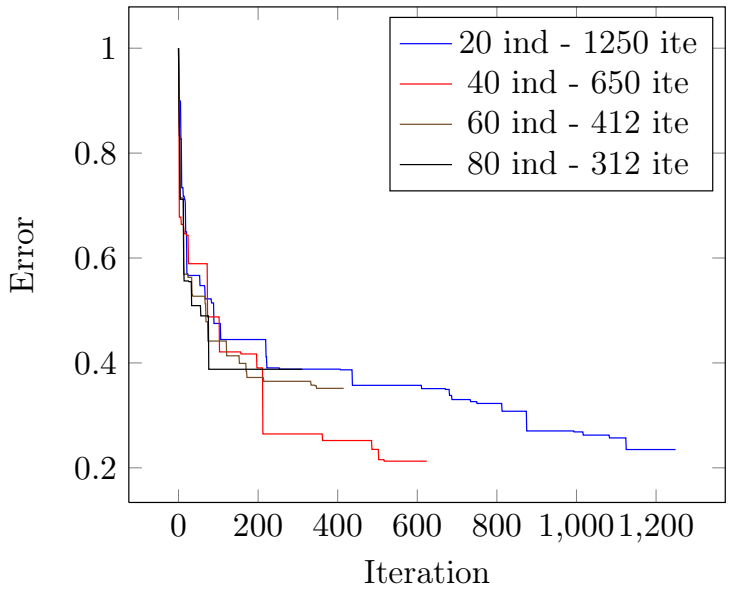

Figure 3-14: Comparison run with different number of individual and maximum iteration.

Mutation Rate	Mating Rate	Best Error
0.1	0.9	0.07
0.9	0.9	0.17
0.9	0.1	0.16
0.7	0.4	0.21
0.4	0.7	0.26
0.5	0.5	0.24

Table 3.2: Mean error values over ten runs of the evolutionary algorithm with different mutation and mating rates.

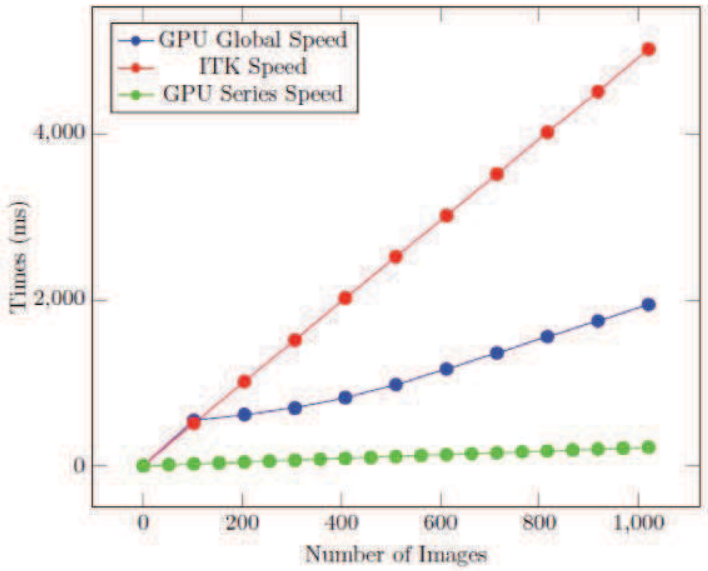

Figure 3-15: Speed test comparison between the CPU design, the GPU blocks design and the GPU series design.

3.5 Iterative Mesh Approach

Even if the proliferation of neurosphere is not a natural process that can be observed *in vivo*, the proliferation is not chaotic or a random process. Each cell behaves following a cycle and the accumulation of the different cell behaviour lead to the proliferation into a neurosphere. To better determine the structure that comes from the cells division and proliferation, we model the neurosphere proliferation through an alternation of the a primal Delaunay Triangulation [27] and its dual Voronoi Tessellation structure. It starts as a triangulated mesh structure where each triangle respects the Delaunay criterion stating that no vertex of the mesh $\mathcal{M}$ should be inside of the circumference circle define by any triangle of $DT(\mathcal{M})$, where DT is Delaunay state of $\mathcal{M}$. The Delaunay Triangulation was proven to be a solution to regular sphere packing problem [117, 93], and we will be using this property for the modelling of neurospheres.

The vertices of the mesh represent the position of a cell. In addition, each vertex has a set of information related to the cell it represents: radius, age and chance of division. The edges of the mesh that link the different vertex of the mesh, represent the connection between cells and provide topological information to the model. Quad Edge Mesh will define the mesh structure and its dual, giving us a lattice on which we will dispatch the cells composition of the neurosphere.

3.5.1 Quad Edge Mesh Structure

We use a *Quad Edge Mesh* structure [39] that is implemented in the Insight ToolKit (ITK)[1] [38]. The *Quad Edge Mesh* data structure in ITK, as depicted in figure 3-16, can handle discrete 2-manifold surfaces. It actually stores the geometry and both primal and dual topology. It has a constant complexity local access a modifications. The *Quad Edge Mesh* data structure is a 3 layers structure in which the bottom layer is called QuadEdge (*QE*) layer that represents the topology, the intermediate layer is called QE Geometric (*QE-Geom*) layer that links topology and geometry and finally the upper layer is native to ITK called ITK layer. The *QE* data structure is presented in detail in [38]. For each edge, there

[1] ITK - `www.itk.org`

are 4 *QE*s in the structure as illustrated in figure 3-16b. It contains two primal *QE*s and two dual *QE*s. For the sake of simplicity, we only draw connection for one point and one face from *QE* to *QEGeom* and *QEGeom* to ITK layer as shown in figure 3-16b, conversely both points and faces are equally linked in the data structure. This data structure only needs three operators as *Rot*, *Onext* and *Splice* to implement all other modifications (Euler operator) and accessibility of the mesh.

We have extended the existing structure in the ITK to stores both primal and dual mesh simultaneously. The new design of *Quad Edge Mesh With Dual* data structure contains double reference i.e., one for primal point to dual cell and one for primal cell to dual point as depicted in figure 3-17a. For the sake of simplicity, we only draw connection from QE layer to QEGeom layer and QEGeom layer to ITK layer for one point and one face instead of both points and both faces as shown in figure 3-17a. The primal and dual overlapping structures of connections at QEGeom layer is shown in figure 3-17b. Furthermore, this class contains three new containers; *DualPointsContainer* for dual points, *DualCellsContainer* for dual cells and *DualEdgeCellsContainer* for boundary edges and three new functions; *AddDualPoint* for adding dual point, *AddDualFace* for dual cells (polygon) and *AddDualEdge* for boundary edges.

In order to keep the primal-dual references in a single data structure, we have two design options. In first design, we maintain two look up tables; one table for storing references of primal cell to dual point and second table for primal point to dual cell. The advantage of this approach is backward compatibility of code and test cases. The bad side of this design is to maintain these tables that having the complexity $nlog(n)$ causing severe degradation of performance in case of large mesh. In second design, we modify the existing data structure by adding two reference pair; primal point to dual cell and primal cell to dual point as shown below. With this design, no look up table is required to maintain the primal and dual references. So it is very efficient approach but not compatible with respect to previous code and test cases.

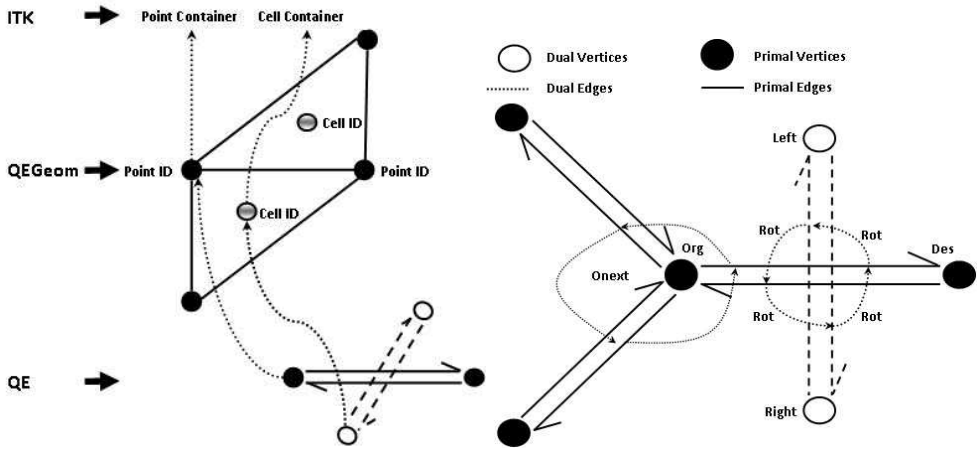

(a) QuadEdgeMesh structure (b) QuadEdge structure

Figure 3-16: Quad Edge Mesh data structures

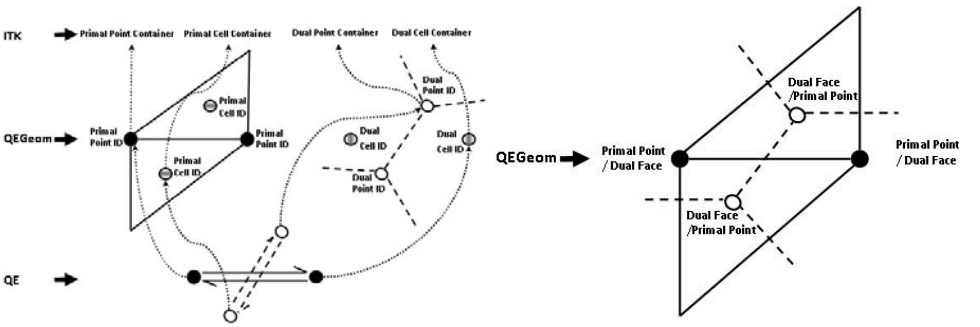

(a) QuadEdgeMeshWithDual's layers (b) QEGeom Layer of Quad Edge Mesh With Dual

Figure 3-17: Quad Edge Mesh With Dual data structure

3.5.2 Incremental Delaunay Triangulation

Several ways exist to generate a Delaunay triangulation: The recursive process of Divide and Conquer [55] or the Sweep Line algorithm (also known as the Fortune's algorithm) [37] for the most advance and optimised, and the flip or the incremental algorithm [25] for the more common and straightforward. The Divide and Conquer and the Sweep Line was put aside as too constrained in term of implementation in order to manage dynamical construction. Our choice went on the Incremental Algorithm for is speed and simplicity.

Let $\mathcal{P}$ a point set and $DT(\mathcal{P}_t)$ the Delaunay triangulation of $\mathcal{P}_t \subset \mathcal{P}$. We construct $DT(\mathcal{P}_{t+1})$ by adding a point p_t randomly taken from $\mathcal{P} \backslash \mathcal{P}_t$ into the $DT(\mathcal{P}_t)$. Then, the triangle t of $DT(\mathcal{P}_t)$ that embed the point p_t is located and subdivided into three new triangle t_1, t_2 and t_3, which share the same vertex p_t.

Initialisation

This algorithm will generate a 2-manifold planar mesh of 1 component and 1 boundary, embedded into a n-dimensional space, but that will be parallel to the plan $(0, x, y)$. This output mesh will respect the Delaunay criterion.

The Incremental algorithm is a step case algorithm which needs initialisation. We initialise $DT(\mathcal{P}_0)$ by creating a four points mesh which encloses all the points of $\mathcal{P}$. Those four points Ω_0, Ω_1, Ω_2 and Ω_3 are at the extremity of the coordinates space of $\mathcal{P}$ (Fig. 3-19a). This is to make sure that their edges will always respect the criterion and will not influence the triangulation. Once the algorithm will have converged, the points will be removed along with all edges connected to them (Fig. 3-19f). In the case of we start the process from an already existing mesh respecting the Delaunay structure, we check if the new points are inside the existing mesh. If they are inside, there is no need for the Ω points.

Main algorithm

At each step of the algorithm, we add a new point p_t to the triangulation (Fig. 3-19c). First we locate the triangle $T(p_i, p_j, p_k)$ of the current triangulation $DT(\mathcal{P}_t)$ the point p_t is going to affect. This is done using a Walk In Triangulation algorithm [31] implemented as an *ITK::WalkInTriangulationFunction* [89] in the ITK.

From the given initial triangle t, we randomly determine q, one of the vertices of t. We rotate around q until the current triangle incident to q is intersecting with the $\overrightarrow{qp}$ vector. Once t is intersecting with $\overrightarrow{qp}$, we test on witch edge e the vector $\overrightarrow{qp}$ is going out of t using the orientation predicate (Eq. 3.10). We move to the neighbour triangle of t that share the edge e and test again, in the new triangle, which edge is crossed by the $\overrightarrow{qp}$. The walk stops when no edge crossing $\overrightarrow{qp}$ is found (Fig 3-18).

$$orientation(\alpha, \beta, \gamma) \;=\; sign\left(\begin{vmatrix} \beta_x - \gamma_x & \alpha_x - \gamma_x \\ \beta_y - \gamma_y & \alpha_y - \gamma_y \end{vmatrix}\right) \tag{3.10}$$

For robustness and exactness in the algorithm, the predicate is done by using an exact discrete geometrical predicate [94] implemented in the ITK [72].

Once the triangle T containing the new point is found, it is removed and replaced by the three triangles $T_1(p_i, p_j, p_t)$, $T_2(p_j, p_k, p_t)$ and $T_3(p_k, p_i, p_t)$ (Fig. 3-19d).

Once a new point is added, the Delaunay criterion is then checked for the newly created triangle T_1, T_2 and T_3 (Fig. 3-19e). It uses the *ITK::PointInCircleGeometricalPredicateFunctor* [72] and verifies, for the given triangle and point, the emptiness of the circumference circle for the adjacent face and opposite to the given point. If the face is not Delaunay conform, we *flip* the diagonal edge of the quadrilateral formed by the triangle and its adjacent triangle using the *ITK::QuadEdgeMeshFlipEdgeEulerOperator*. Because the *flip* can affect the validity of other local edge, the verification is recursively called on the two new triangles created from the edge flipping. The overall process was wrapped in the ITK [88].

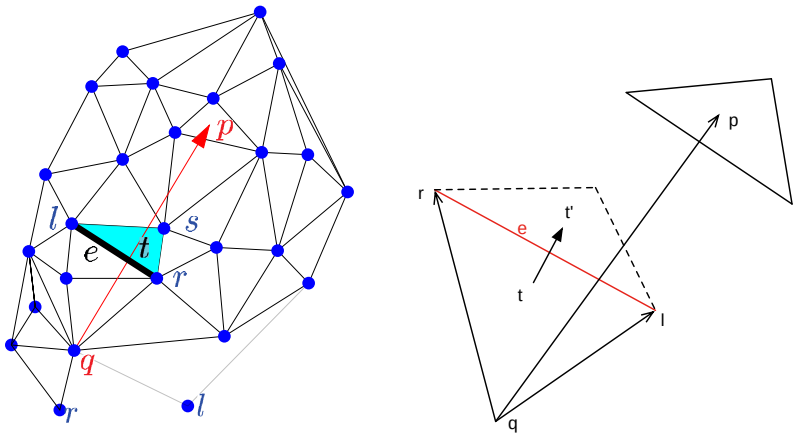

Figure 3-18: Straight Walk in a Triangulation Algorithm. (a) Global view of the walk over a triangulated mesh. (b) Walk from one triangle t to a neighbour triangle t' in direction of the final triangle q.

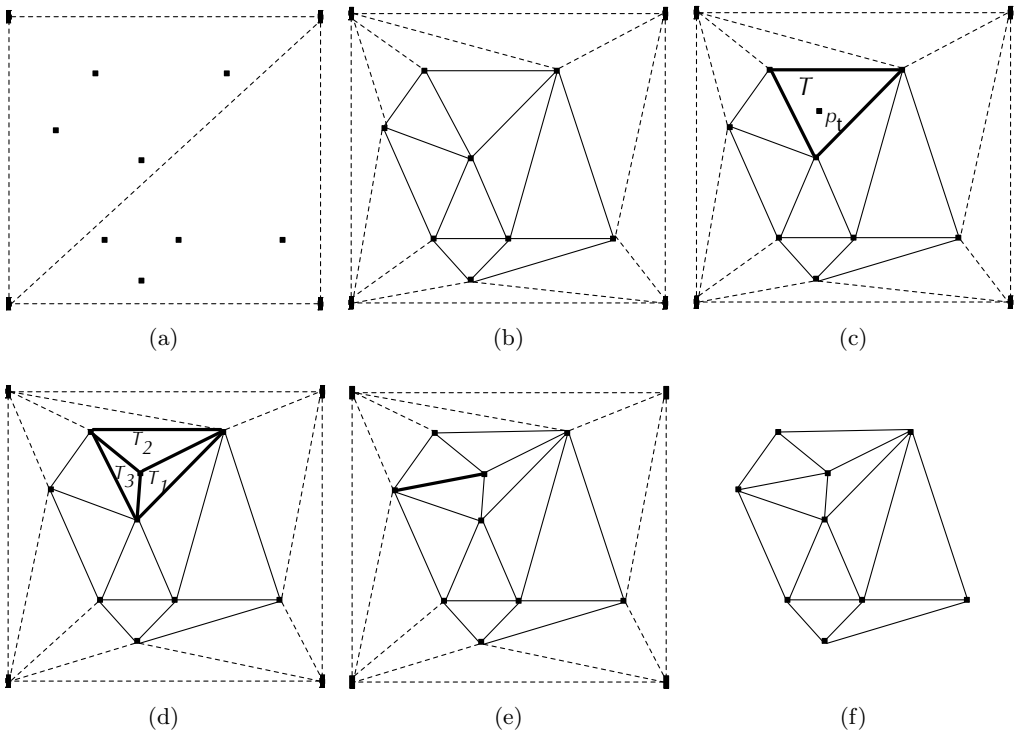

Figure 3-19: Incremental algorithm iteration. (a) Initialisation step. (b) $DT(\mathcal{P}_t)$. (c) Add a point p_t to $DT(\mathcal{P}_t)$. (d) Create three new triangles T_1, T_2 and T_3. (d) Flip illegal edge in order to obtain $DT(\mathcal{P}_{t+1})$. (e) When all point are processed, remove temporary points from the initialisation step. (f) Final $DT(\mathcal{P})$.

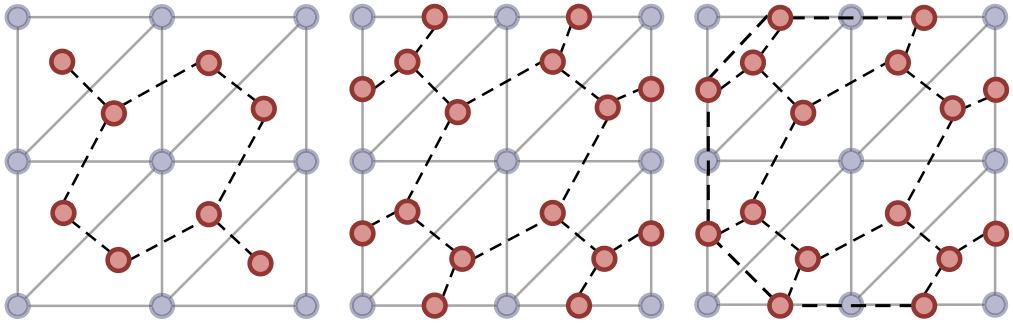

(a) Primal/Dual without dual edge point (b) Primal/Dual with dual edge point (c) Primal/Dual with dual edge point border

Figure 3-20: Primal (in blue) and its Dual (red), in the particular case of Delaunay/Voronoi, with different borders management options

Primal - Dual

Taking a set of points $\mathcal{P}$ in $\mathbb{R}^3$, the Delaunay triangulation of $\mathcal{P}$ is a specific triangulation of $\mathcal{P}$ that respects the Delaunay criterion stating that no point of $\mathcal{P}$ should be inside of the circumference circle of any triangle of the triangulation of $\mathcal{P}$. Taking a set of points $\mathcal{P}$ in $\mathbb{R}^3$, the Voronoi diagram (or tesselation) is the partition of $\mathbb{R}^3$ into n polyhedral regions such as each region T has a set of points in $\mathbb{R}^3$ which are closer to T than to any other region. The Voronoi diagram is the dual of the Delaunay triangulation, and the Delaunay triangulation is the dual structure of the Voronoi diagram (Fig. 3-20). By dual, we mean to draw a line segment between two Voronoi vertices if their Voronoi polygons have a common edge, or in more mathematical terminology: there is a natural bijection between the two that reverses the face inclusions. The duality between Delaunay triangulations and Voronoi diagram is geometric because it depends on the position of its vertices.

The switch between the primal and dual topology of the Quad Edge Mesh was added to the existing ITK structure though our extension [47]. This allow in our case to switch from a primal to a dual in a constant time and to use the dual/primal property to find new position for other layers that keep the packing of sphere to its minimum.

3.5.3 Division Process

The Delaunay gives us a regular structure that assures us to minimise the packing of the cells. The iterative construction of the first layer mesh must now fit to the division process of the cells in the neurosphere. At each new time step of the neurosphere observation, if a new cell appears, we update the current model with a new cell. Each vertex of the mesh is related to a timer and a chance of division, directly given by how long the experiment is running and the division probability given by the figure 3-4. In the case of a division, we define a dividing cell c_m and select a neighbour cell c_n that is an an external border of the mesh (Fig. 3-21b). A new vertex c_1 is created and form a new triangle with c_m and c_n (Fig. 3-22). c_m and c_1 both represent the two new cells issued from the division in the mesh, and c_m is redefine as its daughter c_2.

- The edge between c_2 and c_1 represent the contact between two cells issued from the same division.
- The edge between c_1 and c_n represent the phoneme of agglomeration of the cells and their attraction into a compact structure.
- The edge between c_2 and c_n is kept because of the previous existing edge between c_m and c_n.

Two cases of division can occur: (i) A visible division occur and new cell appear in the observation. (ii) A division occurs but it is not visible in the observation and no new cell is visible. We define the two cases as a visible division and a invisible division.

In the case of an invisible division, we determined the cell that divided with the corresponding division probability. We take the highest one and position a new vertex at an equal distance of $d = 2r$, where r is the defined radius a of cell, from the mother cell and the selected neighbour cell (Fig. 3-22b).

In the case of a visible division, the cell detection process provides the two-dimensional coordinates of the new cell. We can directly use them to place the new vertex related to this new cell, and the closes existing vertex with the highest probability of division will be

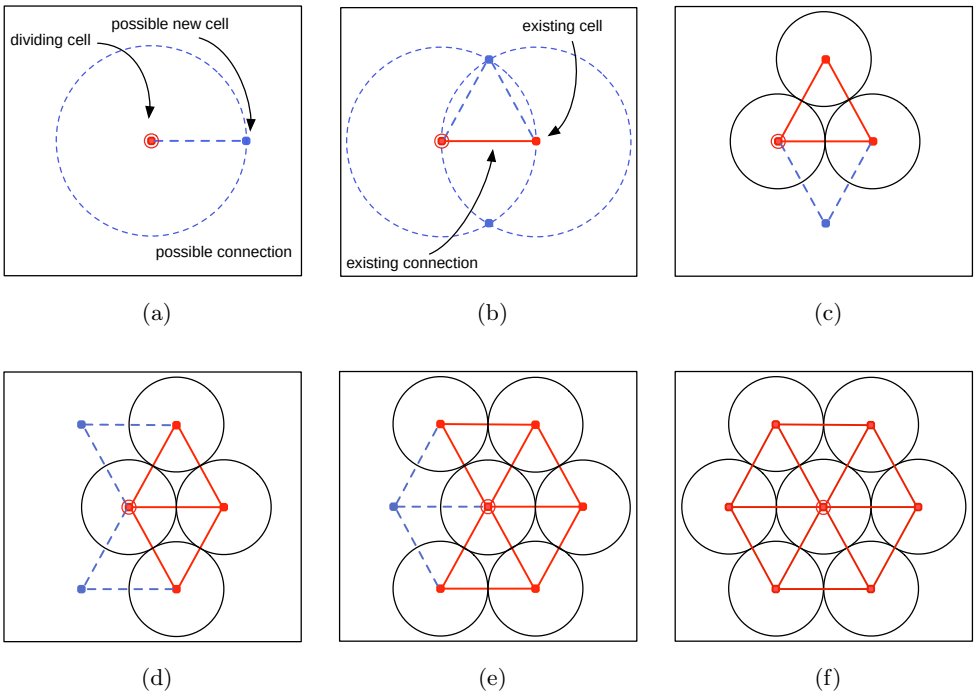

Figure 3-21: Iterative construction of the mesh through the division of the same cell. (a) First division orientation is random on a sphere around the first cell. (b) The second division is predefined by the position of the two first cells. (c-e) Iterative division, each time the new cell is connected to a border cell. (f) The division plan is fully occupied by neighbour cells.

set as the mother cell (Fig. 3-22c). The observation can only provide us with the (x, y) coordinates, and defines the depth $z = 0$.

3.5.4 Depth and Layers

Depth

The first aspect of depth that is introduced in the model occurs after a visible division. The new cell c_{new} will be defined at an equal distance $r \leqslant d \leqslant 2r$ of its two neighbour cells. In the case $d \neq 2r$, the mesh does not respect the Delaunay criterion anymore. Instead of flipping edges to reform a Delaunay structure, we modify the depth value of the cell until c_{new} is a distance $d = 2r$ from its two neighbour cells (Fig. 3-23).

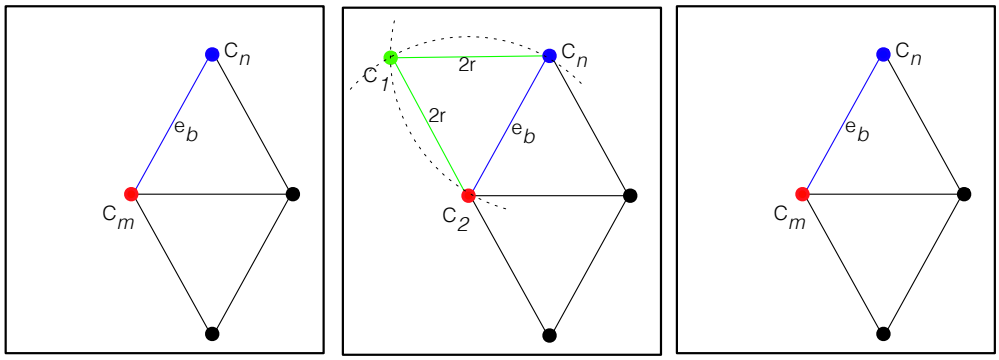

Figure 3-22: Division process. (a) the vertex c_m is dividing, the neighbour border vertex c_n is selected. (b) The division is invisible, we define the new vertex c_1 at $d = 2r$ from c_m and c_n, and c_m is redefine as the second vertex issued from the division. We create the face (c_2, c_1, c_n) to the model. (c) The division is visible, we define the new vertex (c_1 and c_2 and we add the face (c_2, c_1, c_n) to the model.

Layer

We want our model to have a certain compact aspect. The Delaunay triangulation is a solution to the sphere-packing problem. In case all the spheres have the same radius, it will allow each vertex to have a maximum of 6 neighbour vertices, tending to a hexagonal sphere structure (Fig. 3-21f) on a plan. The model is defined as layer of cells. The division will always occur on a layer until the neighbourhood of the dividing cell is fully occupied. The new cell will then create a new layer on the model and position itself on the space created by three cells, equivalent to the barycentre of the face of the layer (Fig. 3-24). The position of the cells on the new layer is defined by the dual of the layer below. Due to the particularity of the Delaunay Triangulation, its dual is a Voronoi Tessellation and it is directly generated by the Quad Edge Mesh structure.

3.5.5 Iterative Mesh Test

We applied our mesh on a regular and perfect structure, all identical size of cells, no overlapping, fix timer and division cycle, and a limitation of the size of a layer. As the implementation allow it, we were able to store the first and second layer respectively corresponding to the Delaunay and the Voronoi, and access to one, the other, or both at the same time in a constant time (Fig. 3-25). For now the structure only allow us to

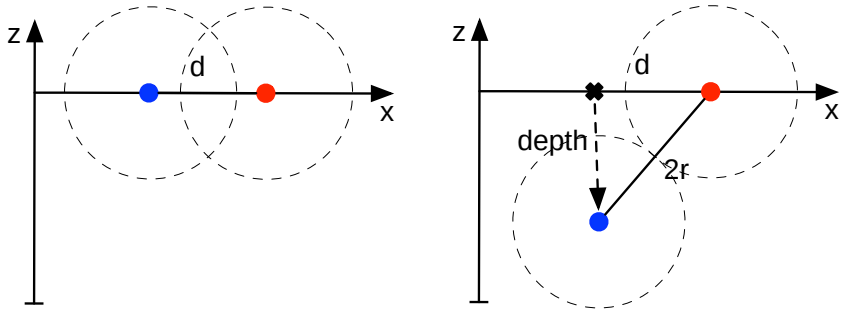

(a) (b)

Figure 3-23: Assuming all the cells have the same size, we determine the depth position of a cell from the Delaunay criterion. (a) The positioned cell after detection though the observation process, with $z = 0$ and distance from neighbour $d < 2r$. (b) Modification of z until we reach a distance of $2r$.

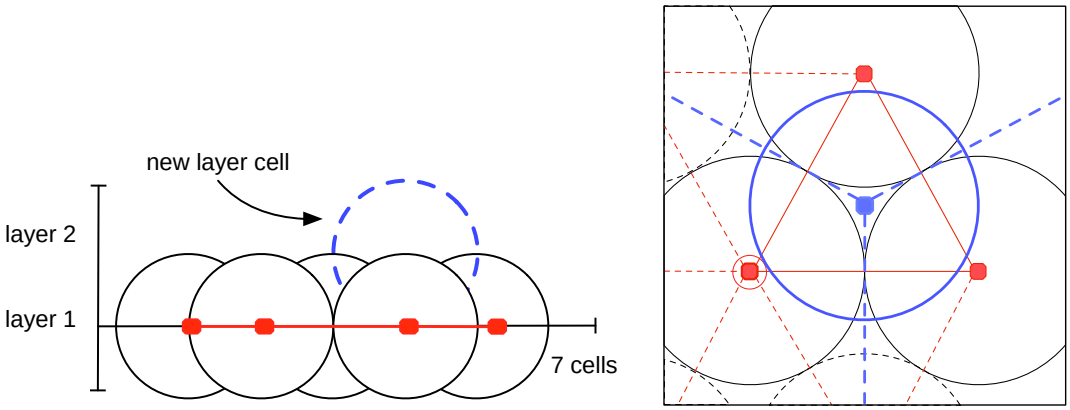

(a) (b)

Figure 3-24: Multi-layer aspect of the model. (a) Position of new layer cell after the neighbourhood of the dividing cell is full. (b) Position of the new cell defined by the barycentre of the face of the under-layer. Also given by the dual of the under-layer.

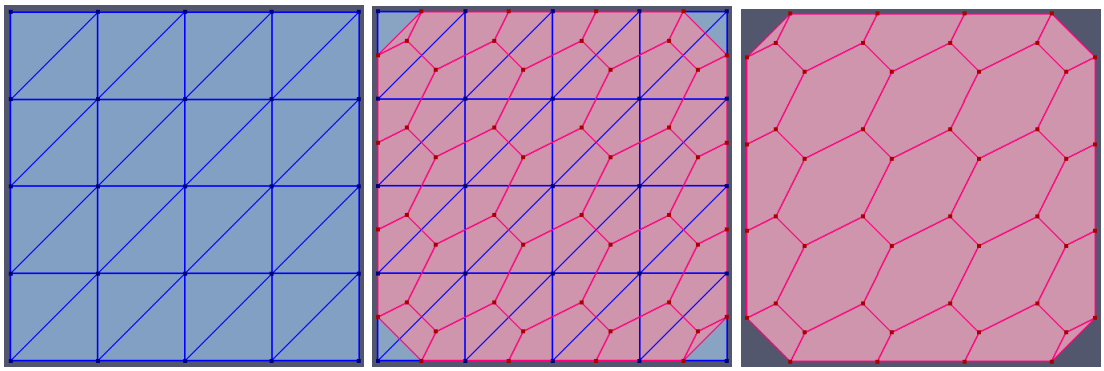

(a) (b) (c)

Figure 3-25: A two layers regular lattice generated using the mesh structure. (a) The primal layer. (b) The primal and dual layer. (c) The dual layer.

have two layers. A higher number of layers would requires either a volume mesh structure, which is not the case of our implementation that focus on generating 2-D surfaces, or a surrounding structure to store the different layers and manage communication between them. As our current experiment does not generate neurospheres with more than two layers of cells, such development is not necessary for the moment. However, we are aware that for further applications on larger neurosphere specimen, our structure is currently limited and may need to be rethink.

3.6 Conclusion

We have defined a set of *prior* knowledge that was considered relevant by the biologist and adapted them into two model generation process. The first model generation process is using evolution algorithm to determine, through an iterative search, a population model that represent a possible configuration of cells. The second approach is using a Delaunay triangulation structure to iteratively position the cells following a proliferation pattern defined by the cells cycle. Both models are then evaluated according to the selection process described in the next chapter.

Chapter 4

Selection:

3-D to 2-D Registration

4.1 Introduction

The third and final module of the framework is represented by the selection one. The purpose of the selection is to associate a score to each model generated by the synthesis in accordance to their likelihood with the microscope observation and the information extracted by the analysis. In order to relate the models to the observation and provide a ranking score, a 3-D to 2-D registration approach is used. According to an evaluation function using shape and texture, it will associate a score to each model and allow us to rank them. A visualisation of the best results is done at the end of the process, merging both image and model into a 3-D display to help the observation and the validation of the process.

4.2 State of the Art Related to Image Registrationt

Registration is a process that determines correspondences between two data. It is mostly used between two images and is applied in various applications. In computer vision and pattern recognition, it can play a role in data comparison, segmentation [20, 112] and tracking [61]. In medical image analysis, it is often used for disease observation. Either to evaluate a patient observation based on healthy observations in order to observe the difference between healthy and unhealthy observation and better understand the effects of a pathology, or to compare two observations of a pathology under the same modality done at different times to observe the evolution the pathology. It also plays an important role in modality fusion, for merging images taken from different but complementary sources such as a MRI image and Positron Emission Tomography (PET) image [63].

In image registration, the correspondence between two images is determined by finding the geometry transform and the intensity transform to pass from one image to the other. One image will be defined as fixed and the other one as moving. Brown [16] defined the registration process for two images, I_{fix} and I_{mov}, as:

$$I_{fix}(x, y) \;\Leftrightarrow\; \xi(I_{mov}(\phi(x, y))) \tag{4.1}$$

where ξ and ϕ are respectively the intensity transform and the geometrical transform that allow to map I_{mov} on I_{fix}. The problem is then to determine the two transforms. This is done through an optimisation process in which an evaluation function, also called criteria or metric function, is defined in order to quantify how well the two images correspond. The process can be applied to register more than two images together through an iterative approach, replacing the moving image with a new one.

As there are various applications to numerous types of images or modalities, there is actually no generic registration method. Although it is possible to define a generic approach [116] on which we can build a registration process (Fig. 4-1). The fitness function, the transform and the optimisation process are to be determined depending on the data and to the problems to be solved. As the geometry transform will provide results in the continuous coordinate space, an interpolation between the fixed and the transformed moving image can be applied.

Registration is not limited to 2-D images but can be applied at higher dimensional data. In medical image analysis, 3-D to 3-D registration is often used when working on volume data such as MRI or CT stacks. Registration method has also been applied for finding the correspondence between data of different dimensions, registering a 3-D volume with a 2-D image for example. Such method is mainly used in image-guided real-time intervention. A 3-D volume of the patient is made before the intervention using a heavy image modality (*e.g.* MRI) and will be used as the fixed data, and a 2-D image of the patient is done during the intervention using a lighter image modality (*e.g.* X-ray or ultrasound) [45].

4.2.1 Evaluation Function

The most important part of a registration algorithm is the evaluation function as it will define the aim of the process. It will rate the correspondences between the fixed and the transformed moving data. The behaviour of the registration algorithm will be therefore defined by the evaluation function. Two main families of functions exist: area-based methods and feature-based methods.

For classical registration problems, such as registration between the two images, for

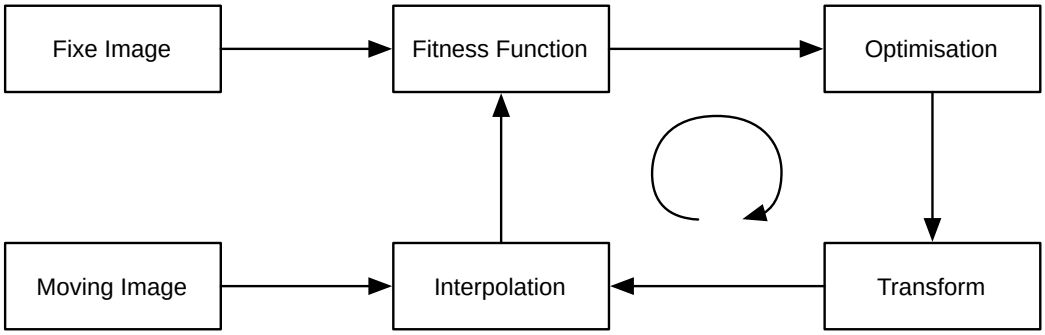

Figure 4-1: Generic image registration pipeline process.

example, several evaluation functions have already been widely explored and used. Such metrics are not necessary limited to image registration and can be applied for registration between other types of data, such as sets of points.

Area-Based Methods

Also called intensity-based methods as they are comparing the images using the intensity value of each pixel. These metrics compare two areas of data. The area can be defined as a sliding window or the whole data itself depending on the method. The most known area based methods are the Mean Square Error (MSE), the Normalised Cross-Correlation (NCC) and the Mutual Information (MI).

MSE is a well-known function to compare two sets of values. This function can be directly used to compare the intensity values of two images. For two images A and B, of the same size, the MSE is

$$MSE(A,B) \;=\; \frac{1}{W*H} \sum_{x=0}^{W} \sum_{y=0}^{H} (\; A(x,y) - B(x,y) \;)^2 \tag{4.2}$$

where W and H are respectively the width and height, in pixel, of the two images. If two images do not have the same size, the MSE can be calculated only on the overlapping information. The main requirement of such method is that the two data have their intensity values in the same range.

NCC [57] is another well-known intensity based method. It computes the cross-correlation for each pair of values and normalises it with the square root of the autocorrelation of the two data. The NCC of two data A and B is defined as

$$NCC(A,B) \;=\; \frac{\sum_i^N (\; A_i \;\cdot\; B_i \;)}{\sqrt{\sum_i^N A_i^2 \;\cdot\; \sum_i^N B_i^2}} \tag{4.3}$$

where N the number of values considered, A_i the i-th value of the data A, and B_i the i-th value of B. As such process is insensitive to a linear transformation, it is usually used to register data that have such relation between their values.

MI [100] measures how much one random variable can provide information about another unknown random variable, and is given by the relation

$$MI(A,B) \;=\; H(A) \;-\; H(B) \;-\; H(A,B) \tag{4.4}$$

where $H(A)$ and $H(B)$ are respectively the entropy values of the data A and B, and $H(A,B)$ the joint entropy. They are respectively defined as:

$$H(A) \;=\; \sum_i^n -p(a_i)\log(p(a_i)) \tag{4.5a}$$

$$H(B) \;=\; \sum_i^n -p(b_i)\log(p(b_i)) \tag{4.5b}$$

$$H(A,B) \;=\; \sum_i^n -p(a_i,b_i)\log(p(a_i,b_i)) \tag{4.5c}$$

where $p(a_i)$ and $p(b_i)$ are respectively the probabilities of the values a_i and b_i in the set and $p(a_i,b_i)$ the joint probability of the two values in the set. The MI is very effective when registering multi-modality data. It is often used in medical image analysis for the fusion of images taken from different modalities, usually anatomical images and functional images, which are very different in term of content.

Feature-Based Methods

In opposition of area-based methods, which compare the entire object, feature-based methods are only comparing salient structures extracted from the data with a specific preprocessing. Such methods are especially used for the registration of sets of points, meshes or graphs. In the case of images, such structures are either extracted from the images, like particular blobs determined by a DoG or a Harris corner, or computed from the image, such as a mesh. Feature-based methods are more efficient in terms of computation as only specific light structures are registered in opposition with area-based approaches that compare all the information contained in the two sets of data. The salient structures to be compared are particular points, edge, structure, which does not contain as much information as they are themselves the information. Much simpler function, like Euclidean distance, can be used to compare them without affecting the efficiency of the comparison. However, the extraction of the salient structure as to be perfectly adapted to the data as any error will directly affect the performance of the registration.

4.2.2 Transform

The transform is the function that is going to alter the moving data in order to make it corresponds to the fixed data. It is usually a geometrical transform but, in some rare applications, it can be another type of transform such as an intensity transform, or even both. The transform is determined by the type of data and problem to be solved [41]. Two main types of transform are used: rigid and non-rigid transform.

Rigid Transformation

A rigid transformation corresponds to a transform that preserves the distance between every pair of points transformed. For two point X and Y:

$$d(g(X), g(Y))^2 = d(X, Y)^2 \tag{4.6}$$

where d the Euclidean distance function and g a rigid transform in $\mathcal{R}^n$. Therefore, by definition, any object transformed by a rigid transformation shall keep its shape and size intact, only its position and orientation will be modified. This corresponds to translation,

rotation and any composition of those transforms. Such transform $\mathcal{T}$, for a point p, can be written as

$$\mathcal{T}(p) \;=\; Rp \;+\; t \tag{4.7}$$

where R a rotation matrix and t a translation vector.

Non-rigid Transformation

Non-rigid transformation does not preserve the distance between every pair of points. They are more complex transforms, which regroups several different types: scaling transform, affine transform and curved transform. Such transforms are usually used in registration problem where the object to be registered is considered as non-rigid. In other words, the shape of the object in the problem to be solved is expected to change. The type of the non-rigid transformation to be used also depends on how the object shape can be altered. Such details are to be defined accordingly to problem to be solved.

Scale Transform are transform corresponding to rigid transform except with a scaling factor $S = diag(s_x, s_y, s_z)$. It has the property to conserve straight lines and angles. Written as:

$$\mathcal{T}(p) \;=\; SRp \;+\; t \quad \text{or} \quad \mathcal{T}(p) \;=\; RSp \;+\; t \tag{4.8}$$

where R a rotation matrix and t a translation vector. The two notations are needed as the order in which the scaling and rotation are done may change the final results.

Affine Transform are transforms that only preserve straights lines but allow modification of the angles. Written as:

$$\mathcal{T}(p) \;=\; Ap \;+\; t \tag{4.9}$$

with no restriction on the value of a_{ij} elements of A, the affine transform matrix. This type of transform includes translation, rotation, scaling, shear, similarity and any composition of them. They are usually noted in homogeneous coordinates.

4.2.3 Optimisation

As it was explained previously, registration finds the best transformation that makes the two data corresponding. When such transform is unknown, we need to perform an iterative search of this transformation. Several methods exist for solving such optimisation problem. We will see some of the most used optimisation algorithms in registration, but it exists various other optimisation algorithms such as Powell's conjugate direction method.

Regular Gradient Descent (RGD) is a method that searches iteratively the solution by following the negative value of the derivative of the function to minimise at the current point. For a function f to be minimised, the process searches the value x that minimises the function through iterative steps

$$x_{n+1} \;=\; x_n \;+\; \lambda \frac{\partial f(x_n)}{\partial x_n} \tag{4.10}$$

where n is the iteration index and λ the learning step.

This optimisation process is used in the registration and in other optimisations. It works well in combination with MSE or NCC fitness function. However, this process has some drawbacks, one of them being a convergence problem. Such method will take important step when the gradient value is high and small step when the gradient value is low, and it is preferable to have the opposite.

Levenberg-Marquardt Algorithm (LMA) [71] is used to minimise non linear least square function and is based on the Gradient Descent.

$$S(x) = \sum_{j}^{N} [y_j - f(x_j)]^2 \tag{4.11}$$

Levenberg-Marquardt blended the RGD and the Gauss-Newton method, taking the advantage of both to propose the following iterative step

$$x_{n+1} \;=\; x_n \;-\; (H + \lambda diag(H))^{-1} \; \frac{\partial f(x_i)}{\partial x_i} \tag{4.12}$$

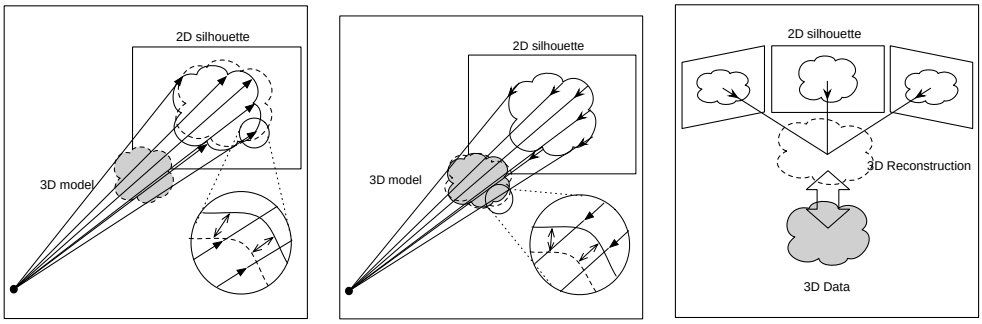

(a) (b) (c)

Figure 4-2: 3-D to 2-D registration strategy. a) Projection strategy b) Back-projection strategy c) Reconstruction strategy

where H the Hessian matrix for x_i and λ the learning step. At each step the error is evaluated, if the error is decreasing, λ is decreased as we are getting closer to the solution, if the error increase, then the step is discarded and λ is increased. The main drawback of such algorithm is the inversion of matrices to be done during the iterative costly step.

4.2.4 3-D to 2-D Registration Strategy

A registration problem between two different dimensional data is not very different from a classic registration problem, and has been explored before [22, 54]. We still want to determine the best geometry transform that relates the two data to each other. The main problem is what type of geometrical transform can be used and what kind of fitness function can rate the correspondence between 2-D and 3-D data. As comparing data of different dimensions is a too complicated problem, the answer proposed is to bring both data into the same dimensional space. Markelj *et.al.* [66], in their review in 3-D to 2-D registration, has determined three main strategies to do so: the *projection strategy*, the *back-projection strategy* and the *reconstruction strategy* (Fig. 4-2). Still, such problem remains by definition, an ill posed problem. It can possibly fail to determine the best solution. This is usually overcome by having multiple 2-D data to register with the 3-D data. Both the 3-D and 2-D data will be either the moving or the fixed data, depending on which strategy is chosen.

Projection Strategy

A projection strategy would be defined as 3-D to 2-D registration. The action would be to project the 3-D data, defined as the moving data, into the 2-D space of the 2-D data (Fig. 4-2a), defined as the fixed data. It can be defined as, for two data set A^{3D} and B^{2D}, we would determine the transformation $\mathcal{T}$ such as:

$$\mathcal{P}(\mathcal{T}(A^{3D})) \;=\; \mathcal{T}(A^{2D}) \;\Leftrightarrow\; B^{2D} \tag{4.13}$$

where $\mathcal{P}$ a projection function that projects A into B dimensional space Ω_B. In the case of multiple 2-D data, in order to improve the registration result:

$$P_i(\mathcal{T}(A^{3D})) \;=\; \mathcal{T}(A^{2D})_i \;\Leftrightarrow\; B_i^{2D} \quad \text{with } i = 1, 2, ..., N \tag{4.14}$$

where N is the total number of 2-D data to be registered. The projection strategy is the most straightforward way to solve data dimension differences.

Back-Projection Strategy

The back-projection strategy is the exact contrary of the projection strategy, and could be defined as a 2-D to 3-D registration. The 2-D data, defined as the moving data, are back-projected into the 3-D space of the 3-D data (Fig. 4-2b), defined as the fixed data. For two data sets A^{3D} and B^{2D}, we would determine the transformation $\mathcal{T}$ such as:

$$\mathcal{T}(A^{2D}) \;\Leftrightarrow\; B^{3D} = \mathcal{B}(B^{2D}) \tag{4.15}$$

where $\mathcal{B}$ a back-projection function. In the case of multiple 2-D data:

$$\mathcal{T}(A^{2D}) \;\Leftrightarrow\; B_i^{3D} = \mathcal{B}_i(B_i^{2D}) \quad \text{with } i = 1, 2, ..., N \tag{4.16}$$

where N is the total number of 2-D data to be registered.

Reconstruction Strategy

The reconstruction strategy is different from the two previous strategies and requires multiple 2-D data. The 2-D data are gathered and used to reconstruct a 3-D model which will be registered with the 3-D data with a 3-D to 3-D registration (Fig. 4-2c). For two data set A^{3D} and B_i^{2D}, for $i = 1, 2, ..., N$ the different 2-D data, we would determine the transformation $\mathcal{T}$ such as:

$$\mathcal{T}(A^{2D}) \Leftrightarrow B^{3D} = \mathcal{R}(B_i^{2D}) \tag{4.17}$$

where $\mathcal{R}$ a reconstruction function.

4.3 Adapting Registration for Neurosphere Model Selection

As we described in the state-of-the-art, registration methods are mainly used for the fusion of two data (multi-modality, *etc.*), or for finding mutual information in two different data (object detection, *etc.*). In our application, we use registration to find mutual information between dimensionally different data and associates score between them. It takes part in the model selection process, and provides a ranking score to each model accordingly on how well they register. Based on the generic pipeline of a registration process, we build a registration pipeline to rank our model according to a set of criteria.

4.3.1 Projection

The first point to define is how to solve the dimensional difference of the two data, the image and the 3-D model. The reconstruction strategy requires a set of multiple 2-D data in order to reconstruct a 3-D model. This is not applicable in our case, as we only have one microscope image at each acquisition time and not a set of images at different angles. The possibility to reconstruct a shape model using multiple images taken at different time t, by using shape from motion [67, 68], was explored but those approaches require a temporal resolution between the images acquired that is not too important in order to make relation between the two images. This is not possible in our case due to the restriction defined by the experiment itself. We put aside the reconstruction strategy for our approach but, com-

bined with a shape from motion method, should not be abandoned for future applications.

The projection and back-projection methods do not have any specific requirement to be applied like the reconstruction approach. During the process of generating the model, we explained that first cells are defined based on the cell detection process done during the analysis module. Therefore our model does not actually have specific defined space except the one defined by its own creation process. On the contrary, the microscope images have a very specific space defined by the microscope parameters. It makes it simpler and straightforward to apply a projection strategy where the 3-D model is projected into the 2-D image space. The back-projection which corresponds to the inverse, the 2-D image is back-projected into the 3-D model space, is applicable but not as intuitive than the projection approach.

The model to be projected does not have any specific orientation except the one that we define for them during the generation. By definition, there are infinite orientations in which we can project the model into the 2-D space. However, we have limited our process to a single axis, the z-axis, which correspond to the depth of the model. Two main reasons for this: It mimics how the microscope acquires the neurosphere; Different projection angle may give the exact same projection, limiting the number of projection angle but increasing the number of different models would converge to the same results and cover the solution space in a similar way.

Two main geometrical projections: orthogonal projection and perspective projection. The first one takes the 3-D object and projects it following the parallel line of the axes, thus its name orthogonal. It is a naive projection which does not create any projection deformation of the model, for example far object will not appear smaller than near object after the projection. The second projection type mimics the projection done by a human eye or a camera, reproducing the deformation due to the distance of the object from the observer. We have focused our efforts on the orthographic projection as it is a fast and straight forward to use. Indeed, an orthographic projection parallel to one of the axis is equivalent to removing the coordinate information related to this axis. For example, a

point $a \rightarrow \mathcal{R}^3$ projected into point $b \rightarrow \mathcal{R}^2$ by an orthographic projection $\mathcal{P}_z$ along the z-axes is given by the equations

$$b_x = s_x a_x + c_x \tag{4.18a}$$

$$b_y = s_y a_y + c_y \tag{4.18b}$$

with s a scale factor, by default equal to 1 and c an arbitrary offset (equal to 0 by default). It can be posed as a matrix multiplication

$$\begin{bmatrix} b_x \\ b_y \end{bmatrix} = \begin{bmatrix} s_x & 0 & 0 \\ 0 & s_y & 0 \end{bmatrix} \begin{bmatrix} a_x \\ a_y \\ a_z \end{bmatrix} + \begin{bmatrix} c_x \\ c_y \end{bmatrix} \tag{4.19}$$

As we can see, the orthographic projection applied a scale factor, here noted s, during the projection. However, all modifications of the model projected should be done via the registration transform, otherwise it will alter the process, so the scale factor is defined as $s = 1$ in order to keep the model aspect. The orthographic projection of the model is done along the z-axis, and following the projection equation 4.19, and project the sphere that constitutes the model. For that, we simply project the centre point of the sphere. From the projected point, we define the disc corresponding to the projection of the sphere using the equation of a circle.

4.3.2 Evaluation Function

After the model projection, we proceed to compare the two-dimension projected model with the microscope observation. For that, we need to define relevant features, to properly compare them and to define evaluation function allowing their comparaison.

From the microscope observation, we were able to extract the neurosphere boundaries, the number of visible cells and their positions and finally the pixel-wise intensity. The first information used is the neurosphere's boundary. We compare the observation silhouette (or shape) with the model-projected silhouette and determine how good the two silhouettes correspond to determine a score. This is a classic feature used in three-dimension

model reconstruction from images [73, 10, 74]. However, the problem we are solving is an ill-posed problem as we only have one silhouette from the observation, and multiple different three-dimension models can produce the same silhouette. Because of this, the process may converge to a good solution but with a false model.

In order to limit the chances of a bad convergence, we do not compare the projected model and the observation on the silhouette but we also look at cell representation level and how a cell should look like under phase contrast. For that, we use an idealised representation of a cell under phase contrast microscopy (Fig. 4-3) and construct, from the model cell configuration projection, a textured representation of the projected model. We then compare the observation image and the textured projected model, to determine a score (Fig. 4-4).

Both comparison criteria, the shape and the model texture, are done on a pixel-wise using a NCC function to be minimisation, such as

$$F_{global}(m) \;=\; F_{external}(m) \;+\; F_{internal}(m) \tag{4.20}$$

where $F_{external}$ corresponding to the external value depending on the likelihood with the observation, and $F_{internal}$ corresponding to the internal value defined by the model itself.

$$F_{global}(m) \;=\; \underbrace{F_{shape}(m) \;+\; F_{texture}(m)}_{\texttt{external}} \;+\; \underbrace{F_{distance}(m)}_{\texttt{internal}} \tag{4.21}$$

with

$$F_{shape}(m) \;=\; likelihood(shape(I), shape(m)) \tag{4.22a}$$

$$F_{texture}(m) \;=\; likelihood(texture(I), texture(m)) \tag{4.22b}$$

$$F_{distance}(m) \;=\; \sum_i \sum_j distance(c_i^m, c_j^m)(\alpha + \beta) - (2\alpha r) \tag{4.22c}$$

where α and β are coefficients to control the flexibility of the model, m the model to be evaluated and m_{c_i} the i^{th} cell of the model, and r the cell radius size.

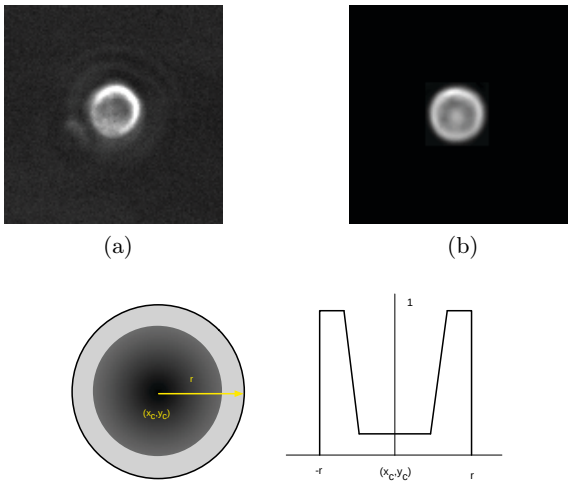

Figure 4-3: Ideal model representation of a cell under phase contrast microscope. (a) A cell under phase contrast. (b) The model representation. (c) The texture model graph.

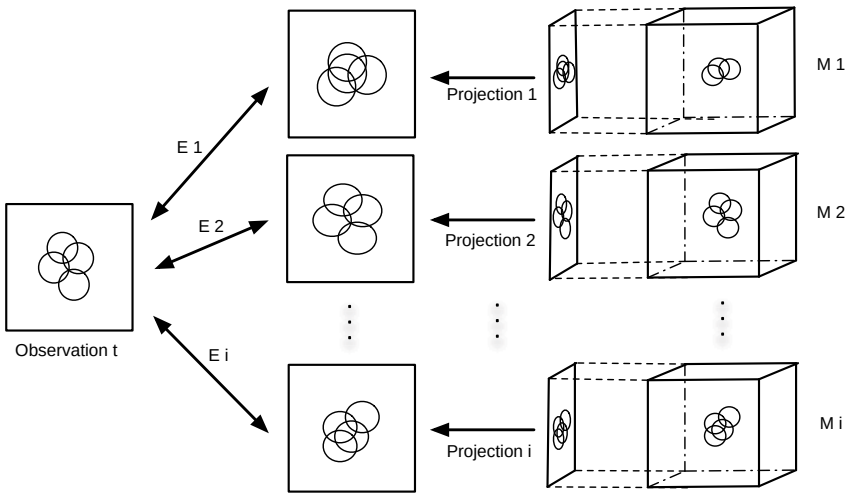

Figure 4-4: Representation of the models evaluation. Each model is projected in the image space and the compared with the observation.

4.3.3 Transform

A rigid transform is used to perform the mapping between the model and the image. The neurosphere is a deformable object, where its shape depends on the organisation of the cells that compose it. The cells that compose it can also be deformed within certain limits. From these statements it would be logical to define the process with a non-rigid transform. However, those observations are correct on the observation of the neurosphere over a long period of time, but they are actually observed on a discretised period of observation. The deformation of cells is not fully observable and the cells keep a spherical aspect as long as they are not observed during a movement. The deformation of the neurosphere is due to the division and proliferation of the cells, the deformation associated those events are managed in the model generation process. Therefore, the object itself can be considered at a time t, as a rigid object.

Another reason that could have justified the use of a non-rigid transformation would be a modification of the observation point by a non-rigid transformation. However, during acquisition and observation process, the microscope objective can only be modified by a translation on the (x, y) plan.
Therefore, we choose a rigid transform composed of a rotation and a translation.

4.3.4 Optimisation

The optimisation process of the registration finds the transform minimising the evaluation function, that compares the observation image and the projected model. We kept the process as straight forward as possible and used a RGD. The optimisation process does not have any important influence on the overall process except on how fast it may converge to an acceptable result. However, the RGD is a proven optimisation process that gave good results for our application.

4.3.5 Visualisation

At the end of the framework, a visualisation process is applied to a selected model. Retrieving the information from the registration process, more specifically the transformation

output of the registration, both the 3-D model and the microscope observation are merged using Visual ToolKit (VTK)[1]. This time, the observation is transposed into the model space. The transformation obtained from the registration is applied to the model. Then both are displayed in the 3-D space of the model. By default, the best model is automatically displayed.

The visualisation has two purposes: First of all, it is used as a qualitative validation of the framework. Indeed, the difficulty to obtain a strong ground truth on our data, such as the position, size, and number of cells present in the observed neurosphere at each time step of the experiment, led us to a visual validation of the model through the user point of view. This validation is simple at early stage of the neurosphere development, but becomes more complicated with the complexification of the neurosphere structure. The second purpose is for information support. The first goal of our framework is to gather information on the structure of the neurosphere and its dynamism over time during the proliferation phase, the model generated can also but seen as a support for other process information such as a cell tracking or annotations from biologist.

4.4 Results and Analysis

We applied our framework on the different sequences for both *Training* and *Test* data sets. We first tried our approach using the random sphere generation process. The method was not adapted in term of speed, taking close to 10 minutes per images, principally due to the selection process over the large number of models. The results obtained on simple configuration were not satisfactory. However, in some cases, the process provided a model close to the observation. The regularity of these good results and the important cost in time, were not enough for a possible application but comfort us in the fact that our approach was viable. Helping us to identify the parts and problems of the current methodology to be improved.

[1]VTK - `www.vtk.org`

4.4.1 Evolution Process

We have run the framework off-line on a sequence of neurosphere forming processes. The *Training* data set does not have a structure that goes higher than 4-cell neurosphere. The *Test* data set has configuration reaching a higher number of divisions. In order to see any variation in the model generation process, we look for the list of best models generated and not just for the best model.

Over a Sequence

We have applied the process to different sequences, in order to observe the evolution of the model over a total sequence and with the growth of the neurosphere. We first applied it in a sequence of the *Training* data set, composed of 134 images that reach a 4-cell configuration (Fig. 4-5). The error is lower than 0.5 over the total sequence of the five best models. With some small variations, we do not see much difference between the different models, showing a similar convergence and results for the five best models. However, we can observe two types of variations: some isolated peaks of errors in the middle of the sequence, and some divergences of the model error at the end of the sequence. The isolated peaks are from a bad model result. The model converged to a close but not exact structure, resulting in a good but not perfect error value. The error variation at the end of the sequence is actually due to the increase of the number of cells leading to higher possible variation in the configuration of cells. The different models are reaching a similar configuration but with some small variation in terms of cells coordinates, especially in terms of depth.

We have run a similar process in a sequence from the *Training* data set, composed of 160 images that reach a 7-cell configuration (Fig. 4-6). Even if the sequence is coming from a different batch experiment, we can observe similar behaviour of the cells and the neurospheres that are observable in the *Training* data set. Isolated peaks appearing a different time step from one or two models, and small variations past the second division when reaching a 4-cell configuration. However, the process manages to keep a good score over the time and the number of cells. We can observe the same behaviour on another sequence from the *Test* data set (Fig. 4-7), similar to the previous one as it reaches a 8-cell

configuration.

At Precise Time Step

Looking only at the evolution of the error of the models does not tell us if the models are correct compared to the observation. In order to see the behaviour of the model, we looked at the model results at different specific times of various sequences.

At simple configuration, from 1-cell to 4-cell, the process converge nearly immediately to its minimum, with all the ten models reaching a score not higher than 0.1 (Fig. 4-8). Some variation in the depth of the cells can be observed but the tenth models are actually very similar to each other. This was expected as the number of cells does not allow much variation in the configuration and show a certain stability in term of convergence of the solution from the generation process.

On more complex structures, reaching 6-cell, even if slower, requiring more iterations to reach a minimum, the convergence is still acceptable in term of time. However, in the same case as for the 4-cell and lower, the process manages to generate configuration scores lower than 0.1 (Fig. 4-9b). We can start observing some wrong generated models appearing with the increase of complexity of the structure. Six over ten models are correct, but the four others (Fig. 4-9d, 4-9f, 4-9k, 4-9l) are close to the solution but not correct. They have correctly positioned cells in the x, y-plan,but appear to have a wrong depth position.

Still on 5-cell and 6-cell neurosphere, we have this time tested with a non-planar configuration, where one cell is out of focus, located in front. We managed again a relatively fast convergence to a 0.1 score or lower (Fig. 4-10b). However, in this case, the models generated vary more. Indeed, over the ten selected models, four models are considered as inaccurate (Fig. 4-10h, 4-10j, 4-10k, 4-10l) as they position all the cells at the same depth, and we do not detect the actual correct configuration. On the six other models, four are correctly generated (Fig. 4-10c, 4-10e, 4-10f, 4-10g). The two left models have the correct configuration but the position of the sixth cell is wrong. The last cell is positioned behind the five first cells and is not visible. This variation is mainly due to how we score the

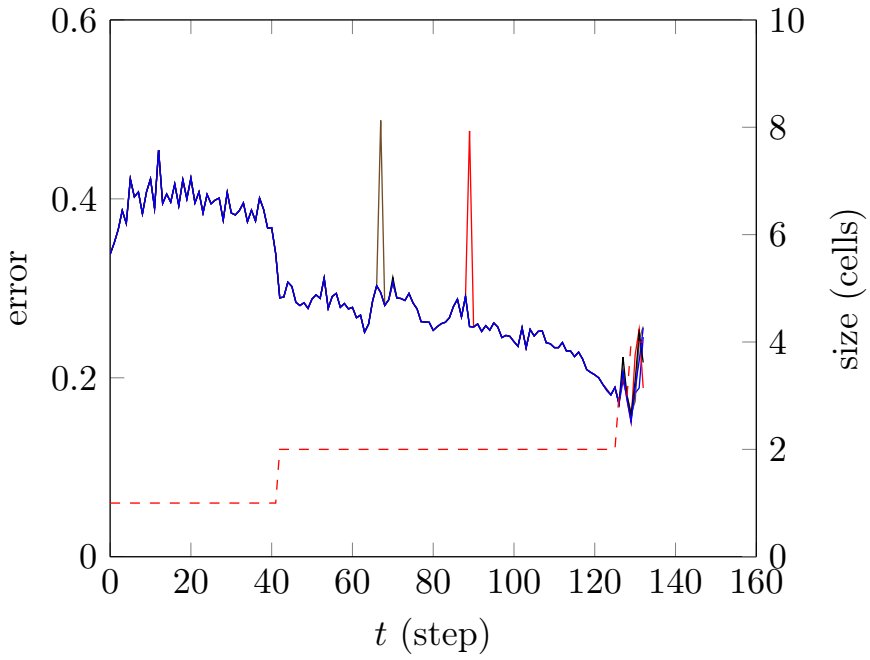

Figure 4-5: Evolution of the error on a five best evolution model over time and over the number of cells (in dashed red) on a sequence from the *Training* data set.

models, using the shape and the texture. Only the texture helps the positioning of the last cell and it seems to not always be enough to successfully place the cell on all the model.

4.4.2 Iterative Mesh Process

We tested the iterative mesh process on the same data set used for the evolution algorithm tests. First using the *Training* data set, then using the *Test* data set to observe the limits of the process.

Over a Sequence

First, on early stage sequence from the *Training* data set, containing low number of cells (Fig. 4-11). The overall results are better than the results of the evolutionary algorithm, with a lower error over the global sequence. This is due to the fact that the model's cells are, at the beginning of the growth, directly generated and positioned from the detected cells in the sequence. There positioning and size is therefore more accurate than the with the evolutionary algorithm. The high stability of the score over the sequence is due to the

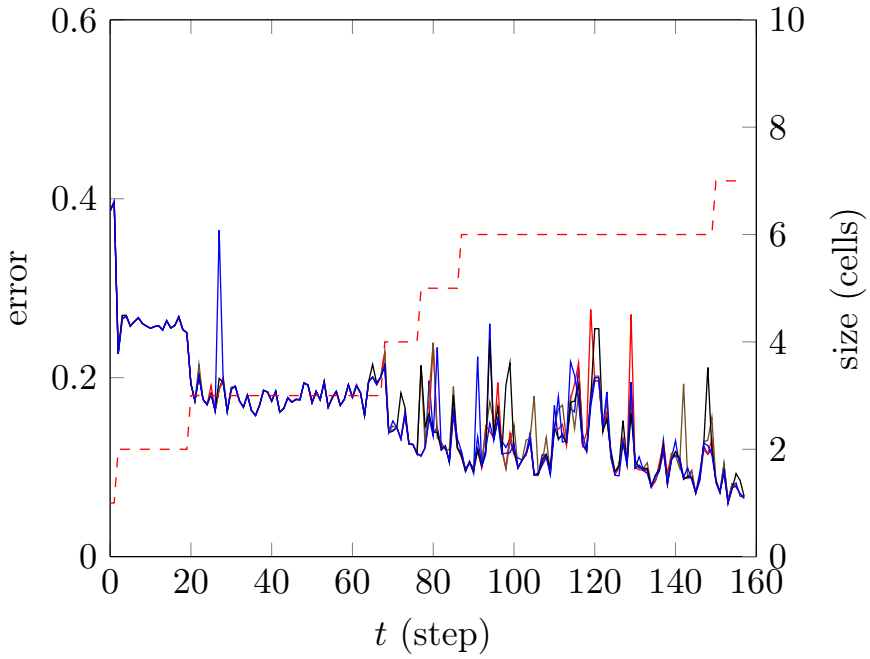

Figure 4-6: Evolution of the error on a five best evolution model over time and over the number of cells (in dashed red) on a sequence from the *Test* data set that reach a 7-cell configuration.

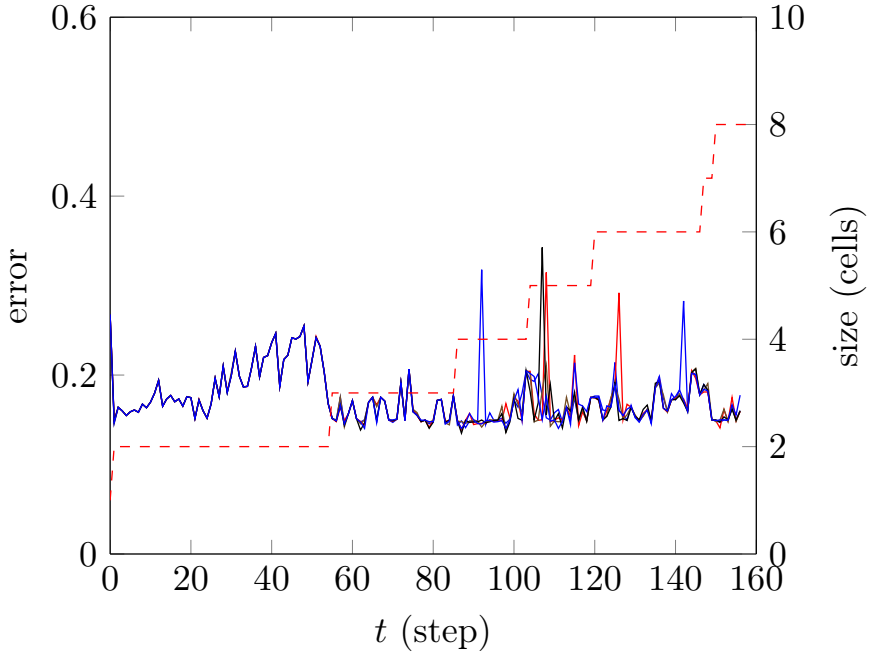

Figure 4-7: Evolution of the error on a five best evolution model over time and over the number of cells (in dashed red) on a sequence from the *Test* data set that reach a 8-cell configuration.

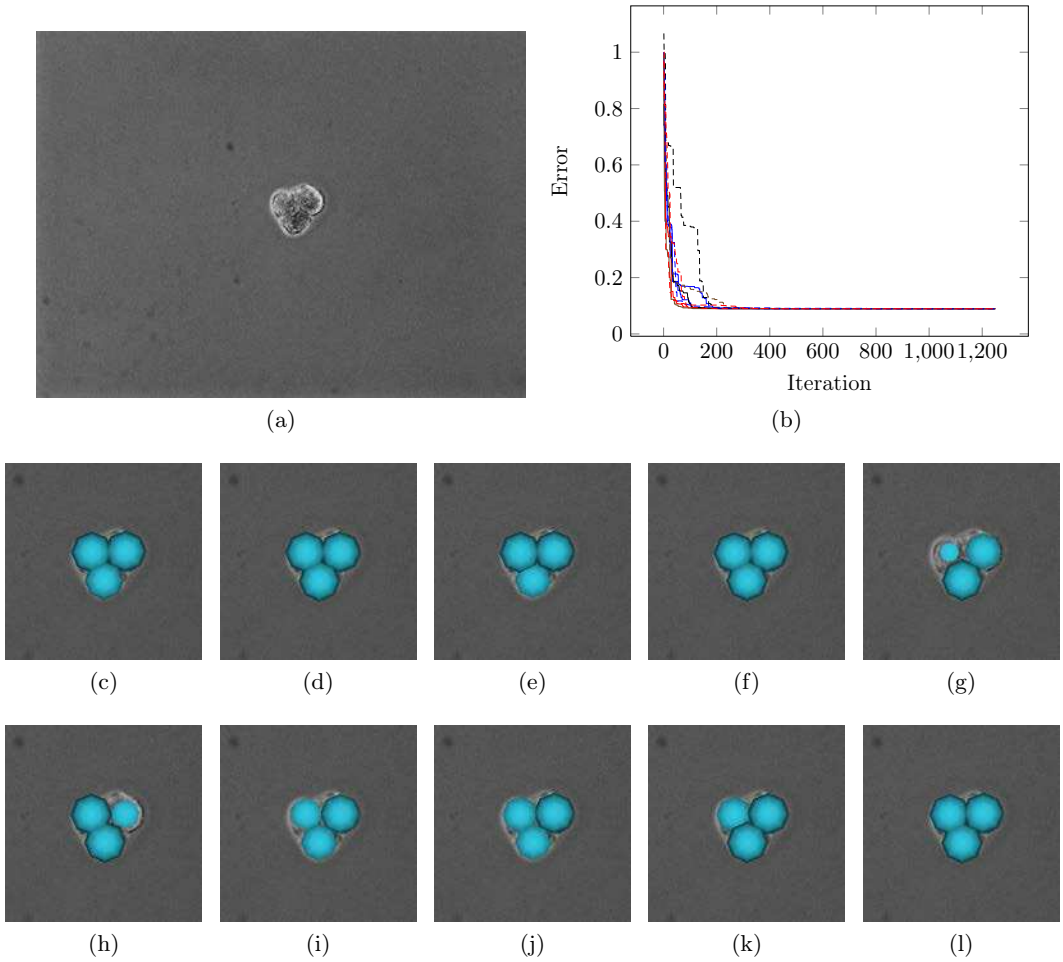

Figure 4-8: Ten model generated from the image (a) containing a 3-cell neurosphere. With the exception of the model (g), all the model are accurate in term of configuration.

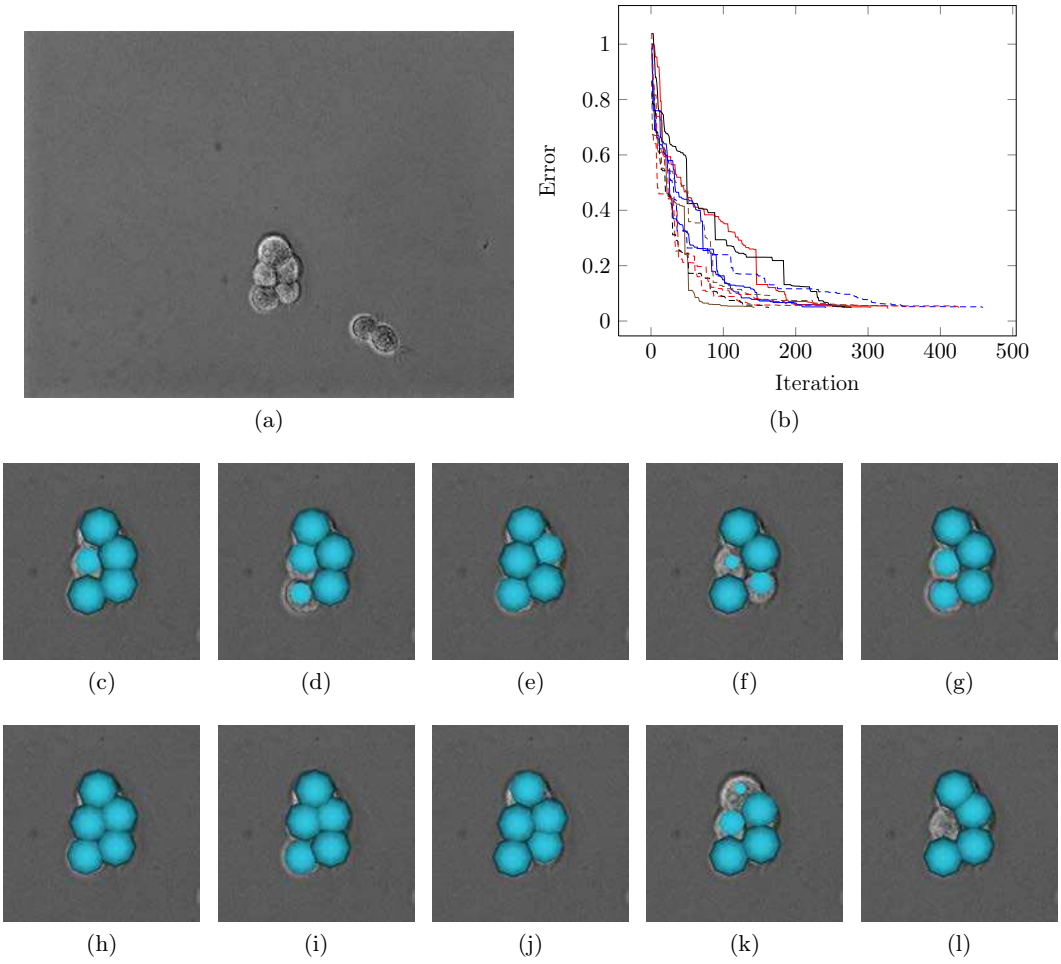

Figure 4-9: Ten models generated from the image (a) containing a 5-cell neurosphere. The majority of the models are correct, but the models (d), (f), (k) and (l) have one cell with a wrong depth position.

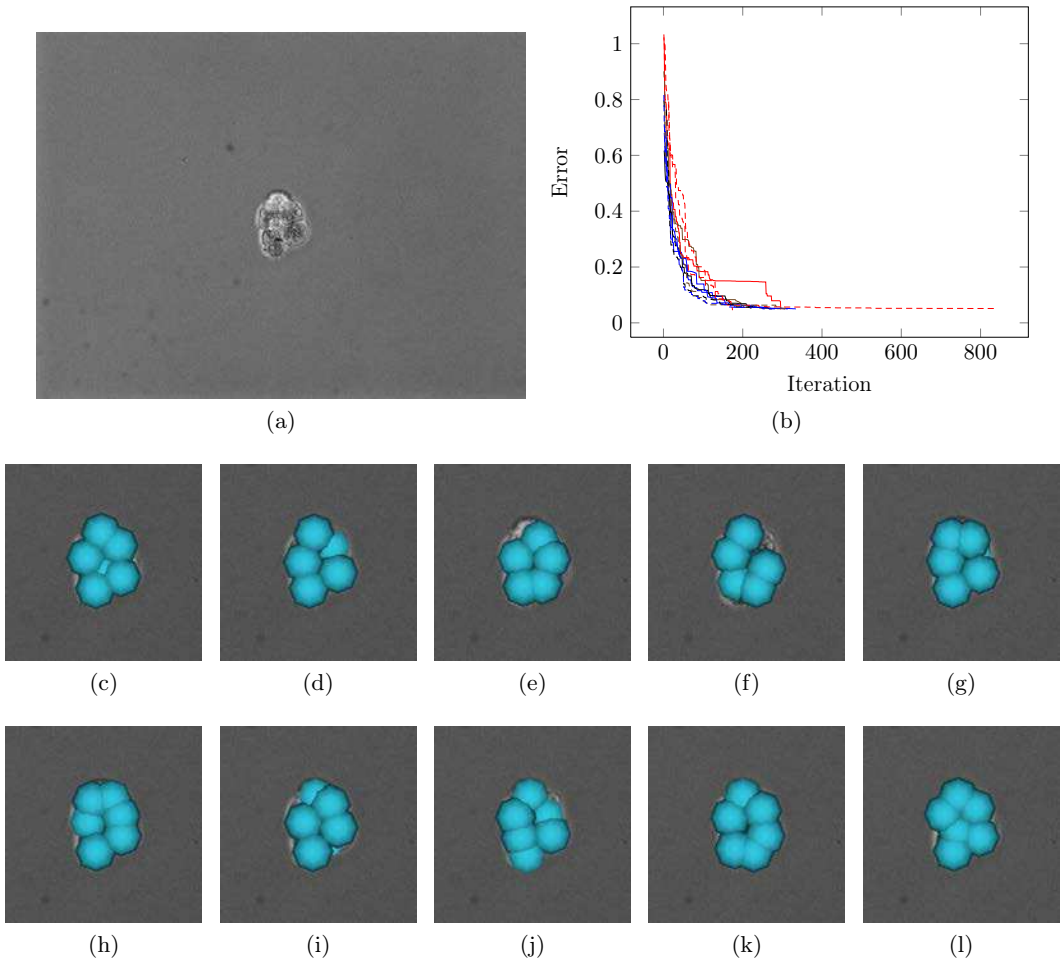

Figure 4-10: Ten best models generated from the observation (a) containing a 6-cell neurosphere. The results (c), (e), (f) and (g) are correct models with some acceptable variation on the position of the cells. (d) and (i) are not correct but still close to the actual cell configuration, with some depth value of cells not exact. (h), (j), (k) and (l) are too far from the correct configuration, in this case the six cells are on the same plan.

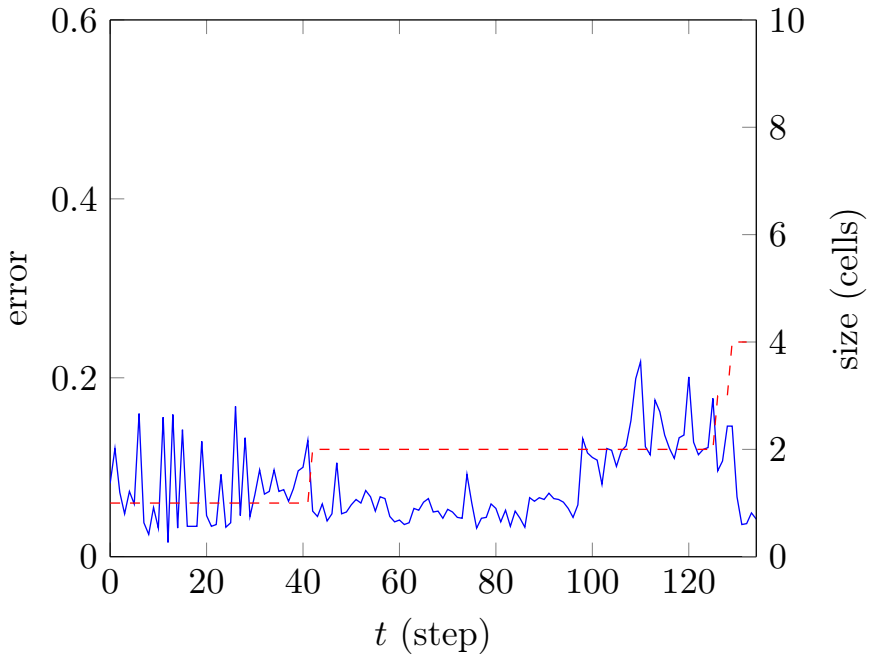

Figure 4-11: Evolution of the error on a mesh model over time and over the number of cells (in dashed red) on a sequence from the *Training* data set that reach a 4-cells configuration.

fact that, in opposition to the evolution process, the mesh is not generated in a random search but directly based on the previous step. Still some loss of precision is noticeable at similar steps where the evolution process failed.

We applied the same process to the *Test* data set which contains more advanced neurosphere configuration. Similar results than with the *Training* data set was observable at the beginning of the sequences. We see a low error at the beginning of the sequence, when the configuration remains simple. However, after reaching 5-cell configuration, the model has more difficulty fitting the observations as well as the evolution process (Fig. 4-12, 4-13). We can observe an increase of the error value when the configuration reaches 4-cell or higher.

At Precise Time Step

We observe some miss placement of one or two cells while reaching complex configuration, raising the error to more than 0.5 (Fig. 4-15a). This is due to the fact that, on the *Test* data set, the observable configurations does not seems as regular and organised

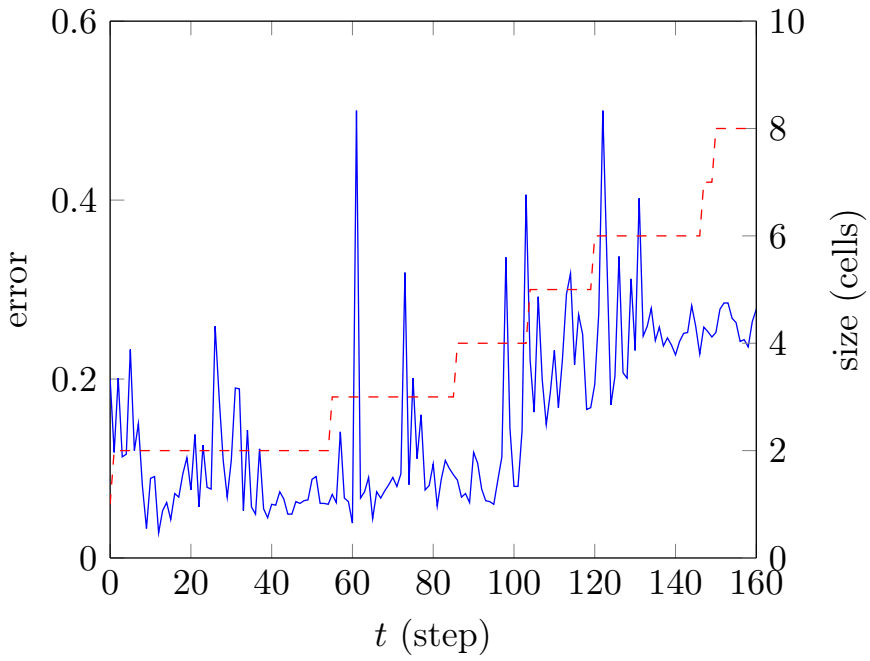

Figure 4-12: Evolution of the error on a mesh model over time and over the number of cells (in dashed red) on a sequence from the *Test* data set that reach a 8-cell configuration.

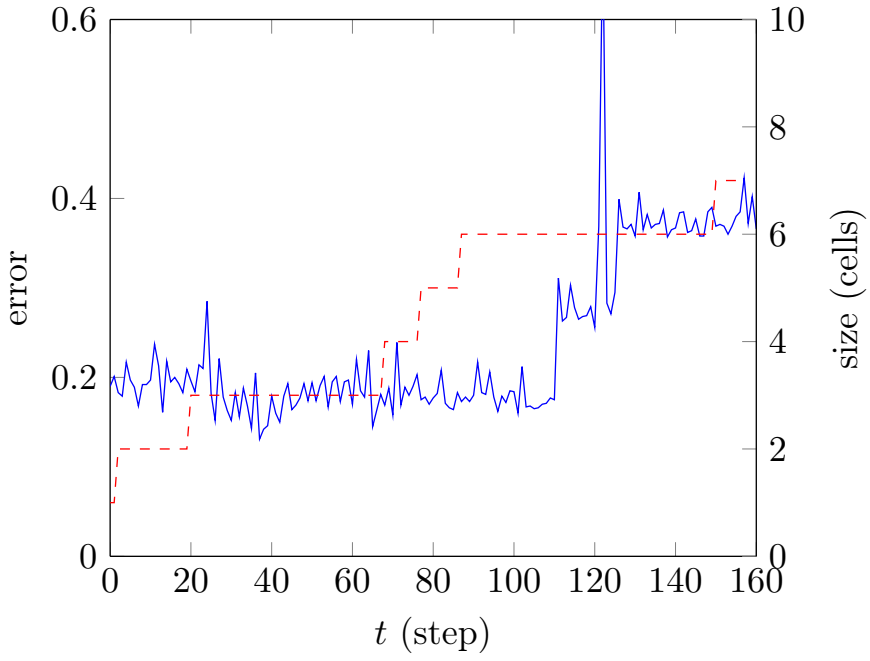

Figure 4-13: Evolution of the error on a mesh model over time and over the number of cells (in dashed red) on a sequence from the *Test* data set that reach a 8-cell configuration.

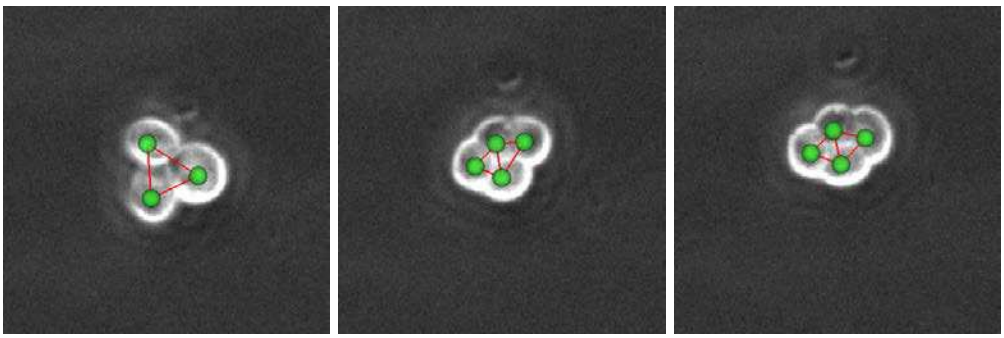

(a) (b) (c)

Figure 4-14: Iterative mesh model results on early stage neurospheres.

as we thought. The iterative mesh approach is following a regular construction that is guided through with the information extracted from the analysis module. The process is not adapted to chaotic structures that appear in the *Test* data set. Despite the increase of the error, the process still manage, when the configuration of the neurosphere return to a more regular aspect, to manage to fit the observation (Fig. 4-15b).

With those results, we can observe that the highly controlled Delaunay mesh structure is not enough flexible for our data. The rules that we have defined are well adapted for early stage, during which the proliferation seems to perfectly follow a regular pattern, but they are not fully adapted for later proliferation observation during which the structures appear to have various possible configurations that does not follow a regular growth. This loss of regularity can come from the fact that neurosphere are not only neural stem cells but also progenitor cells. They may not have the same time cycle and may divide much more rapidly than neural stem cell. In addition, a movement of the cells, internally of the neurosphere may be also a factor to this irregularity of the proliferation.

4.4.3 Parallel Model Synergism

In our initial observation of the neurosphere proliferation process, we assumed that the growth was following a development pattern. While this remains observable in most of the time, especially in early stage, our results shown that some unexpected configuration can be observed in some sequences. This is mostly due to possible events:

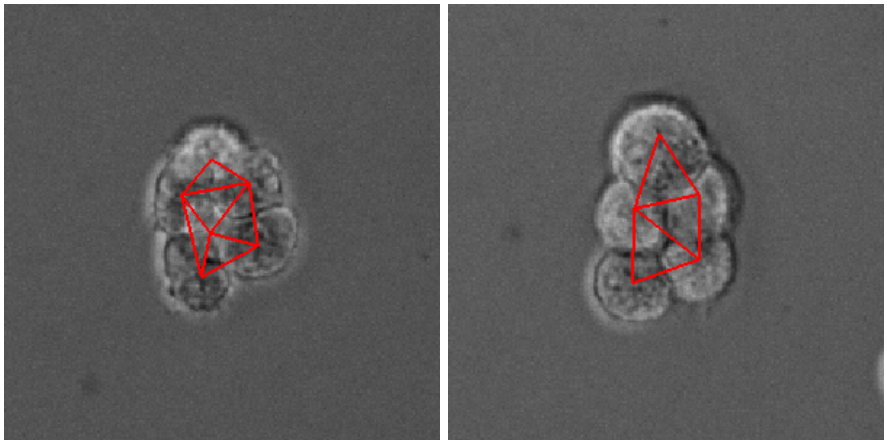

(a) (b)

Figure 4-15: Iterative mesh model results on early stage neurospheres.

- Cell movements inside the neurosphere.
- Different cell cycle between neural stem cells and neural progenitor cells.

Those events are currently not taken in consideration in our framework. The iterative mesh method shows very good results on early stage neurosphere, providing a dynamical construction of the model over time. However, due to the over control aspect of this method, the model does not manage to fit unexpected complex configurations, which does not follow the growth pattern related to the iterative mesh construction. The evolution algorithm process, based on a random search approach, is more flexible in terms of possible configurations. It shows good adaptation over the different sequences and manages to keep up with the different observed configurations even though this may not have followed a logical pattern development. However, this high adaptability is managed through the last of the dynamical aspect of the model construction.

A possible approach, using both models at the same time is considered (Fig. 4-16). The goal would be, at each step, to use both approaches to generate two models: one mesh model and one evolution model, both with their associated fitness score. Both would be compared, using an Iterative Closest Point (ICP) process or another meshes/points comparison approach, and validate each other. In the case of conflict, the model with the lowest fitness score takes over and the other model may be reprocessed in order to copy the

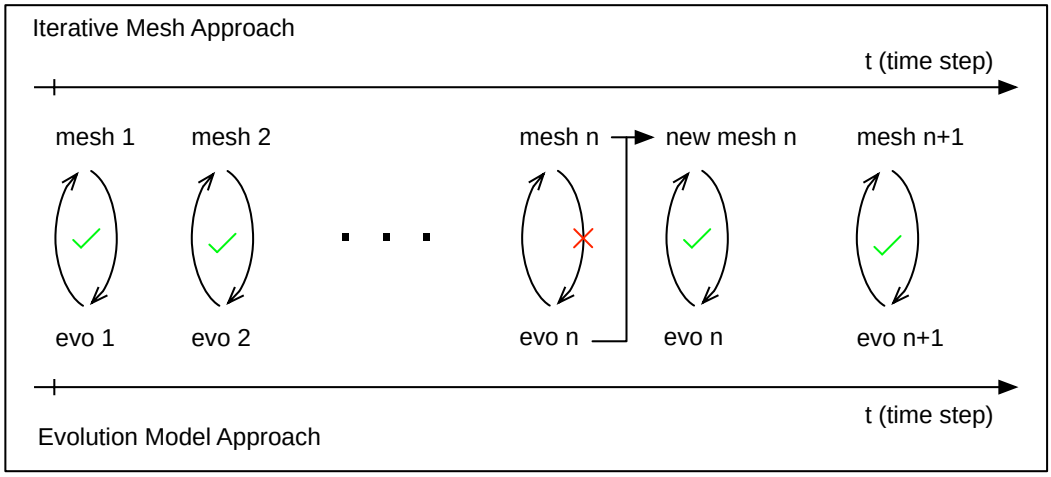

Figure 4-16: Iterative and evolution mutual validation process. Both models verify each other. If a model is discard, a new model is regenerated using the alternative approach as verification.

valid model. Both approaches would work in synergy, compensating each other downfalls.

4.5 Conclusion

We have presented the methodology of models scoring and selection using 3-D to 2-D registration method, by evaluating them according the shape and the texture of their projection into the microscope space. We observed the results provided by both of the two model generation methods described in the previous chapter. Even if, in terms of pure results, the evolution algorithm provides better overall results, especially on more complex configuration, the mesh structure model displayed some promising results and may be improved for higher complexity neurospheres. Through the visualisation step, the different results can be observed and evaluated by the biologist, who could use the proposed method as an augmented reality observation and validation support.

Conclusion and Outlooks

Conclusion

In this study, we have been working on elaborating a framework solution for the visualisation and the monitoring of neural stem cells and their proliferation into neurosphere, through the NFA experiment. The NFA has proven to be an important part of the neural stem cells research field, providing to the biologist a culture protocol and also a test experiment for screening possible drugs and behaviour analysis. The recent evolutions in NFA researches have shown important impacts on brain cancer research and on regenerative medicine solution for brain injuries or degenerative diseases. From these evolutions, we deduce the need of improving the research on neural stem cells through exploring new aspects of the field and developing new tools for their analysis.

Even though different cell analysis solutions already exist in the literature, most of them are either adapted for already differentiated progenitor cells, or are elaborated for flat culture experiment. These experiments, as they force the cells on a flat structure, do not allow a clear observation of their proliferation, and may also modify their global behaviour. With the collaboration of the Institute of Medical Biology and the Institute of Bio-Informatics of Singapore, we explored the development of new solutions for the observation and analysis of neural stem cells in floating culture, through the NFA. This work was carried on in the context of the IVS4NCS project[2], an 3 years A*STAR JCO project between the Institute of Medical Biology, the Bio-Informatics Institute and the Institute Infocomm Research, from which the Image and Pervasive Access Laboratory is part of, focusing on the development and deployment of observation and analysis solutions, adapted to the NFA.

In the context of this project, we have conceived and implemented an innovative framework for the observation of neurosphere formation and the extraction of the cells configuration through a 2-D to 3-D modelling process. Using registration and comparison process, this framework is build on merging 2-D and 3-D information. The 2-D information is extracted directly from the microscope monitoring the NFA using image processing and

[2]IVS4NSC - Intelligent Biomedical Vision System: `http://ipal.cnrs.fr/project/ivs4nsc-intelligent-biomedical-vision-system`

analysis methods. The 3-D information is generated from a set of *prior* knowledge defined from the biologist observations and knowledge of the NFA experiment using computer graphics and modelling solutions. The main goal on which we have focused in this thesis is the extraction of a model structure that fits the observations of the neurosphere, either off-line from a previous NFA experiment, or in real time during the experiment. The model extracted through this approach may be use for the elaboration of a database of neurosphere configuration for possible research and analysis. The model as more globally, the framework, provide also the possibility of visualisation for direct monitoring for the biologist and a display support for other process applied during the experiment, such as tracking, mitosis activity, and so on.

The framework is composed of three modules: analysis, synthesis and selection. The analysis module, in charge of extracting the 2-dimensional information from the microscope image, regroups a set of image processing methods. First, an image reconstruction process first proposed by Li *et.al.* [59], based on the phase contrast physics, generating an artefacts free image with an improved contrast, facilitating the segmentation and detection process that will follow. Second, a detection algorithm for highly clustered cell was developed, using the global shape of the cluster and partial circular boundaries of the cluster to detect the position of the cells. The synthesis module is in charge of generating all possible configuration solutions, using the information extracted from the analysis module, such as the number of cells present at a certain time, and the *prior* knowledge brought by the biologist. We came with two possible processes for the model generation: one using an evolution algorithm and another one based on an iterative mesh construction. Both have different advantages and interests. The evolution algorithm, through the flexibility and adaptation of his nature, manages to adapt and to provide interesting results, even with unexpected configuration of neurospheres. The iterative mesh structure, through the Delaunay lattice, gave a more controlled construction of the model, with an important topological information linked to its generation. In both cases, a set of possible models that can fit the current observation, is defined. The selection process is the final process that will select the best-generated model, by comparing, using registration methods, each model to the observation and by ranking, based on how close they are, to the reality. The

comparison is done through shape and texture comparison. The registration allows a fusion of both the microscopic image and the model, for visualisation and validation.

In summary, this work presents an innovative framework for:

- The monitoring of the NFA experiment;
- The extraction of neurosphere configuration over time for future analysis;
- A platform for neurosphere visualisation and the incorporation of future NFA analysis tools (tracking, *etc.*).

For the elaboration of this framework, we proposed:

- A new method for high clustered cells detection under phase contrast microscopy;
- Two modelling generation algorithms for neurospheres:
  - using Evolution Algorithm;
  - using Delaunay / Voronoi lattice.
- A registration process from 3-D to 2-D base on shape and textural information.

Outlooks

The modelling framework has been applied to different sets of neurosphere proliferation, generated by the Institute of Medical Biology, provided accurate and interesting results.

With both the evolution algorithm and the mesh construction, our process is either very flexible with few control, or highly controllable but with low flexibility. A mix of both would be a good possible solution to develop in a near future. The detection of clustered cells, providing good results on our data, could be adapted to manage the ellipsoidal structure, in order to be used in different cell detection applications.

On a longer perspective, now that a solution is given to extract the configuration of neurosphere, a database of neurosphere evolution can be built in order to determine

a possible relation between the configuration at early stage and the survivability of the neurosphere over time. Similar studies can be done to determine the possible effects of drugs on the proliferation and structural aspect of the neurosphere.
Also, the model provides a perfect visualisation for future processing, such as cells tracking and lineage tracing. The improvement of the NFA protocol can also lead to the possibility of using fluorescence information.

A new A*STAR JCO Grant Integrated Autonomous Microscopy Systems project[3], regrouping the Institute of Medical Biology, the Bio-Informatics Institute and the Institute for Infocomm Research which the Image and Pervasive Access Laboratory is part of, was launched in the continuity of the previous one. This new project focuses on more generic 3-D microscopy in order to propose new opportunities of application and evolution to the framework, through the use of a light sheet modality. It will continue to focus on stem cell research, as they represent an important field of research, but will stay flexible to different type of stem cells and not only neural stem cells.

[3]IAMS - `http://www.ipal.cnrs.fr/project/iams-integrated-autonomous-microscopy-systems`

Bibliography

[1] Sohail Ahmed. The culture of neural stem cells. *Journal of cellular biochemistry*, 106(1):1–6, 2009.

[2] Omar Al-Kofahi, Richard J Radke, Susan K Goderie, Qin Shen, Sally Temple, and Badrinath Roysam. Automated cell lineage construction: A rapid method to analyze clonal development established with murine neural progenitor cells. *Cell Cycle*, 5(3):327–335, 2006.

[3] F. Ambriz-Colin, M. Torres-Cisneros, J.G. Avina-Cervantes, J. E. Saavedra-Martinez, O. Debeir, and J.J. Sanchez-Mondragon. Detection of biological cells in phase-contrast microscopy images. In *Artificial Intelligence, 2006. MICAI '06. Fifth Mexican International Conference on*, pages 68–77, 2006.

[4] A. Arvidsson, T. Collin, D. Kirik, Z. Kokaia, and O. Lindvall. Neuronal replacement from endogenous precursors in the adult brain after stroke. *Nature medicine*, 8(9):963–970, 2002.

[5] M. Athelogou, M. Eblenkamp, G. Schmidt, F. Novotny, E. Wintermantel, and G. Binnig. Single-cell detection and classification in phase contrast images. In *Information Technology and Applications in Biomedicine (ITAB), 2010 10th IEEE International Conference on*, pages 1–4, 2010.

[6] J.G. Avia-Cervantes, M. Torres-Cisneros, F. Ambriz-Colin, O. Debeir, and J.J. Sanchez-Mondragon. Detection of biological cells in phase-contrast video microscopy. In *Electronics and Photonics, 2006. MEP 2006. Multiconference on*, pages 239–243, 2006.

[7] Hassan Azari, Sharon A Louis, Sharareh Sharififar, Vinata Vedam-Mai, and Brent A Reynolds. Neural-colony forming cell assay: an assay to discriminate bona fide neural stem cells from neural progenitor cells. *Journal of visualized experiments: JoVE*, (49), 2011.

[8] Hassan Azari, Maryam Rahman, Sharareh Sharififar, and Brent A. Reynolds. Isolation and expansion of the adult mouse neural stem cells using the neurosphere assay. *Journal of visualized experiments: JoVE*, 45, 2010.

[9] Hassan Azari, Sharareh Sharififar, Maryam Rahman, Saeed Ansari, Brent A Reynolds, et al. Establishing embryonic mouse neural stem cell culture using the neurosphere assay. *Journal of visualized experiments: JoVE*, 47, 2011.

[10] Simon Baker, Takeo Kanade, et al. Shape-from-silhouette across time part i: Theory and algorithms. *International Journal of Computer Vision*, 62(3):221–247, 2005.

[11] D.H. Ballard. Generalizing the hough transform to detect arbitrary shapes. *Pattern Recognition*, 13(2):111 – 122, 1981.

[12] Zhirong Bao, John I. Murray, Thomas Boyle, Siew Loon Ooi, Matthew J. Sandel, and Robert H. Waterston. Automated cell lineage tracing in caenorhabditis elegans. *Proceedings of the National Academy of Sciences of the United States of America*, 103(8):2707–2712, 2006.

[13] Britta Basse, Bruce C. Baguley, Elaine S. Marshall, Wayne R. Joseph, Bruce van Brunt, Graeme Wake, and David J. N. Wall. A mathematical model for analysis of the cell cycle in cell lines derived from human tumors. *Journal of Mathematical Biology*, 47(4):295–312, 2003.

[14] Andrew J. Becker, Ernest A. McCulloch, and James E. Till. Cytological demonstration of the clonal nature of spleen colonies derived from transplanted mouse marrow cells. *Nature*, 197(4866):452–454, 1963.

[15] Savile Bradbury and Brian Bracegirdle. *Introduction to light microscopy*. Bios Scientific Publishers, 1998.

[16] Lisa Gottesfeld Brown. A survey of image registration techniques. *ACM Comput. Surv.*, 24(4):325–376, 1992.

[17] Vicent Caselles, Ron Kimmel, and Guillermo Sapiro. Geodesic active contours. *International journal of computer vision*, 22(1):61–79, 1997.

[18] Ying Chen, Ena Ladi, Paul Herzmark, Ellen Robey, and Badrinath Roysam. Automated 5-d analysis of cell migration and interaction in the thymic cortex from time-lapse sequences of 3-d multi-channel multi-photon images. *Journal of Immunological Methods*, 340(1):65 – 80, 2009.

[19] Jierong Cheng and J.C. Rajapakse. Segmentation of clustered nuclei with shape markers and marking function. *Biomedical Engineering, IEEE Transactions on*, 56(3):741–748, 2009.

[20] Shao-Yi Chien, Shyh-Yih Ma, and Liang-Gee Chen. Efficient moving object segmentation algorithm using background registration technique. *Circuits and Systems for Video Technology, IEEE Transactions on*, 12(7):577–586, 2002.

[21] Andrew R Cohen, Francisco L A F Gomes, Badrinath Roysam, and Michel Cayouette. Computational prediction of neural progenitor cell fates. *Nat Meth*, 7(3):213–218, 2010.

[22] C.M. Cyr, A.F. Kamal, T.B. Sebastian, and B.B. Kimia. 2d-3d registration based on shape matching. In *Mathematical Methods in Biomedical Image Analysis, 2000. Proceedings. IEEE Workshop on*, pages 198–203, 2000.

[23] Ondřej Daněk, Pavel Matula, Carlos Ortiz-de Solórzano, Arrate Muñoz-Barrutia, Martin Maška, and Michal Kozubek. Segmentation of touching cell nuclei using a two-stage graph cut model. In Arnt-Børre Salberg, JonYngve Hardeberg, and Robert Jenssen, editors, *Image Analysis*, volume 5575 of *Lecture Notes in Computer Science*, pages 410–419. Springer Berlin Heidelberg, 2009.

[24] Jesse Davis and Mark Goadrich. The relationship between precision-recall and roc curves. In *Proceedings of the 23rd International Conference on Machine Learning*, ICML '06, pages 233–240. ACM, 2006.

[25] Mark De Berg, Otfried Cheong, Marc van Kreveld, and Mark Overmars. *Computational geometry*. Springer, 2008.

[26] O. Debeir, P. Van Ham, R. Kiss, and C. Decaestecker. Tracking of migrating cells under phase-contrast video microscopy with combined mean-shift processes. *Medical Imaging, IEEE Transactions on*, 24(6):697–711, 2005.

[27] Boris Delaunay. Sur la sphere vide. *Izv. Akad. Nauk SSSR, Otdelenie Matematicheskii i Estestvennyka Nauk*, 7(793-800):1–2, 1934.

[28] Loic P Deleyrolle, Geoffery Ericksson, Brian J Morrison, J Alejandro Lopez, Kevin Burrage, Pamela Burrage, Angelo Vescovi, Rodney L Rietze, and Brent A Reynolds. Determination of somatic and cancer stem cell self-renewing symmetric division rate using sphere assays. *PLoS One*, 6(1):e15844, 2011.

[29] Loic P Deleyrolle and Brent A Reynolds. Identifying and enumerating neural stem cells: application to aging and cancer. *Prog Brain Res*, 175:43–51, 2009.

[30] Loic P Deleyrolle and Brent A Reynolds. Isolation, expansion, and differentiation of adult mammalian neural stem and progenitor cells using the neurosphere assay. *Methods Mol Biol*, 549:91–101, 2009.

[31] Olivier Devillers, Sylvain Pion, and Monique Teillaud. Walking in a triangulation. *International Journal of Foundations of Computer Science*, 13(02):181–199, 2002.

[32] A. Dufour, V. Shinin, S. Tajbakhsh, N. Guillen-Aghion, J-C Olivo-Marin, and C. Zimmer. Segmenting and tracking fluorescent cells in dynamic 3-d microscopy with coupled active surfaces. *Image Processing, IEEE Transactions on*, 14(9):1396–1410, 2005.

[33] O. Dzyubachyk, W.A. Van Cappellen, J. Essers, W.J. Niessen, and E. Meijering. Advanced level-set-based cell tracking in time-lapse fluorescence microscopy. *Medical Imaging, IEEE Transactions on*, 29(3):852–867, 2010.

[34] I. Ersoy, F. Bunyak, M. A. Mackey, and K. Palaniappan. Cell segmentation using hessian-based detection and contour evolution with directional derivatives. In *Image Processing, 2008. ICIP 2008. 15th IEEE International Conference on*, pages 1804–1807, 2008.

[35] M. J. Evans and M. H. Kaufman. Establishment in culture of pluripotential cells from mouse embryos. *Nature*, 292:154–156, 1981.

[36] E.I. Fomchenko and E.C. Holland. Origins of brain tumors? A disease of stem cells? *Nature Clinical Practice Neurology*, 2(6):288–289, 2006.

[37] Steven Fortune. A sweepline algorithm for voronoi diagrams. *Algorithmica*, 2(1-4):153–174, 1987.

[38] Alexandre Gouaillard, Leonardo Florez-Valencia, and Eric Boix. Itkquadedgemesh: A discrete orientable 2-manifold data structure for image processing. *The Insight Journal*, 2006.

[39] Leo J. Guibas and Jorge Stolfi. Primitives for the manipulation of general subdivisions and the computation of voronoi diagrams. In *Proceedings of the fifteenth annual ACM symposium on Theory of computing*, STOC '83, pages 221–234, New York, NY, USA, 1983. ACM.

[40] John W. Haycock. 3d cell culture: A review of current approaches and techniques. In John W. Haycock, editor, *3D Cell Culture*, volume 695 of *Methods in Molecular Biology*, pages 1–15. Humana Press, 2011.

[41] M. Holden. A review of geometric transformations for nonrigid body registration. *Medical Imaging, IEEE Transactions on*, 27(1):111–128, 2008.

[42] Chao-Hui Huang, S. Sankaran, D. Racoceanu, S. Hariharan, and S. Ahmed. Online 3-d tracking of suspension living cells imaged with phase-contrast microscopy. *Biomedical Engineering, IEEE Transactions on*, 59(7):1924–1933, 2012.

[43] Seungil Huh and Mei Chen. Detection of mitosis within a stem cell population of high cell confluence in phase-contrast microscopy images. In *Computer Vision and Pattern Recognition (CVPR), 2011 IEEE Conference on*, pages 1033–1040, 2011.

[44] Seungil Huh, D.F.E. Ker, R. Bise, Mei Chen, and T. Kanade. Automated mitosis detection of stem cell populations in phase-contrast microscopy images. *Medical Imaging, IEEE Transactions on*, 30(3):586–596, 2011.

[45] William M. Wells III, Paul Viola, Hideki Atsumi, Shin Nakajima, and Ron Kikinis. Multi-modal volume registration by maximization of mutual information. *Medical Image Analysis*, 1(1):35 – 51, 1996.

[46] J. Illingworth and J. Kittler. A survey of the hough transform. *Computer Vision, Graphics, and Image Processing*, 44(1):87 – 116, 1988.

[47] Humayun Irshad, Stéphane U. Rigaud, and Alexandre Gouaillard. Primal/dual mesh with application to triangular/simplex mesh and delaunay/voronoi. *Insight Journal*, 2012.

[48] Chanho Jung and Changick Kim. Segmenting clustered nuclei using h-minima transform-based marker extraction and contour parameterization. *Biomedical Engineering, IEEE Transactions on*, 57(10):2600–2604, 2010.

[49] Bradley A. Justice, Nadia A. Badr, and Robin A. Felder. 3d cell culture opens new dimensions in cell-based assays. *Drug Discovery Today*, 14(1–2):102 – 107, 2009.

[50] Jos Käfer. Des cellules aux tissus : modélisation physique du comportement collectif des cellules embryonnaires des cellules aux tissus : modélisation physique du comportement collectif des cellules embryonnaires, 2008.

[51] Ruth L Kirschstein and Lana R Skirboll. *Stem cells: scientific progress and future research directions*. National Institutes of Health, Department of Health and Human Services, 2001.

[52] Hiroaki Kobayashi, I. Ishimaru, Ryoji Hyodo, Toshiki Yasokawa, Katsumi Ishizaki, Shigeki Kuriyama, Tsutomu Masaki, Seiji Nakai, Kaoru Takegawa, and Naotaka Tanaka. A precise method for rotating single cells. *Applied Physics Letters*, 88(13):131103–131103–2, 2006.

[53] Hiroaki Kobayashi, Ichirou Ishimaru, Toshiki Yasokawa, Katsumi Ishizaki, Shigeki Kuriyama, Tsutomu Masaki, Seiji Nakai, Kaoru Takegawa, and Naotaka Tanaka. Three-dimensional phase-contrast imaging of single floating cells. *Applied Physics Letters*, 89(24):241117, 2006.

[54] Panos D Kotsas and Tony Dodd. A review of methods for 2d/3d registration. *Word Academy of Science, Engineering and Technology*, 59:606–609, 2011.

[55] Geo Leach. Improving worst-case optimal delaunay triangulation algorithms. In *4th Canadian Conference on Computational Geometry*, pages 340–346. Citeseer, 1992.

[56] Jungwoo Lee, Meghan J Cuddihy, and Nicholas A Kotov. Three-dimensional cell culture matrices: state of the art. *Tissue Engineering Part B: Reviews*, 14(1):61–86, 2008.

[57] JPl Lewis. Fast template matching. In *Vision Interface*, volume 95, pages 15–19, 1995.

[58] Kang Li, Mei Chen, Takeo Kanade, Eric D Miller, Lee E Weiss, and Phil G Campbell. Cell population tracking and lineage construction with spatiotemporal context. *Medical image analysis*, 12(5):546, 2008.

[59] Kang Li and Takeo Kanade. Nonnegative mixed-norm preconditioning for microscopy image segmentation. In JerryL. Prince, DzungL. Pham, and KyleJ. Myers, editors, *Information Processing in Medical Imaging*, volume 5636 of *Lecture Notes in Computer Science*, pages 362–373. Springer Berlin Heidelberg, 2009.

[60] L. A G Lin, A.Q. Liu, Y. F. Yu, C. Zhang, C. S. Lim, S. H. Ng, P. H. Yap, and H. J. Gao. Cell compressibility studies utilizing noncontact hydrostatic pressure measurements on single living cells in a microchamber. *Applied Physics Letters*, 92(23):233901–233901–3, 2008.

[61] M. Lorenzo-Valdés, G.I. Sanchez-Ortiz, R. Mohiaddin, and D. Rueckert. Atlas-based segmentation and tracking of 3d cardiac mr images using non-rigid registration. In *Medical Image Computing and Computer-Assisted Intervention — MICCAI*, volume 2488 of *Lecture Notes in Computer Science*, pages 642–650. Springer Berlin Heidelberg, 2002.

[62] Valentin Lulevich, Tiffany Zink, Huan-Yuan Chen, Fu-Tong Liu, and Gang-yu Liu. Cell mechanics using atomic force microscopy-based single-cell compression. *Langmuir*, 22(19):8151–8155, 2006.

[63] JB Antoine Maintz and Max A Viergever. An overview of medical image registration methods. *UU-CS*, (1998-22), 1998.

[64] R. Malladi, J.A. Sethian, and B.C. Vemuri. Shape modeling with front propagation: a level set approach. *Pattern Analysis and Machine Intelligence, IEEE Transactions on*, 17(2):158–175, 1995.

[65] A. Manzanera and J.C. Richefeu. A new motion detection algorithm based on $\sigma - \delta$ background estimation. *Pattern Recognition Letter*, 28(3):320–328, 2007.

[66] P. Markelj, D. Tomaževič, B. Likar, and F. Pernuš. A review of 3d/2d registration methods for image-guided interventions. *Medical Image Analysis*, 16(3):642 – 661, 2012. <ce:title>Computer Assisted Interventions</ce:title>.

[67] M. Marques and J. Costeira. Optimal shape from motion estimation with missing and degenerate data. In *Motion and video Computing, 2008. WMVC 2008. IEEE Workshop on*, pages 1–6, 2008.

[68] Manuel Marques and João Costeira. Estimating 3d shape from degenerate sequences with missing data. *Computer Vision and Image Understanding*, 113(2):261 – 272, 2009.

[69] Tim McInerney and Demetri Terzopoulos. Deformable models in medical image analysis: a survey. *Medical Image Analysis*, 1(2):91 – 108, 1996.

[70] E. Meijering. Cell segmentation: 50 years down the road. *Signal Processing Magazine, IEEE*, 29(5):140–145, 2012.

[71] Jorge J Moré. The levenberg-marquardt algorithm: implementation and theory. In *Numerical analysis*, pages 105–116. Springer, 1978.

[72] B. Moreau and A. Gouaillard. Exact geometrical predicate: Point in circle. *Insight Journal*, 2011.

[73] A.Y. Mulayim, U. Yilmaz, and V. Atalay. Silhouette-based 3-d model reconstruction from multiple images. *Systems, Man, and Cybernetics, Part B: Cybernetics, IEEE Transactions on*, 33(4):582–591, 2003.

[74] Wolfgang Niem. Error analysis for silhouette-based 3d shape estimation from multiple views. In *Proc. Int. Workshop on Synthetic-Natural Hybrid Coding and Three-Dimensional Imaging*, 1997.

[75] Björn Nilsson and Anders Heyden. Segmentation of complex cell clusters in microscopic images: Application to bone marrow samples. *Cytometry Part A*, 66A(1):24–31, 2005.

[76] J. Orikawa and T. Tanaka. Cell segmentation from phase-contrast images using hybrid watershed and region growing algorithm for genomic drug discovery. In *SICE Annual Conference 2010, Proceedings of*, pages 84–88, 2010.

[77] Nobuyuki Otsu. A threshold selection method from gray-level histograms. *Automatica*, 11(285-296):23–27, 1975.

[78] P. Perona and J. Malik. Scale-space and edge detection using anisotropic diffusion. *Pattern Analysis and Machine Intelligence, IEEE Transactions on*, 12(7):629–639, 1990.

[79] Steven M. Pollard, Koichi Yoshikawa, Ian D. Clarke, Davide Danovi, Stefan Stricker, Roslin Russell, Jane Bayani, Renee Head, Marco Lee, Mark Bernstein, Jeremy A. Squire, Austin Smith, and Peter Dirks. Glioma stem cell lines expanded in adherent culture have tumor-specific phenotypes and are suitable for chemical and genetic screens. *Cell Stem Cell*, 4(6):568–580, 2009.

[80] Przemyslaw Prusinkiewicz. Modeling plant growth and development. *Current Opinion in Plant Biology*, 7(1):79 – 83, 2004.

[81] Przemyslaw Prusinkiewicz and Anne-Gaëlle Rolland-Lagan. Modeling plant morphogenesis. *Current Opinion in Plant Biology*, 9(1):83 – 88, 2006.

[82] Maryam Rahman, Loic Deleyrolle, Vinata Vedam-Mai, Hassan Azari, Muhammad Abd-El-Barr, and Brent A Reynolds. The cancer stem cell hypothesis: failures and pitfalls. *Neurosurgery*, 68(2):531–545, 2011.

[83] B A Reynolds and S Weiss. Generation of neurons and astrocytes from isolated cells of the adult mammalian central nervous system. *Science*, 255(5052):1707–1710, 1992.

[84] Brent A Reynolds and Rodney L Rietze. Neural stem cells and neurospheres[mdash]re-evaluating the relationship. *Nat Meth*, 2(5):333–336, 05 2005.

[85] Brent A Reynolds and Angelo L Vescovi. Brain cancer stem cells: Think twice before going flat. *Cell Stem Cell*, 5(5):466–467, Nov 2009.

[86] J.C. Richefeu and A. Manzanera. A new hybrid differential filter for motion detection. *Computer Vision and Graphic*, pages 727–732, 2006.

[87] Rodney L. Rietze and Brent A. Reynolds. Neural stem cell isolation and characterization. In *Adult Stem Cells*, volume 419 of *Methods in Enzymology*, pages 3 – 23. Academic Press, 2006.

[88] Stéphane U. Rigaud and Alexandre Gouaillard. Incremental delaunay triangulation. *Insight Journal*, 2012.

[89] Stéphane U. Rigaud and Alexandre Gouaillard. Walk in a triangulation: Straight walk. *Insight Journal*, 2012.

[90] P.K Sahoo, S Soltani, and A.K.C Wong. A survey of thresholding techniques. *Computer Vision, Graphics, and Image Processing*, 41(2):233 – 260, 1988.

[91] S. Sakuma and T. Tanaka. Cell extraction method from phase contrast microscopy image. In *SICE Annual Conference (SICE), 2011 Proceedings of*, pages 1485–1488, 2011.

[92] Jeremy B Sanderson. *Phase Contrast Microscopy*. John Wiley & Sons, Ltd, 2001.

[93] B Segre and K Mahler. On the densest packing of circles. *The American Mathematical Monthly*, 51(5):261–270, 1944.

[94] Jonathan Richard Shewchuk. Adaptive precision floating-point arithmetic and fast robust geometric predicates. *Discrete & Computational Geometry*, 18:305–363, 1997.

[95] Kazutoshi Takahashi and Shinya Yamanaka. Induction of pluripotent stem cells from mouse embryonic and adult fibroblast cultures by defined factors. *Cell*, 126(4):663–676, 2006.

[96] P. Thevenaz, R. Delgado-Gonzalo, and M. Unser. The ovuscule. *Pattern Analysis and Machine Intelligence, IEEE Transactions on*, 33(2):382–393, 2011.

[97] Paul Thevenot, Ashwin Nair, Jagannath Dey, Jian Yang, and Liping Tang. Method to analyze three-dimensional cell distribution and infiltration in degradable scaffolds. *Tissue engineering. Part C, Methods*, 14(4):319–331, 2008.

[98] James A. Thomson, Joseph Itskovitz-Eldor, Sander S. Shapiro, Michelle A. Waknitz, Jennifer J. Swiergiel, Vivienne S. Marshall, and Jeffrey M. Jones. Embryonic stem cell lines derived from human blastocysts. *Science 6*, 282(5391):1145–1147, 1998.

[99] Tony Y. Wang, Arindom Sen, Leo A. Behie, and Michael S. Kallos. Dynamic behavior of cells within neurospheres in expanding populations of neural precursors. *Brain Research*, 1107(1):82 – 96, 2006.

[100] William M Wells, Paul Viola, Hideki Atsumi, Shin Nakajima, and Ron Kikinis. Multi-modal volume registration by maximization of mutual information. *Medical image analysis*, 1(1):35–51, 1996.

[101] Mark Winter, Eric Wait, Badrinath Roysam, Susan K Goderie, Rania Ahmed Naguib Ali, Erzsebet Kokovay, Sally Temple, and Andrew R Cohen. Vertebrate neural stem cell segmentation, tracking and lineaging with validation and editing. *Nat. Protocols*, 6(12):1942–1952, 2011.

[102] Connie C Wong, Kevin E Loewke, Nancy L Bossert, Barry Behr, Christopher J De Jonge, Thomas M Baer, and Renee A Reijo Pera. Non-invasive imaging of human embryos before embryonic genome activation predicts development to the blastocyst stage. *Nat Biotech*, 28(10):1115–1121, 2010.

[103] Kenong Wu, D. Gauthier, and M.D. Levine. Live cell image segmentation. *Biomedical Engineering, IEEE Transactions on*, 42(1):1–12, 1995.

[104] Qiang Wu, Fatima Merchant, and Kenneth Castleman. *Microscope image processing*. Elsevier, 2010.

[105] Sufan Wu, Yoshihisa Suzuki, Masaaki Kitada, Kazuya Kataoka, Miyako Kitaura, Hirotomi Chou, Yoshihiko Nishimura, and Chizuka Ide. New method for transplantation of neurosphere cells into injured spinal cord through cerebrospinal fluid in rat. *Neuroscience Letters*, 318(2):81 – 84, 2002.

[106] Wei Xiong, Shue-Ching Chia, Joo-Hwee Lim, S. Shvetha, and S. Ahmed. Detection of unstained living neurospheres from phase contrast images with very large illumination variations. In *Engineering in Medicine and Biology Society,EMBC, 2011 Annual International Conference of the IEEE*, pages 6154–6157, 2011.

[107] Lei Xu, Erkki Oja, and Pekka Kultanen. A new curve detection method: Randomized hough transform (rht). *Pattern Recognition Letters*, 11(5):331 – 338, 1990.

[108] Fuxing Yang, MichaelA. Mackey, Fiorenza Ianzini, Greg Gallardo, and Milan Sonka. Cell segmentation, tracking, and mitosis detection using temporal context. In JamesS. Duncan and Guido Gerig, editors, *Medical Image Computing and Computer-Assisted Intervention – MICCAI 2005*, volume 3749 of *Lecture Notes in Computer Science*, pages 302–309. Springer Berlin Heidelberg, 2005.

[109] Zhaozheng Yin, Takeo Kanade, and Mei Chen. Understanding the phase contrast optics to restore artifact-free microscopy images for segmentation. *Medical Image Analysis*, 16(5):1047–1062, 2012.

[110] Weimiao Yu, Hwee Kuan Lee, Srivats Hariharan, Wenyu Bu, and Sohail Ahmed. Quantitative neurite outgrowth measurement based on image segmentation with topological dependence. *Cytometry Part A*, 75A(4):289–297, 2009.

[111] Weimiao Yu, Hwee Kuan Lee, Srivats Hariharan, Shvetha Sankaran, Pascal Vallotton, and Sohail Ahmed. Segmentation of neural stem/progenitor cells nuclei within 3-d neurospheres. In *Advances in Visual Computing*, volume 5875 of *Lecture Notes in Computer Science*, pages 531–543. Springer Berlin Heidelberg, 2009.

[112] V. Zagrodsky, V. Walimbe, C.R. Castro-Pareja, Jian Xin Qin, Jong-Min Song, and R. Shekhar. Registration-assisted segmentation of real-time 3-d echocardiographic data using deformable models. *Medical Imaging, IEEE Transactions on*, 24(9):1089–1099, 2005.

[113] Frits Zernike. How i discovered phase contrast. *Science*, 121(3141):345–349, 1955.

[114] C. Zimmer, E. Labruyere, V. Meas-Yedid, N. Guillen, and J.-C. Olivo-Marin. Segmentation and tracking of migrating cells in videomicroscopy with parametric active contours: a tool for cell-based drug testing. *Medical Imaging, IEEE Transactions on*, 21(10):1212–1221, 2002.

[115] C. Zimmer, Bo Zhang, A. Dufour, A. Thebaud, S. Berlemont, V. Meas-Yedid, and J.-C.O. Marin. On the digital trail of mobile cells. *Signal Processing Magazine, IEEE*, 23(3):54–62, 2006.

[116] Barbara Zitová and Jan Flusser. Image registration methods: a survey. *Image and Vision Computing*, 21(11):977 – 1000, 2003.

[117] Chuanming Zong. *Sphere packings*. Springer, 1999.